AIR AND WATER GAP MULTISTAGE MEMBRANE DISTILLATION SYSTEM FOR WATER DESALINATION

BY

SUHAIB MUSTAFA ALAWAD AHMED

A Thesis Presented to the

DEANSHIP OF GRADUATE STUDIES

KING FAHD UNIVERSITY OF PETROLEUM & MINERALS

DHAHRAN, SAUDI ARABIA

In Partial Fulfillment of the
Requirements for the Degree of

MASTER OF SCIENCE

In

MECHANICAL ENGINEERING

DECEMBER 2016

KING FAHD UNIVERSITY OF PETROLEUM & MINERALS

DHAHRAN- 31261, SAUDI ARABIA

DEANSHIP OF GRADUATE STUDIES

This thesis, written by **SUHAIB MUSTAFA ALAWAD AHMED** under the direction of his thesis advisor and approved by his thesis committee, has been presented and accepted by the Dean of Graduate Studies, in partial fulfillment of the requirements for the degree of **MASTER OF SCIENCE IN MECHANICAL ENGINEERING.**

Dr. Atia E. Khalifa
(Advisor)

Dr. Zuhair Mattoug Gasem
Department Chairman

Dr. Mohammed A. Antar
(Member)

Dr. Salam A. Zummo
Dean of Graduate Studies

Dr. Fahad A. AL-Sulaiman
(Member)

31/1/17

Date

This work is dedicated to my family

ACKNOWLEDGMENTS

First of all, praise be to Allah almighty, most beneficent and merciful. I would like to thank King Fahd University of petroleum and minerals (KFUPM) for offering me this opportunity to accomplish my Master of Science in mechanical engineering and providing me the environment to achieve this level of study.

I would like to express my sincere gratitude to my advisor Dr. Atia E. Khalifa for his guidance, enthusiasm, encouragement and the imparting of his knowledge and expertise. He is not only helpful with deep vision and understanding but also most importantly a kind person. Beside him, I would like to express my appreciation to my committee members Dr. Mohammed Antar and Dr. Fahad Al-Sulaiman for their valuable assistance, guidance and constructive advice which really help me to successfully complete my thesis.

I would like to thank Mr. Mohammed Karam and Mr. Ali Kamal for their technical support in the experimental work. I would equally like to thank all my friends and colleagues for their encouragement. I am very grateful to the entire Sudanese and Muslim community at KFUPM for their moral support and encouragement. Finally, I express my gratefulness to my parents, family and friends for endless love, supplication.

TABLE OF CONTENTS

LIST OF TABLES

LIST OF FIGURES

LIST OF NOMENCLATURES

Q_f	Convective heat transfer in the feed side [w]
h_f	Convective heat transfer coefficient in the feed side [w/m^2. k]
T_{bf}	Bulk feed temperature [k]
T_{mf}	Membrane surface temperature in the feed side [k]
A_f	Heat transfer area in the feed side [m^2]
Q_{mem}	Heat transfer through membrane matrix [w]
A_m	Heat transfer area through the membrane [m^2]
Q_{cm}	Conduction heat transfer through the membrane material [w]
k_m	Thermal conductivity of membrane matrix [w/m. k]
δ	Membrane thickness [m]
T_{ms}	Membrane surface temperature in the support side [k]
k_{gas}	Thermal conductivity of the gas entrapped in membrane pores [w/m. k]
k_{mem}	Thermal conductivity of membrane material [w/m. k]
ε	Membrane porosity
Q_v	Evaporative heat transfer through the membrane pores [w]
J_w	Permeate flux [kg/m^2. s]

ΔH_v	Enthalpy of vaporization of water [J/kg]
Q_{support}	Conductive heat transfer through the support plate [w]
k_{suppot}	Thermal conductivity of the support plate [w/m. k]
δ_{suppot}	Support plate thickness [m]
$\mathrm{A}_{\text{support}}$	Heat transfer area of support plate [m^2]
T_{sg}	Support plate surface temperature in the gap side [k]
Q_{gap}	Conductive heat transfer through the gap [w]
k_{gap}	Thermal conductivity of the gap [w/m. k]
δ_{gap}	Gap thickness [m]
A_{gap}	Heat transfer area through the gap [m^2]
T_{pg}	Condensation plate surface temperature in the gap side [k]
Q_{plate}	Conductive heat transfer through the condensation plate [w]
k_{plate}	Thermal conductivity of condensation plate [w/m. k]
δ_{plate}	Condensation plate thickness [m]
A_{plate}	Heat transfer area in the condensation plate [m^2]
T_{pc}	Condensation plate surface temperature in the coolant side [k]
Q_c	Convective heat transfer in the coolant side [w]

h_c	Convective heat transfer coefficient in the coolant side [w/m^2. k]
A_c	Heat transfer area in the coolant side [m^2]
T_{bc}	Bulk coolant temperature [k]
Nu_f	Nusselt number for feed stream
Nu_c	Nusselt number for coolant stream
k_{wf}	Thermal conductivity of feed water [w/m. k]
k_{wc}	Thermal conductivity of coolant water [w/m. k]
D_{hf}	Hydraulic diameter of feed flow channel [m]
D_{hc}	Hydraulic diameter of coolant flow channel [m]
Re_f	Reynolds number for feed stream
Re_c	Reynolds number for coolant stream
Pr_f	Prandtl number for feed stream
Pr_c	Prandtl number for coolant stream
ΔP_m	Vapor pressure difference across the membrane [pa]
γ_{wf}	Activity coefficient
X_{wf}	Mole fraction of water in feed solution
X_{Nacl}	Mole fraction of NaCl in the feed solution

R_{MD}	Equivalent mass transfer resistance
R_{km}	Knudsen diffusion resistance
R_{Mm}	Molecular diffusion resistance
M_w	Molar mass of water vapor molecule
τ	Membrane tortuosity
T_m	Mean temperature across the membrane [k]
$P_{air,pore}$	Log-mean air pressure at both sides of the membrane [pa]
P	Total pressure of water vapor and air [pa]
$D_{w,a}$	Diffusion coefficient of the vapor through the air
EE	Evaporative efficiency
θ	Temperature polarization coefficient
β	Concentration polarization coefficient
C_{mf}	Concentration at membrane feed surface
C_{bf}	Concentration at feed water
GOR	Gain output ratio
C_p	Specific heat capacity [kJ/kg. K]
D_{pore}	Pore diameter [m]
L	Length of channel [m]
p_v	Vapor pressure [Pa]

R	Gas constant [J/Kmol]
μ	Viscosity [N.s/m^2]
ρ	Density [kg/m^3

ABSTRACT

Full Name : Suhaib Mustafa Alawad Ahmed

Thesis Title : Air and Water Gap Multistage Membrane Distillation System for Water Desalination

Major Field : Mechanical Engineering

Date of Degree : December 2016

Membrane distillation (MD) is one of the promising techniques for water desalination and treatment. It is a thermally driven membrane technique for separating water vapor from a saline solution where a micro-porous hydrophobic membrane is used to separate the water vapor from the hot feed water. The vapor permeation is driven by the vapor pressure difference across the membrane. The MD process is considered low energy consumption desalination technique with good productivity. The working temperature of the feed water ranges from 40^{o}C to 90^{o}C which can be easily secured by renewable energy or waste heat resource.

In this study, the performances of Multistage Air Gap Membrane Distillation (MS-AGMD) and Multistage Water Gap Membrane Distillation (MS-WGMD) systems are experimentally investigated and compared. Different flow arrangements for the feed stream and coolant stream are investigated for both MS-AGMD and MS-WGMD configurations. Parallel, series, and combined parallel-series connections for feed and coolant are considered. A mathematical model based on the analysis of heat and mass transfer within the MD module has been developed to predict the performance of the single stage water gap membrane distillation system under variable operating conditions. Moreover, initial testing of the MD

system combined with an outdoor solar system is carried out in the outdoor climate in the city of Dhahran.

The permeate flux increases with increasing feed temperature and feed flow rate, and with decreasing the gap width for both air gap and water gap systems. However, it decreases with increasing feed salinity and coolant temperature. The system performance is mostly dominated by the effect of feed temperature and gap width. Other variables have relatively smaller effects on the output flux. The parallel flow arrangement is found to produce higher output flux and lower power consumption. The evacuated tube solar collector is able to provide feed water at 85°C for the MD system while the temperature of water inside the collector tank reaches 101°C in the month of May.

The results of the theoretical model are in good agreement with the experimental data for the water gap MD system. The model is able to reflect the effects of different operating and design conditions on the MD system performance as validated by the experimental measurements.

ملخص الرسالة

الاسم الكامل: **صهيب مصطفى العوض أحمد**

عنوان الرسالة: تحلية المياه باستخدام التقطير بالغشاء متعدد المراحل

التخصص: الهندسة الميكانيكية

تاريخ الدرجة العلمية: **ديسمبر 2016**

عملية التقطير بالاغشية هي واحدة من التقنيات الواعدة لتحلية ومعالجة المياه. عملية التقطير بالاغشية هي عملية معالجة حرارية لفصل بخار الماء من المحلول الملحي. في عملية التقطير بالاغشية، يتم استخدام غشاء للفصل بين اثنين من السوائل احدهما ساخن ومالح وهو السائل المراد فصل الاملاح منه (معالجته) بينما الآخر بارد. تحدث عملية الفصل عن طريق انتقال البخارمن الجانب الساخن الى الجانب البارد من خلال الغشاء الرقيق الذي يسمح بمرور البخار ولا يسمح بمرور الماء. ويستند مبدأ التقطير بالاغشية على اختلاف ضغط البخار بين جانبي الغشاء. عملية التقطير بالاغشية لديها مزايا هامة على عمليات التحلية الأخرى ولكن واحدة اهم المميزات ان درجة الحرارة المطلوبة للتسخين تتراوح من 40 الى 90 درجة مئوية، ودرجة الحرارة هذه يمكن الحصول عليها بسهولة عن طريق الحرارة الناتجة عن حرق النفايات أو موارد الطاقة المتجددة مثل الطاقة الشمسية.

في هذه الدراسة، تم التحقق من اداء منظومة فجوة الهواء متعددة المراحل (MS-AGMD) و منظومة فجوة الماء متعددة المراحل (MS-WGMD) وايضا مقارنة اداء المنظومتين. كما تم اختبار كفاءة استخدام توصيلات تدفق مختلفة لتيار التغذية وتيار المبرد لكلا المنظومتين (على التوالي، على التوازي، و على التوالي و التوازي معا). كما تم تطوير نموذج رياضي لانتقال الحرارة والكتلة للتنبؤ بمعدل السريان والأداء لمنظومة فجوة الماء احادية المرحلة. اضافة الى ذلك، تم تنفيذ الاختبار الأولي للمنظومة مع نظام الطاقة الشمسية لدراسة أداء المنظومة مع الإشعاع الشمسي المتغير لمدينة الظهران.

معدل التدفق يزيد مع زيادة درجة حرارة ماء التغذية ومعدل التدفق لماء التغذية، ومع تناقص عرض الفجوة لكلا المنظومتين. و ايضا ينخفض معدل التدفق مع زيادة ملوحة ماء التغذية ودرجة حرارة سائل التبريد. وقد وجد ان المتغيرات الأخرى لها تأثير اقل على معدل التدفق. وقد وجد ان للتوصيل على التوازي اعلى معدل تدفق واقل استهلاك

للطاقة. تم الحصول على درجة حرارة تصل ل 85 درجة مئوية، كما ان درجة حرارة الماء داخل خزان المجمع الشمسي تصل ل 101 درجة مئوية في شهر مايو. وبشكل عام، فان نتائج النموذج النظري متوافقة بشكل جيد مع انتائج التجربة.

CHAPTER 1

INTRODUCTION

1.1 Water scarcity problem worldwide

The possibility of having clean water is reducing every day, meanwhile the requirement of potable water is increasing dramatically. Most of diseases that afflict the human are due to contaminated water resources. Even nowadays, developed countries and developing countries face many problems due to water scarcity because of misuse of available water and the pollution due to industrial activities. Drinking water scarcity is believed to be the biggest problem of the world due to the increase in industrial activities and population growth. Impurity of water resources by industrial wastes has heightened the problem [1]. On our blue planet, there are 1.4 billion cubic meters of water, but only 2.5% are freshwater and therefore directly usable for humans or animals. Of this 2.5% round, about 70% is frozen in glaciers and ice caps. The remaining 30 percent is divided into 97% ground water and 3% surface water, like rivers, lakes or marshes. A detailed overview of the water distribution on earth is shown in Figure 1.1. As can be seen the amount of usable freshwater is negligible.

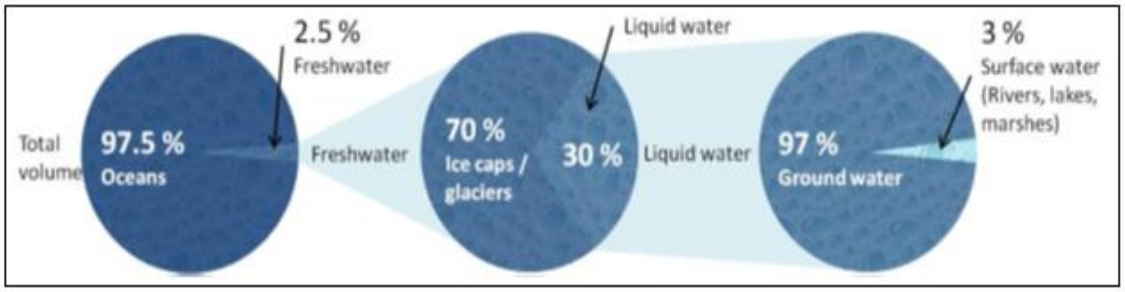

Figure 1.1: Saltwater and freshwater distribution in the world [2]

1.2 Humans consumption and needs for fresh water

Humans cannot live without enough freshwater supply. On average, humans only live for three days without freshwater. On the other hand, they can live for more than two weeks without food. This shows the importance of the freshwater. So, clean water should be availed to all humans and animals. Through the next years, the world population grows and the need for freshwater also increases. The problem is that the water need does not rise linearly, it increases much faster. Therefore, methods must be found to produce the necessary freshwater in an environmentally friendly way [3].

1.3 Desalination role

A lot of people do not have access to freshwater because of the low amount of renewable freshwater resources. In addition, many current freshwater resources are contaminated with waste water that comes from the industry, cultivation, and human beings. Also, the need for freshwater increases, due to the expected global warming, because local mean temperatures increase and this has a direct effect on the freshwater demand. This shows that desalination remains the vital alternative solution to water scarcity problem.

1.4 Seawater properties

Seawater is the water from ocean or sea. The physical properties of salty water depend on the relative proportions and the concentration of the salts it contains. The average salinity of seawater is about 35 g/L. That means every one kilogram of water has about 35 grams of dissolved salts (like chloride and sodium ions as in Figure 1.2 and Table 1.1). The average density of seawater is about 1025 g/L, and it is higher than the density of fresh water which about 1000 g/L because the increase in mass due to dissolved salts is more than the increase in volume. The salty water freezing point (at typical salinity) is about -2^{o}C, and it is less than the freezing point of fresh water (0^{o}C), because as the salt concentration in water increases the freezing point decreases [4].

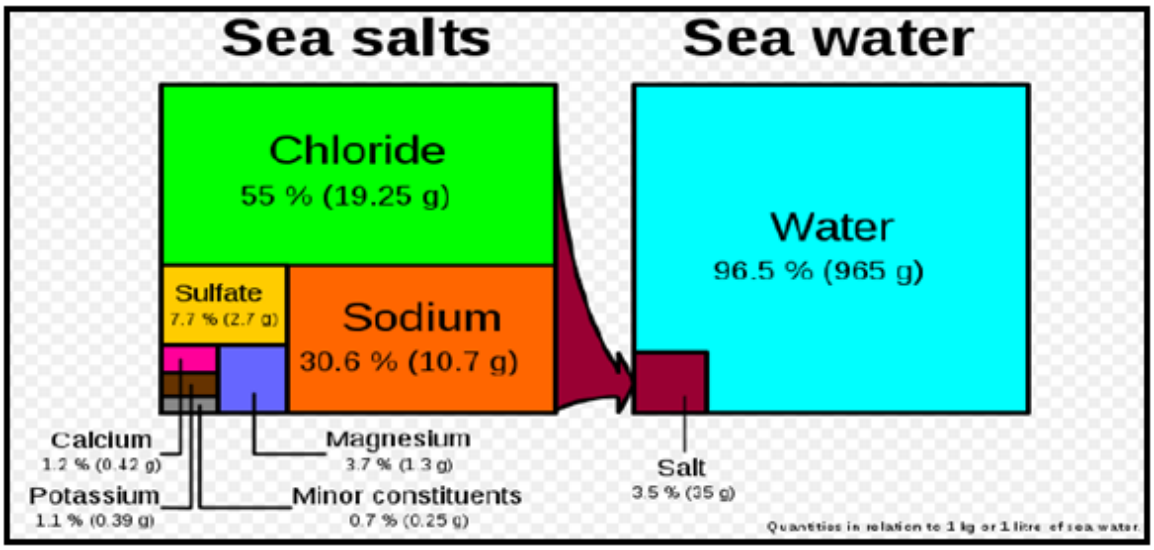

Figure 1.2: The major components of seawater

Table 1.1: Major constituents of seawater and their origins for salinity 35 g/L [5]

Element	Symbol	Name as found in seawater	Ionic state	Concentration in seawater		Sources
				mmol/kg	% by weight g/kg	
Chlorine	Cl	Chloride	Cl^-	545.88	19.353	Volcanic gases
Sodium	Na	Sodium	Na	468.96	10.781	Crust
Magnesium	Mg	Magnesium	Mg^2	52.83	1.284	Crust
Sulfur	S	Sulphate	SO_4^{2-}, $NaSO_4^-$	28.23	2.712	Volcanic gases
Calcium	Ca	Calcium	Ca^2	10.28	0.4119	Crust
Potassium	K	Potassium	K^+	10.21	0.399	Crust
Carbon	C	Bicarbonate	HCO_3^-	2.06	0.126	Volcanic gases, crust, sedimentary rocks
Bromine	Br	Bromide	Br^-	0.844	0.0673	Volcanic gases
Boron	B	Borate	$H_2BO_3^-$	0.416	0.0257	Volcanic gases
Strontium	Sr	Strontium	Sr	0.0906	0.00794	Crust
Fluorine	F	Fluoride	F^-	0.068	0.00130	Crust

1.5 Water-energy nexus

Energy and water systems were mostly treated individually. Recently, because of quick population rise, and increasing consciousness of in-the-wind changes in water cycle and regional climate, the need for combining design and planning of water and energy systems has been growing [6]. Using the water in the energy sector mainly takes place in two processes: generation of electricity and production of fuel. Both of electricity generation and fuel production can utilize different techniques that have quite different requirements for using the water. Also, energy is needed in the water sector for purification (for water treatment and water desalination), abstraction (for pumping ground or surface water), distribution (for transporting the water in urban supply networks and over long distance pipelines), disposal (for industrial wastewater and on-site urban), and utilization (for irrigation applications, for domestic use, and for heating the water in industrial applications) [7].

1.6 Problems facing desalination

Desalination is the main solution for water scarcity issue, but there are several problems related to water desalination:

1. The huge amount of energy used in desalination participate to climate change causing emissions of greenhouse gas.
2. The outlet brine from desalination plants is very salty for the marine life that it comes into contact with.
3. Intake water from the sea always contains some fish and other sea life and passing the water through the desalination system kills these creatures.

1.7 Current desalination techniques

The water desalination systems can be classified into membrane based desalination systems and thermal desalination systems.

1.7.1 Membrane based desalination

In membrane desalination systems such as Revers Osmoses (RO) and Electro-Dialyses (ED), membrane is used to separate the salt from the seawater to generate freshwater. After the desalination process, brine is left and must be disposed off in an environmental friendly way.

1.7.1.1 Reverse Osmosis (RO)

In reverse osmosis process (Figure 1.3), the salty water or the brackish water is compressed through a membrane with high pressure to overcome the osmotic pressure. The common application of reverse osmosis is the separation of fresh water from salty water and brackish

water; salty water or brackish water is pressurized against one surface of the membrane, causing transport of salt-depleted water across the membrane and emergence of potable drinking water from the low-pressure side [8].

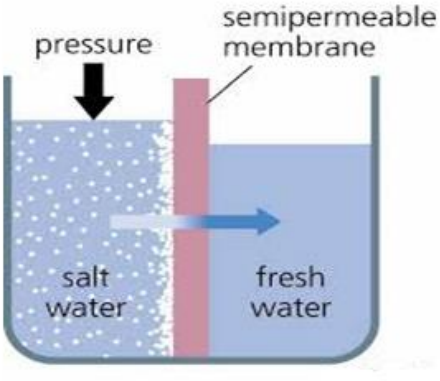

Figure 1.3: Reverse Osmosis Process

1.7.1.2 Electro-Dialysis (ED)

In electro-dialysis process, electrical current is used for separating the salt from the seawater by using an ion exchange. As shown in Figure 1.4, the electrical power is directly proportional to the concentration of the seawater. The higher the salt concentration, the higher is the demand of the electrical power. So, electro-dialysis process is only economic for brackish water (low salinity water). The main advantage of electro-dialysis process over reverse osmosis is that, electro-dialysis can produce more freshwater out of the same amount of saltwater or brackish water (high recovery ratio).

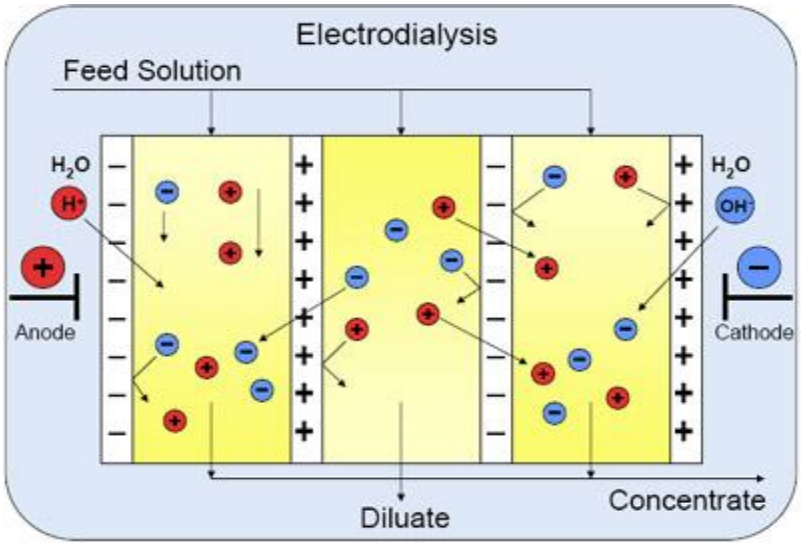

Figure 1.4: Electro-Dialysis

1.7.1.3 Membrane Distillation (MD)

Membrane distillation (MD) process is one of the promising techniques for water desalination and water treatment. It is a thermal-membrane technique for separating water vapor from a saline solution. In MD process, a micro-porous, hydrophobic membrane is placed between two fluids as in Figure 1.5. In MD, the separation process occurs by transfer of the vapor through the hydrophobic membrane due to the vapor pressure difference between the two sides of the hydrophobic membrane [9].

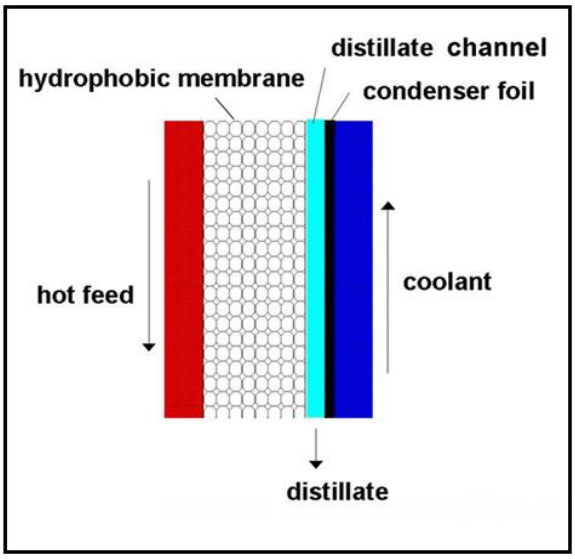

Figure 1.5: Membrane Distillation

1.7.2 Thermal desalination

In these thermal processes, a heat source is used to heat up the water to an acceptable temperature. The source of heat can be acquired from nuclear energy, fossil-fuel, geothermal energy, and solar energy. The most common types of thermal desalination techniques are multi-stage flash (MSF) desalination, multi-effect distillation (MED), multi-effect distillation with thermal vapor compression (MED-TVC) and multi-effect distillation with mechanical vapor compression (MED-MVC).

1.7.2.1 Multi-Stage Flash (MSF) desalination

In Multi-Stage Flash system as in Figure 1.6, seawater is heated up to a high temperature (90 – 120^{o}C). Then, hot seawater enters a low-pressure chamber. The seawater starts flashing because of lower pressure, and only a small amount of the seawater evaporates in the first chamber. The water vapor rises to the top of the first chamber where it condenses using the colder feed saltwater, which is preheated due to this heat exchange process and then heats up to a higher temperature later. Then the condensed freshwater is extracted

from the first chamber. The remaining brine is reused in the next chamber (which is maintained at a lower pressure) as a feed water source. After the last chamber, the brine must be discharged. The amount of freshwater depends on the temperature and the pressure of the seawater in each chamber [10].

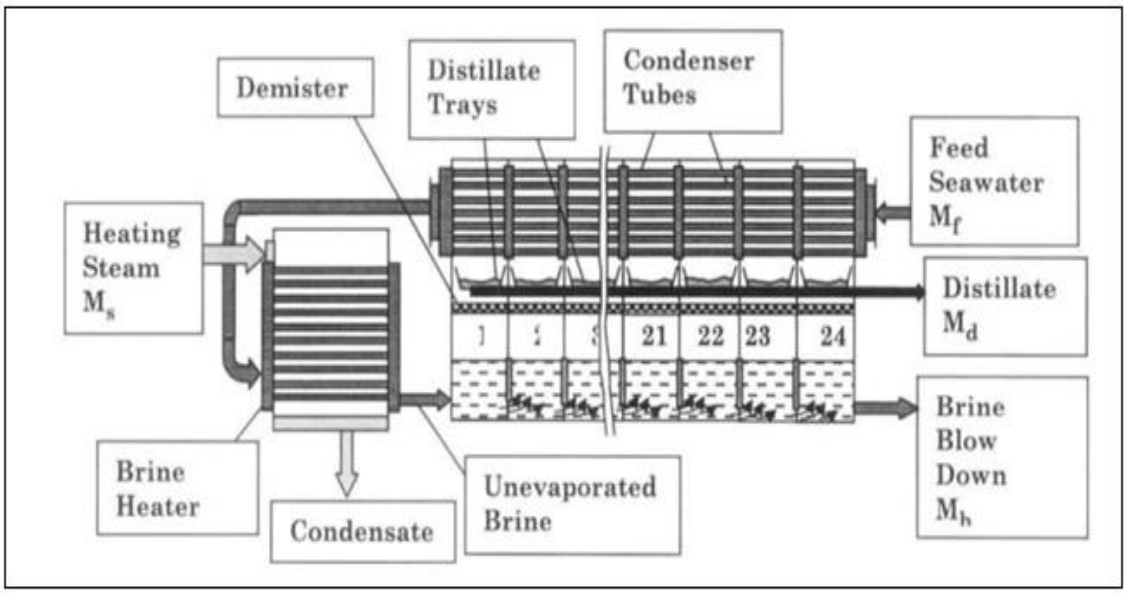

Figure 1.6: Multi-Stage Flash Desalination [4]

1.7.2.2 Multi-Effect Desalination (MED)

In MED process (Figure 1.7), seawater enters each effect at the top and is sprayed inside the effect. It is normally distributed onto the surface of tubes. The sprayed seawater is heated up in the first effect up to the boiling point using an external hot steam from a power plant. The water vapor that leaves the first effect is used in the next effect as a source of heat for the next vaporization process. Due to the heat release, the water vapor condenses and leaves the second effect as freshwater. The sprayed salty water in the second effect is vaporized and again be used in the next effect [11].

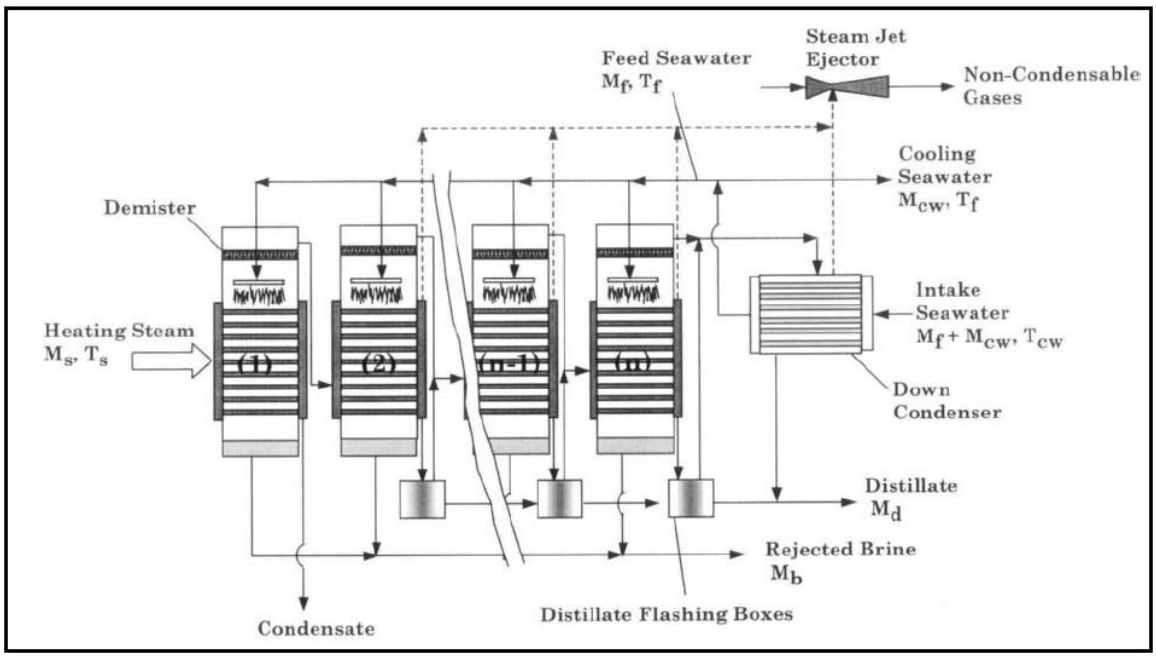

Figure 1.7: Multi-Effect Desalination (MED) [4]

1.7.2.3 Thermal Vapor Compression (TVC)

To improve the efficiency of the MED system, the system is fitted with a thermal vapor compressor as shown in Figure 1.8. Seawater is sprayed onto tube bundles; it is heated up by condensing steam. So, part of the seawater film on the tube outer surface evaporates. The vapor formed in each effect is used as source of heat in the next effect, where it condenses again inside the tubes. In TVC, motive steam from a power plant is mixed with a part of the vapor generated in the last stage are recompressed in the thermo-compressor to heat seawater sprayed in the first effect and evaporate a part of it. The MED-TVC process has several advantages:

- MED-TVC can be used with large and small plants.
- Minimized scaling risk.
- Lower investment cost.

- Reduced corrosion risk.
- Lower thermal energy consumption.
- Lower operating cost.
- Efficient use.

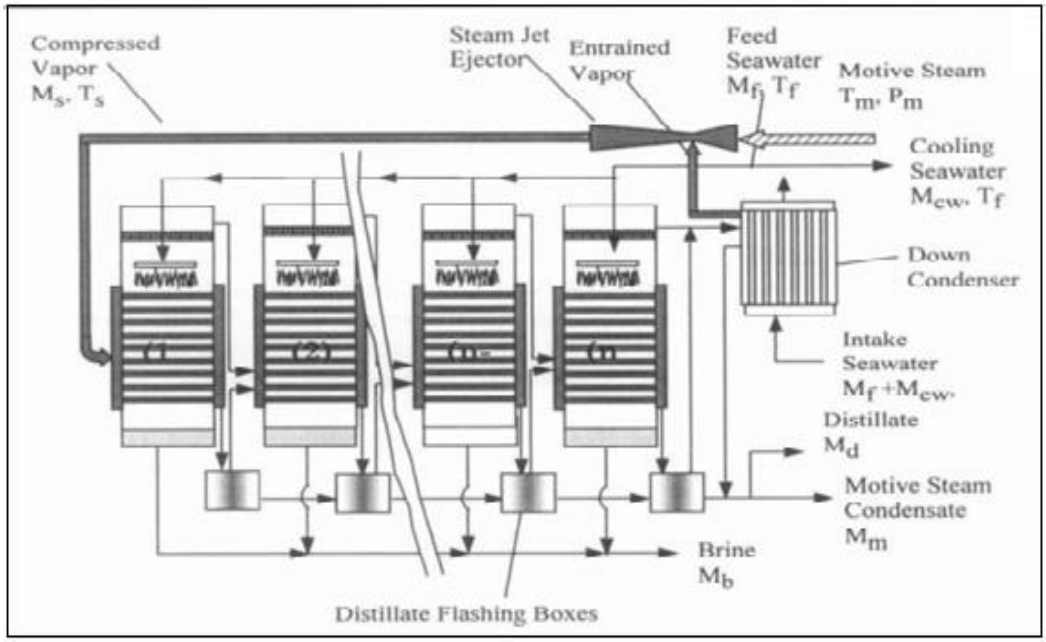

Figure 1.8: Thermal Vapor Compression (TVC) [4]

1.7.2.4 Mechanical Vapor Compression (MVC)

The MED systems with Mechanical Vapor Compression (MED-MVC) shown in Figure 1.9 are used for freshwater production from seawater and brackish water. The deference between the MED-MVC desalination process and the MED-TVC process is that, the steam required to evaporate the seawater is derived from an electric mechanical vapor compressor. The MED-MVC process has several advantages:

- Minimized corrosion risk.
- Reduced scaling risk.

- No need for external thermal energy.
- Process stability.
- Stand-alone system.

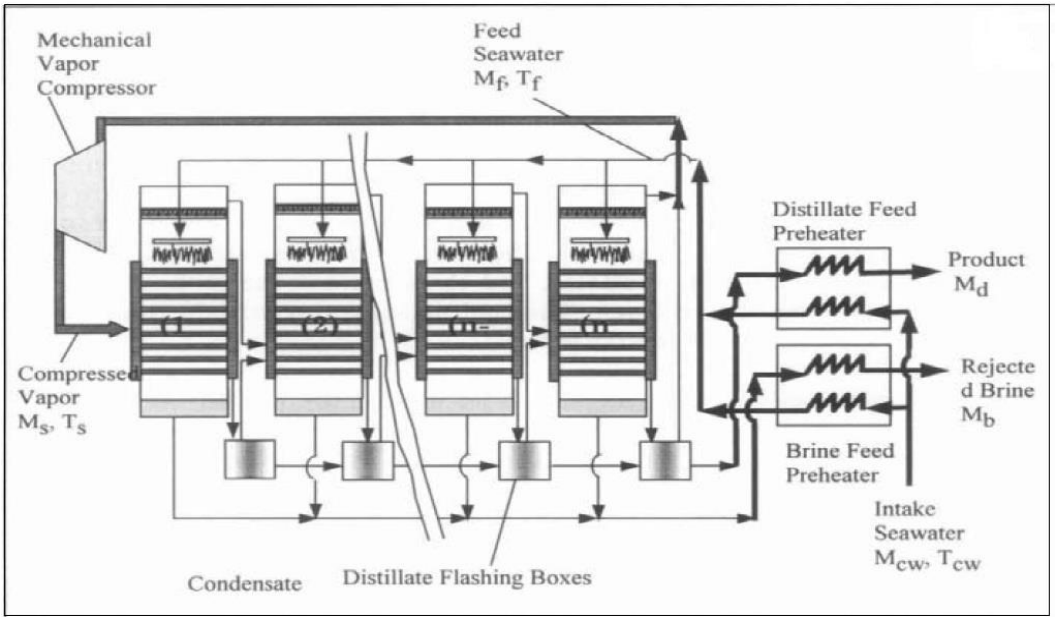

Figure 1.9: Mechanical Vapor Compression (MVC) [4]

1.8 New emerging desalination technologies

1.8.1 Forward Osmosis (FO)

Forward Osmosis (FO) is a process for separating the salts from seawater to get potable water using a semi-permeable membrane. The separation process in Forward Osmosis (FO) is due to gradient of osmotic pressure. In forward osmosis a solution of high concentration is used to drive water (with low salt concentration) flow through the membrane into the high concentration water, and that helps in separating water from saline solution effectively [12].

1.8.2 Dew Evaporation

In dew evaporation process, air as a carrier gas is used to transfer the water vapor from evaporation channel to adjacent, descending dew-forming channels. The required heat for evaporation is obtained from the dew condensation on opposite sides of a heated wall. The condensing cooler air is kept on the cool side because only a small pressure difference is held [13].

1.8.3 Capacitive Deionization (CDI)

Capacitive Deionization (CDI) is a process to remove the ions or ionic constituents from seawater. An electrical potential difference is applied on two porous carbon electrodes. This process removes negative charge ions and anions from the water and then stores them in the positively polarized electrode. Also, positive charge cations are stored in negatively polarized electrode (cathode). The main use of Capacitive Deionization (CDI) is for desalination of brackish water which is the low concentration water (salinity below 10 g/L) [14].

1.8.4 Geothermal Desalination

Geothermal desalination is a new process for producing fresh water that uses geothermal heat to warm the seawater. Geothermal desalination has some advantages over reverse osmosis membrane processes, such as lower maintenance requirements and because of using geothermal heat as the primary energy input, which is a low-environmental-impact source of energy [15].

1.8.5 Solar Desalination

The solar energy is used for water desalination either by heating the seawater directly or by creating the electricity needed for driving the membrane systems [16]. Using the solar energy in seawater desalination can be divided into two methods as shown in Figure 1.10:

1. Direct use for heating.
2. Conversion solar energy to electricity.

In the direct way, a solar collector is used to heat up the saltwater directly as in the solar still [17]. The output freshwater in the direct method is proportional to the incidence angle and the area of the solar collector.

Two separate systems are used in the Indirect solar desalination; a photovoltaic (PV) panels, and a separate conventional desalination system. The direct way is used with many desalination technologies such as the Multi-Stage Flash (MSF), Multi-Effect Humidification (MEH), Multi- Effect Boiling (MEB), Multi-Effect Distillation (MED), Freeze effect distillation, Reverse Osmosis (RO), and Humidification Dehumidification (HDH) [18].

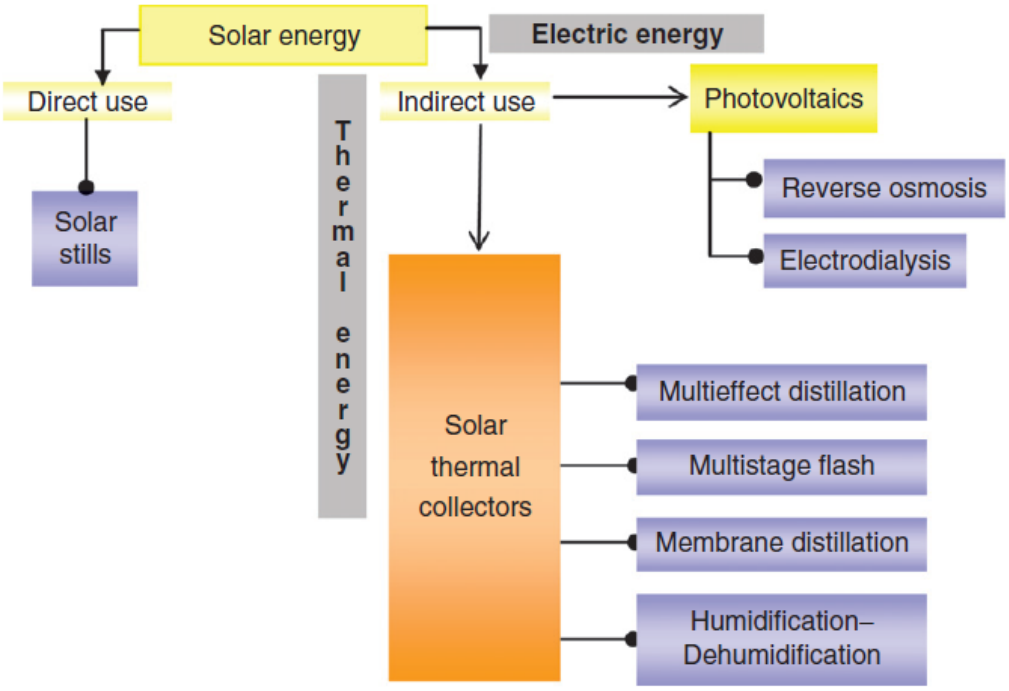

Figure 1.10: Solar Desalination [19]

1.9 Motivation

The MD process is considered low energy consumption desalination technique with good productivity. The working temperature of the feed water ranges from 40°C to 90°C which can be easily secured by renewable energy or waste heat resource. The main problems and which are the major limitation for MD industrialization are that, the consumption of excessive cooling water, the absence of perfect design and the ideal module, and the hydrophobic membrane type. Therefore, the new design of multistage membrane distillation (MSMD) process is needed for industrial applications. This multi stage technique combines the advantages of MD process and multi stages to accomplish higher heat recovery as compared with single MD technology.

1.10 Research Objectives

The objective of this work is to investigate experimentally the performance of multistage membrane distillation system for water desalination. The specific objectives are as follows:

- To investigate the performance of a laboratory-scaled multistage air gap membrane distillation (MS-AGMD) system.
- To investigate the performance of a laboratory-scaled multistage water gap membrane distillation (MS-WGMD) system.
- To study the effect of the main operating conditions such as feed temperature, coolant temperature, feed flow rate, coolant flow rate, gap width, and feed concentration on the permeate flux for both MS-AGMD and MS-WGMD systems.
- To perform energy and efficiency analyses for both MS-AGMD and MS-WGMD systems.
- To study and develop a mathematical model for predicting the performance of single stage water gap membrane distillation process.
- To construct an outdoor solar system, with evacuated tube solar collector, for heating the feed water of the developed MD system (Preliminary work).

1.11 Research Methodology

The above-mentioned objectives are achieved through the following steps:

- Collection of information about water scarcity problem worldwide, human consumption and the needs for fresh water, desalination role, desalination technologies, etc.

- A comprehensive literature review on multistage membrane distillation and solar desalination systems, and a critical review on air gap and water gap membrane distillation systems.
- A mathematical heat and mass transfer model using **E**ngineering **E**quation **S**olver (**EES**) program in order to perform a parametric study on water gap membrane distillation (WGMD) system.
- A comprehensive investigation on the performance of MS-AGMD and MS-WGMD system at different operating parameters and experimental conditions.

CHAPTER 2

MEMBRANE DISTILLATION: BACKGROUND AND LITERATURE REVIEW

2.1 Membrane distillation

Membrane distillation (MD) is a developing method for water treatment and desalination. It is a thermally driven separation process that uses a micro-porous, hydrophobic membrane for separating water vapor from salty water. In MD, the separation process is completed by the water vapor mass transfer through the hydrophobic membrane. The vapor pressure difference between the two sides of membrane is the driving force in MD process [20, 21]. The MD has been widely studied for the different processes such as concentration of solutions, volatile organic compounds removal, desalination of brackish water or seawater, removal of toxic elements and heavy metals from water and additional purification, and separation processes [22–25]. MD has considerable advantages over other desalination methods for example it has lower operating temperature, the possibility to work at lower pressure. Thus, waste heat or solar heat can be used for heating the water [20, 21].

2.2 MD Configurations

Depending on the application of the membrane distillation, different configurations for MD module have been used. The MD configurations differs from each other in the way the module is designed. The four basic configurations mainly used in MD processes are as the following:

2.2.1 Direct Contact Membrane Distillation (DCMD)

In DCMD type (Figure 2.1.a), the feed water is in direct contact with the hot surface of the membrane and cold permeate is in direct contact from the other side. So, water evaporation occurs at the hot surface of membrane. Vapor is passed across the membrane to the cold side due to the pressure difference and condenses inside the membrane module with the cold permeate stream. Direct Contact Membrane Distillation is widely used in water desalination processes because it is the simplest MD type. DCMD is used in many other applications such as in food industries [26, 27], and the manufacturing of acids [28]. The conduction losses are the main drawback of this design.

2.2.2 Air Gap Membrane Distillation (AGMD)

In AGMD there is a direct contact between feed water and hot surface of membrane only. A gap is placed between the membrane cold surface and the condensation surface and is filled by a stagnant air as shown in Figure 2.1.b. Vapor passes across the air gap and condenses on the condensation plate. The advantage of the air gap is to reduce the conduction heat losses. Because the air gap exists, the permeate flux is reduced, which is considered a disadvantage of AGMD compared to DCMD. AGMD is used for removal of volatile organic compounds and for water desalination [29].

2.2.3 Sweeping Gas Membrane Distillation (SGMD)

In SGMD configuration (Figure 2.1.c), as in the previous types there is direct contact between feed water and membrane feed surface. In the permeate side, vapor is swept using an inert gas and then condensation occurs outside the membrane module. This type is like air gap but in this case the gas is moving to enhance the coefficient of mass transfer. The SGMD configuration is used for removal of volatile organic compounds [28]. The sweeping gas membrane distillation gives a small permeate flux with large sweeping gas volume, and this is the main disadvantage of this type.

2.2.4 Vacuum Membrane Distillation (VMD)

In vacuum membrane distillation configuration, a vacuum in the cold side of membrane is created by using a vacuum pump as shown in Figure 2.1.d. Condensation occurs outside the membrane module. One of the VMD advantages is that, the heat lost by conduction is negligible [29]. This type of MD is used also for removal of volatile organic compounds.

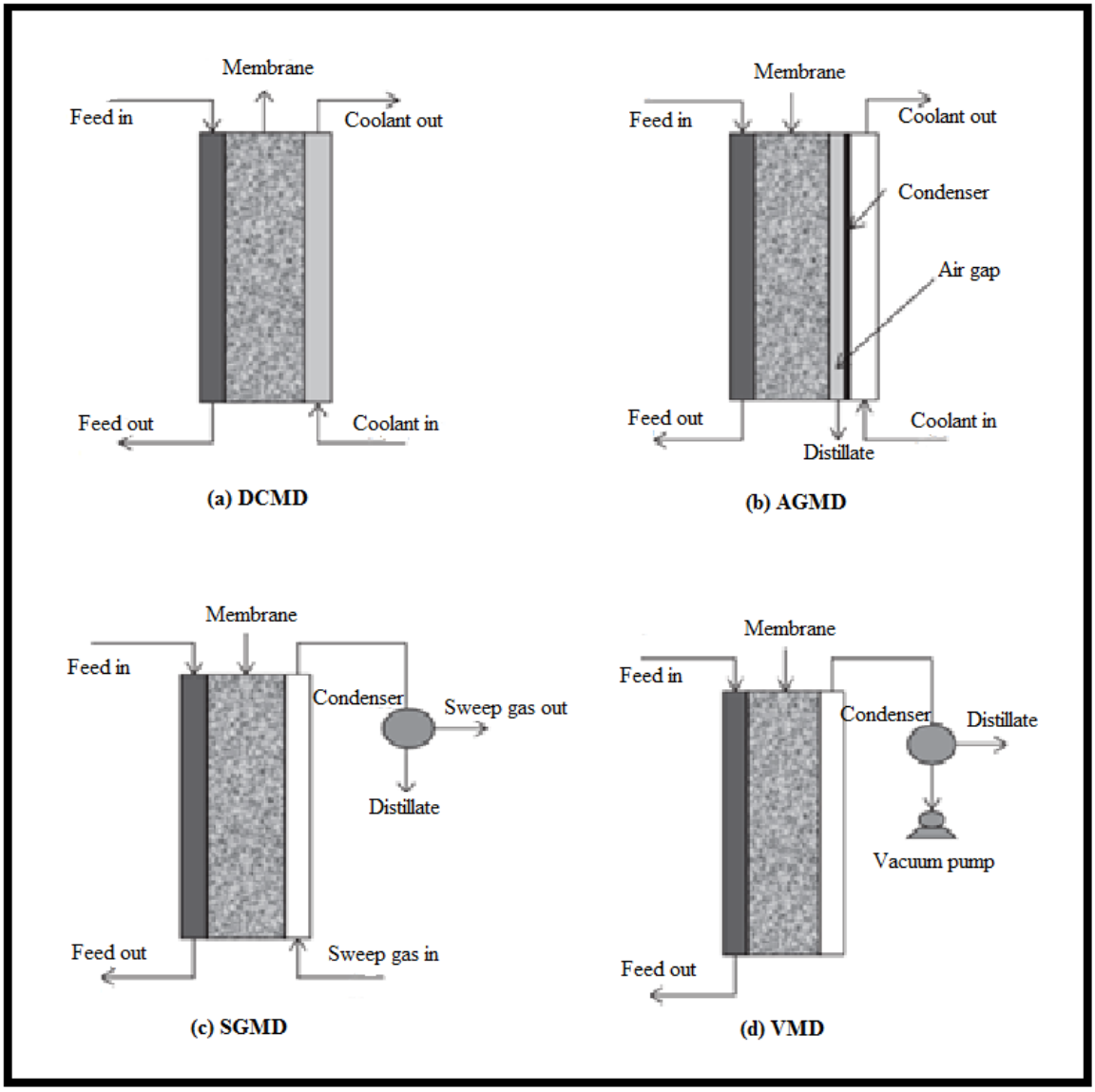

Figure 2.1: MD module configurations [28]

2.3 Main advantages of membrane distillation

- Lower operating temperatures (from 40^{o}C to 90^{o}C).
- Waste heat and renewable energy can be used to heat the feed water.
- Lower operating hydrostatic pressures.
- Membrane fouling in MD is not a problem.

- Cost effective, less expensive material can be used such as plastics.
- No corrosion problems (since plastic can be used).
- High salt rejection factor (almost 100%).

2.4 Main disadvantages of membrane distillation

- The permeate flux is still lower than current conventional desalination techniques.
- Membrane wetting is a possible problem.

2.5 Membrane applications

MD has many applications; initially it started in the food industry. Later, it was introduced to heavy metal removal and recently it is tested and slightly implemented in water desalination and fresh water production. Most of the process applications are in small scale plants and laboratory.

2.6 Membrane modules

There are four common types of membrane modules as the follows:

2.6.1 Plate and Frame Module

The spacers and the membrane are welded to each other between two plates as in Figure 2.2. So, it is very easy to replace or clean. On the other hand, a membrane support is needed because the packing density is small and the ratio of membrane area to packing volume is small [28].

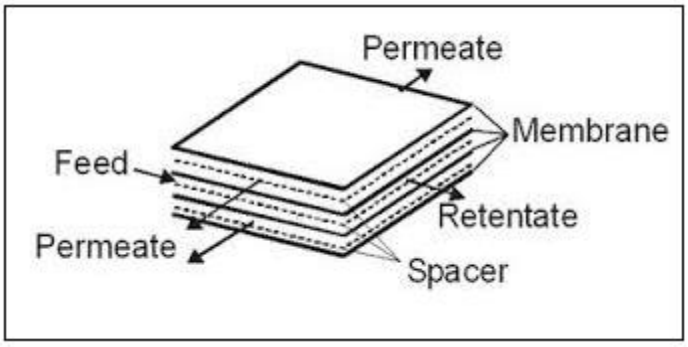

Figure 2.2: Plate and Frame Module

2.6.2 Hollow fiber module

The hollow fiber configuration (Figure 2.3) involves many hollow fibers bundled and sealed in a tube. In this type, the seawater flows outside the fiber and freshwater is produced inside the membrane fiber (outside- inside), or the seawater flows inside the fiber and freshwater is produced outside the membrane fiber (inside- outside). The hollow fiber module has lower energy consumption and higher packing density. These are the main benefits of hollow fiber module; However, the drawbacks are the high tendency of fouling and difficulty of cleaning and maintenance.

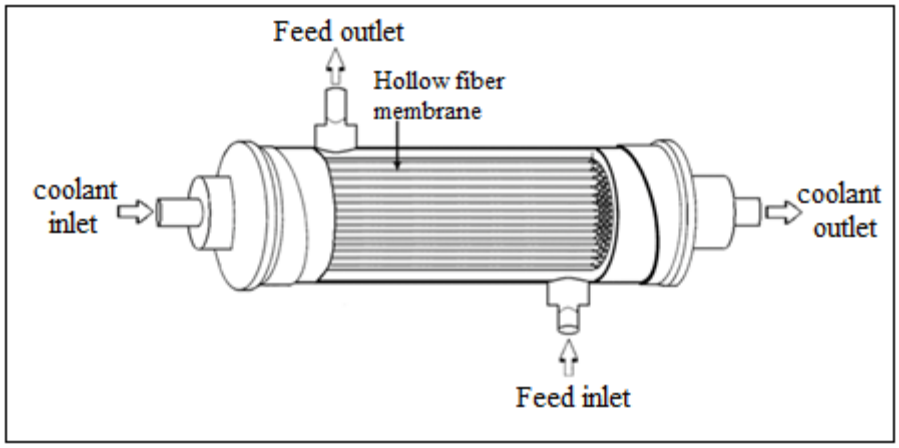

Figure 2.3: Hollow fiber module

2.6.3 Tubular membrane module

In tubular membrane module, the membrane is tubular and fixed between cold and hot cylindrical chambers as shown in Figure 2.4. The tubular membrane module is more preferred due to its low tendency of fouling, easy cleaning and higher effective areas. Conversely, it has low packing density and high operating costs.

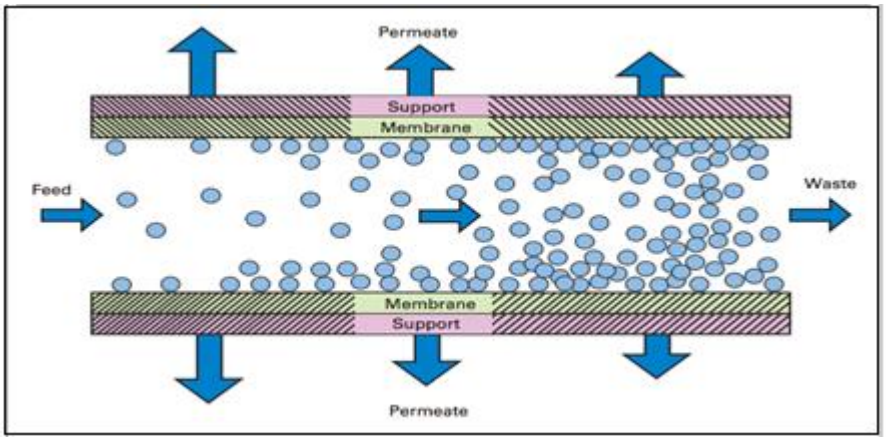

Figure 2.4: Tubular membrane module

2.6.4 Spiral wound membrane module

The spiral wound membrane (Figure 3.5) consists of perforated central collection tube, spacers and flat sheet membrane wrapped and rolled around the tube. The feed flows in an axial direction through the membrane surface, while the freshwater moves to the center and leaves from the outlet pipe. Spiral wound module is the most commonly used membrane type for the desalination of seawater and brackish water. Because of greater control module design of membrane, the tendency toward concentration polarization for the spiral wound membrane is lower than hollow fiber module. The spiral wound module is designed to keep high fluid flow parallel to the membrane surface to enhance mixing of feed at the surface of membrane to reduce the thickness of the boundary layer [30].

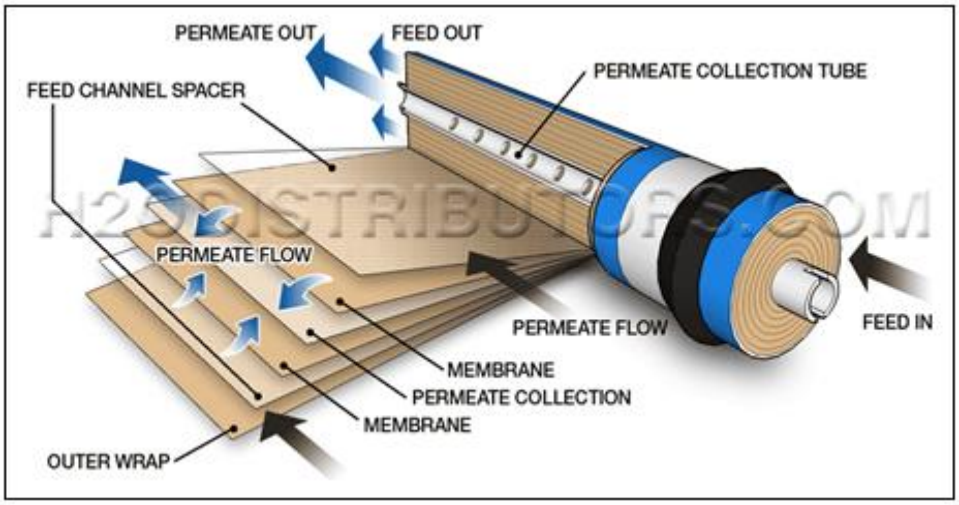

Figure 2.5: Spiral Wound Membrane

2.7 Membrane characteristics

2.7.1 Membrane material

Membranes in the aquatic environment have a repulsive or attractive response to water. The wettability of the membranes is affected by its material composition and its corresponding surface chemistry. The surface tension between the hydrophobic particles is low because the hydrophobic particles tend to cluster together and that increase the surface area. Most hydrophobic membranes are made of polypropylene (PP), polyethylene (PE), poly-tetra-fluoroethylene (PTFE) and polyvinylidene fluoride (PVDF). In general, the membrane used in the MD process should have lower thermal conductivity to minimize heat loss through the membrane and low mass transfer resistance. Furthermore, the membrane should have higher resistance to chemicals and high thermal stability at higher temperatures [28]. The common membranes used in MD are shown in Table 2.1.

Table 2.1: Common membranes commercially used in MD [28]

Trade name	Manufacturer	Material	Mean pore size (μm)	LEP_W (kPa)
TF200	Gelman	PTFE/PP[a]	0.20	282
TF450	Gelman	PTFE/PP	0.45	138
TF1000	Gelman	PTFE/PP	1.00	48
GVHP	Millipore	PVDF[b]	0.22	204
HVHP	Millipore	PVDF	0.45	105[c]
FGLP	Millipore	PTFE/PE[a]	0.20	280
FHLP	Millipore	PTFE/PE	0.50	124
Gore	Millipore	PTFE	0.20	368[c]
Gore	Millipore	PTFE	0.45	288[c]
Gore	Millipore	PRFE/PP[a]	0.20	463[c]

2.7.2 Liquid entry pressure (Wetting pressure)

The wetting pressure, is one of the most important characteristic of membrane. The feed water must not enter the pores of membrane. So, the pressure applied while the water passes over the hydrophobic membrane should not exceed the limit (the wetting pressure). The wetting pressure depends on the membrane hydrophobicity and the maximum pore size. The liquid entry pressure is directly related to feed concentration [31].

2.7.3 Membrane thickness

Another significant membrane characteristic is the membrane thickness. The permeate flux is inversely proportional to the membrane thickness. When the membrane thickness increases, the resistance of mass transfer increases and then the permeate flux decreases. The optimum membrane thickness varies from 30 μm to 60 μm [28].

2.7.4 Mean pore size and size distribution

Membranes used in MD systems usually have pore size between 100 nm to 1 μm. The output flux decreases with decreasing the pore size. Usually, the mean pore size is used for

the vapor flux determination. A small pore size is needed to prevent liquid penetration, while the pore size should be large for higher vapor flux. In other words, the mean pore size should not be too big nor too small. Therefore, the optimum mean pore size for a given membrane should be determined for both operating condition and feed solution [28].

2.7.5 Membrane thermal conductivity

The membrane thermal conductivity is a function of the thermal conductivities of both membrane material and gas surrounding it. The material thermal conductivity depends on shape of crystal, degree of crystallinity, and temperature [28]. A high thermal conductivity in the membrane means the system is not as thermally effective, since the temperature gradient is affected by the heat conduction of the membrane. An ideal case would be a completely insulated membrane.

2.7.6 Membrane porosity and tortuosity

Membrane porosity is the ratio of pores volume to the total volume of the membrane. The membranes with higher porosity have a higher evaporation surface area. For membrane porosity estimation, two types of liquids are used, the first one penetrates the membrane pores, while the other does not. Generally, a membrane with high porosity has lower conductive heat loss and higher permeate flux [28]. Membrane tortuosity is the ratio of pore length to membrane thickness.

2.8 Air gap membrane distillation desalination

Liu et al. [32] carried out experimental and theoretical studies on AGMD for different hydrous solutions, salted water, tap water, alkali solution, acid solution, and dyed solution.

They obtained simple equations of permeate flux and thermal efficiency of AGMD with respect to the temperature difference across the membrane. They analyzed the effects of the air gap width and solution concentration on AGMD. The experiment was made using 1 μm PTFE membrane, and temperature difference of 55^{o}C. The permeate flux was about 28 kg/m^2 h. There was a good match between the theoretical and experimental results.

Lawal and Khalifa [33] investigated the performance of double-stage AGMD unit. They presented the effect of different operating variables such as feed flow rate, feed temperature, coolant flow rate, coolant temperature, and air gap width. They found that the maximum permeate flux for double stage AGMD unit is 128.46 kg/m^{2}h, and a total (average) output flux of 65.81 kg/m^{2}h for a single stage AGMD.

Alklaibi, and Lior [24] presented the effect of operating conditions on the output flux of an AGMD desalination system. They found that the operating conditions of MD system have the following effects :(a) Both air gap distance and feed temperature have significant effects on the flux (the flux increases by more than 3 times as the feed temperature increases from 323 K to 343 K. Decreasing the gap width by 4 mm increases the flux by 2.3 times), (b) Increasing the feed flow rate by 3-times increases the flux by 1.3 times, where increasing the feed salinity by 5 times decreases the flux by 1.15 times only, (c) The cold side parameters have lower effects on the flux than the feed side parameters.

Lior and Alklaibi [9] improved an AGMD model by applying heat and mass equations for the feed and coolant solutions. They studied the variation of the permeate flux with the operating conditions and concluded that: (a) The air gap reduced the conductive heat loss in the system, (b) The permeate flux increases 2.6-times when the gap width decreasing

five-times, (c) The flux increases nine times where the feed temperature increasing from 40 to 80^{o}C (d) The feed concentration and coolant temperature have a lower effect on the permeate flux and thermal efficiency.

Khayet, and Cojocaru [34] constructed an experimental model depending on the Artificial Neural Network (ANN) to study the performance of AGMD process under different operating variables. The input variables of the system were the feed temperature, and the feed flow rate, where the permeate flux was the response variable. The results showed that, the optimum operating variables are 344 K feed temperature, 3 mm air gap width, 286.9 K coolant temperature, and 205 L/h feed flow rate. The maximum value of the permeate flux was 51.075 kg/m^2 h.

Khayet, and Cojocaru [35] applied a response surface method for optimization and modeling for AGMD process used for desalination. They used regression models to estimate the permeate flux and the specific permeate flux by taking the energy consumption into consideration. For the permeate flux, the optimum operating conditions were, 286.9 K coolant temperature, 344 K feed temperature, and 3.05 L/min feed flow rate. Under these operating conditions the permeate flux was 47.189 kg/m^2.h. This was the highest value for the flux through the experiments. For the specific permeate flux, the optimum operating conditions were, 286.9 K coolant temperature, 332 K feed temperature, and 3.4 L/min feed flow rate. Under these operating conditions, the specific permeate flux was 188.7 kg/kW.h, and this was found to be the highest value for the specific performance among all experiments. The energy consumption was about 5.3 kW.h/m^3. Also, they found that the salt rejection factor to be higher than 99.9%.

Hilal et al. [36] carried out an AGMD desalination experiment using high concentrations of Na_2CO_3, Na_2SO_4, NaCl, and $MgCl_2$. They measured the permeate fluxes for different membrane pore sizes (0.2 μm and 0.45 μm) and different feed salinities. They found that the productivity increases with increasing the pore size, and decreases with increasing the feed salinity, the hydrophobicity of TF200 membrane was better than TF450. Also, they concluded that the energy consumption is independent of feed concentration, salt type in the feed and salt concentration.

Ghaffour et al. [37] developed a one-dimensional AGMD model. The model was based on the mass and heat equations for single stage AGMD system. They compared the theoretical results with experimental results acquired under different operating conditions. They calculated the permeate flux for two feed concentrations, different air gap widths, and two membrane types. The operating conditions were: red sea water as feed, 9 mm gap width, 0.2 μm membrane pore size, 1.5 L/min cold water flow rate, 1.5 L/min feed flow rate, 20^{o}C coolant temperature, and 80^{o}C feed temperature. They found that, the maximum permeate flux was about 6 kg/m^2.hr. The theoretical values for the flux were strongly correlated with the experimental values.

Li et al. [38] developed a new AGMD module for water desalination process with internal recovery of the latent heat. The module consisted of parallel hollow fiber membranes and hollow fibers heat exchanger. They studied the effect of operating conditions such as concentration, flow rate, and temperature on permeate flux. The maximum value of the output flux was 5.30 kg/m^2 h and 5.7 was the gained output ratio (GOR).

Li et al. [39] carried out an experimental study of the NaCl aqueous solution desalination using an AGMD module with energy recovery. They developed a regression model using Response Surface Methodology (RSM) to investigate the effect of operating conditions on the permeate flux and gain output ratio of the AGMD system. Based on the regression model. They found that the feed inlet temperature has highest effect on the GOR and the flux. Under the optimum operating conditions, the higher permeate flux and GOR could reach 5.07 $L/m^2 \cdot h$ and 8.78 respectively.

Khalifa et al. [40] presented comprehensive experimental and theoretical studies on AGMD system. For the experimental study, they reported the effect of the operating variables on the flux. They tested two different pore size membranes. Their results presented that both air gap distance and feed temperature have significant effects on the system performance. The flux increases by 550% to 750% when the feed temperature increasing from 40 °C to 80 °C. The flux increases by more than 130% when the air gap width decreasing from 7 to 3 mm. The maximum value of the permeate flux was 71.1 $kg/m^2.hr$, with more than 99.9% salt rejection factor. For the theoretical model a 15% maximum deviation is observed when the results are compared with experimentally measured values.

Khalifa and Lawal [41] presented comprehensive experimental and theoretical studies on AGMD system. For the experimental study, they reported the effect of the operating and design variables on the permeate flux. For the theoretical study, they used Taguchi method and applied regression to model and optimize the performance of the AGMD system. They found that the optimal fluxes are 76.0457 and 74.5916 $kg/m^2.h$; respectively. Also, the

percentage error between the experimental and theoretical results at optimum conditions is 1.95%.

2.9 Liquid gap membrane distillation desalination

A theoretical model has been proposed by Ugrozov et al. [42] to analyze a liquid gap membrane distillation process (LGMD). They derived an analytical expression for the permeate flux in a LGMD-module. They also analyzed the effect of the operating conditions and membrane characteristics on the permeate flux. They used hydrophobic micro-porous membrane in the experiment to examine the effect of feed concentration, feed temperature, and feed flow rate. The maximum value for the permeate flux was 0.0045 $kg/m^2.s$ at 90^oC feed temperature, 20 L/hr feed flow rate, and 10^oC coolant temperature. They found a good matching between the experimental values and the theoretical of the LGMD process.

Essalhi and Khayet [43] compared two different membrane distillation (MD) types, air gap (AGMD) and liquid gap (LGMD), by using the same system and operating conditions. They performed their experiments at different feed concentration and different feed temperatures. They found that (1) Though the resistance of mass transfer in LGMD is greater, the permeate flux for LGMD is slightly higher (from 2.2 to 6.5%) compared to that of AGMD, (2) The salt rejection factors for both MD configurations are almost the same, higher than 99.61%, (3) The thermal efficiency for LGMD is higher compared to AGMD, (4) The internal heat loss for AGMD is higher compared to LGMD, (5) For both MD types, the thermal efficiency increases when the feed inlet temperature increasing, (6) The heat transfer rate and the heat transfer coefficient of the coolant side are higher for LGMD

compared to AGMD, (7) Because of its higher permeate flux, LGMD has slightly higher concentration polarization coefficient compared to AGMD, whereas the temperature polarization coefficient for AGMD is slightly higher than that for LGMD.

Kataeva and Ugrozov [44] calculated the power consumption through the production of fresh water for three different liquid gap membrane distillation modules assembled from heat exchanger, electric heater, and separate liquid gap membrane cells. They found that for all tested MD configurations, the value of power consumption increases proportionally with the productivity and the temperature variance between the inlet and exit of MD module, also it decreases with increasing the membrane surface.

Ghaffour et al. [45] proposed and tested a material gap membrane distillation (MGMD). They used three different materials (air, sand, and DI water) to fill the gap between the condensation plate and the membrane. They found that, the permeate flux increases by about 200–800 % when the gap is filled by DI water and sand. They also studied the effect of material thickness and characteristics and found that increasing the water gap width from 9 mm to13 mm increases the water vapor flux. WGMD has higher values of the permeate flux compared with AGMD.

The performance of AGMD and WGMD systems is compared by Khalifa [46] for the same MD module by studying the effect of operating variables such as feed concentration, feed and coolant flow rates, feed and coolant temperatures, gap thickness, and the material of membrane support on the productivity of the system. Results presented that (1) The permeate flux increases significantly for WGMD design, (2) For the same feed temperature difference the permeate flux increases by 140% when the WGMD is used instead of

AGMD, (3) Under the same operating conditions AGMD has higher gap temperature than WGMD, (4) For both systems, when the gap width decreases the permeate flux increases, but the WGMD is less sensitive to gap thickness, (5) When the feed salinity increases, the permeate flux decreases due to the concentration polarization effect, (6) The salt rejection factor is up to 99.98% for both systems.

2.10 Multistage membrane distillation desalination

Lee and Kim [47] simulated a multi stage vacuum membrane distillation (MSVMD) system by using a one-dimensional in-house code with heat and mass transfer equations and momentum and energy balance equations. They used different arrangements for the system (series, parallel, and mixed) as in Figure 2.6. They evaluated the water product cost by considering the maintenance cost, capital cost, operation cost, and spare parts cost. They analyzed the membrane wetting problem, the productivity, and the water product cost in order to find the best arrangement. Results showed that, (1) The mixed MVMD system with 20 stages has the less water product cost ($\$1.16/m^3$), less maximum trans-membrane pressure difference (93.8 kPa), and highest productivity (3.79 m^3/day). (2) Using the waste heat source with MSVMD system can reduce the water product cost from $\$1.16/m^3$ to $\$0.52/m^3$.

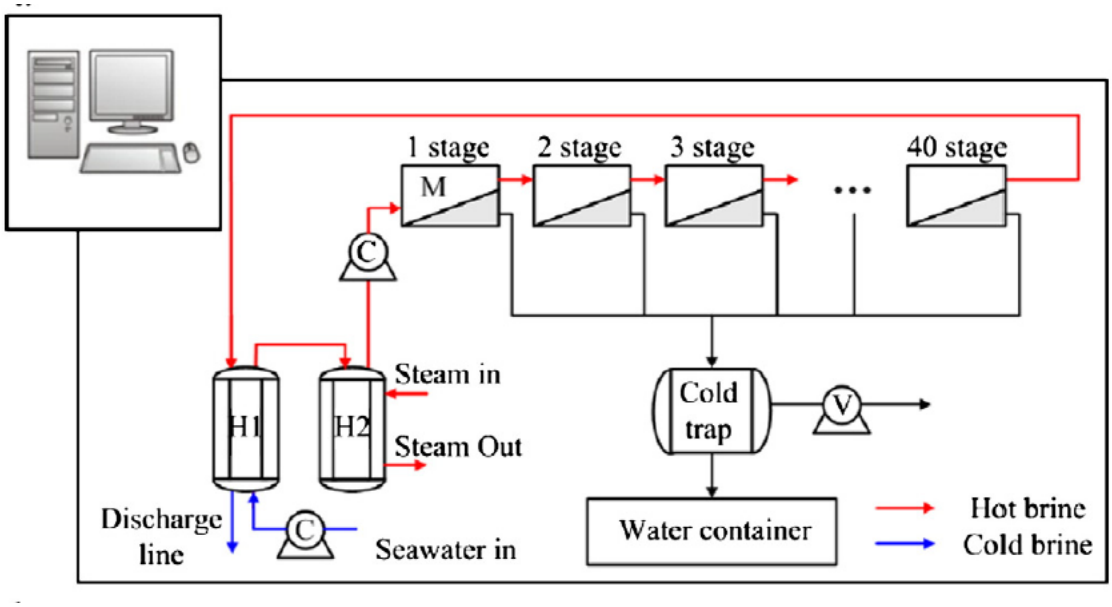

Figure 2.6.a: Series arrangement [47]

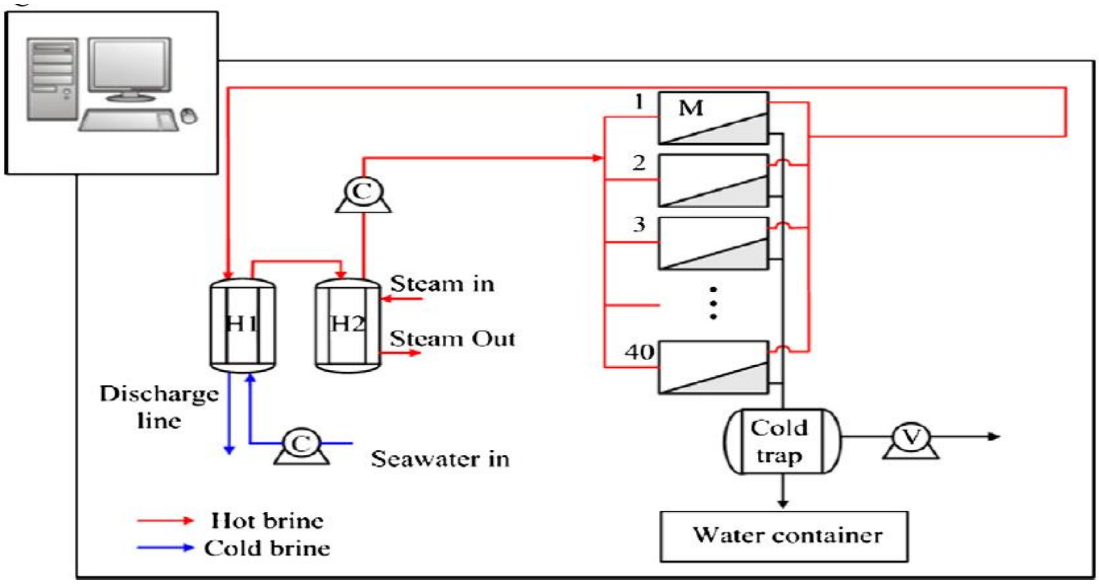

Figure 2.6.b: Parallel arrangement [47]

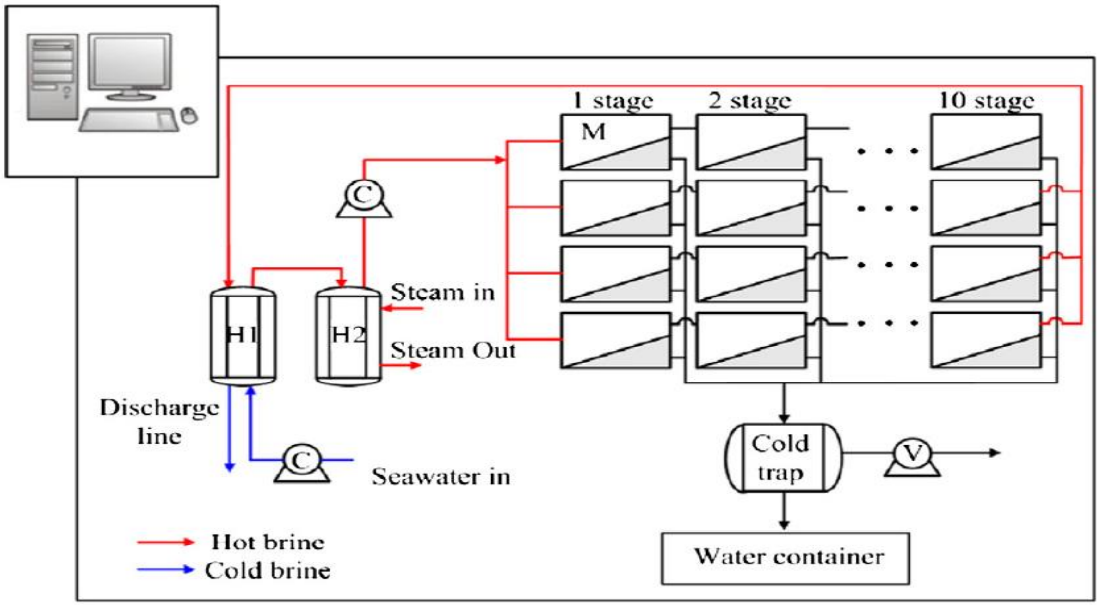

Figure 2.6.c: Mixed arrangement [47]

Kim et al. [48] introduced an integrated pressure-retarded osmosis (PRO) with multi-stage vacuum MD system. They used a recycling flow scheme (MVDM-R) for highly concentrated brine and to produce the fresh water continuously. They used the concentrated brine that is produced from the system to generate the power in the pressure-retarded osmosis system. They also theoretically evaluated the power production and distillate flow rate of the system with respect to the recycling flow ratio and the inlet feed flow rate in the system. They found that (1) At constant feed flow rate, the output flux increases when the recycling flow decreasing, (2) The higher brine concentration from the system is 1.9 M NaCl where 90% recycling flow and 3 kg/min feed flow rate are used, (3) At constant hydraulic pressure difference and using the river water as a feed water with 0.5 kg/min flow rate the maximum power density of 9.7 W/m^2 was achieved.

Kima et al. [49] described the improvement of a solar multi-stage vacuum membrane distillation system. The system consists of temperature modulating (TM) scheme to

measure the variation of the feed seawater temperature, a unit to recover energy from the water vapor to the seawater, and hydrophobic fibers membrane module. They developed a mathematical model to study the system for different numbers of heat recovery units. Results showed that, (1) The total productivity for the system with 10 energy recovery units and 24-stages is about 3.37 m^3/day, and it is about 34% more than the system with one energy recovery unit, (2) For a vacuum membrane distillation system without solar-thermal unit, when the number of heat recovery units increased from 1 to 10, the overall specific thermal energy consumption (OSTEC) decreased by 20 %, (3) The overall specific thermal energy consumption for the system without the solar thermal unit was 28 –36% higher than the solar-thermal system.

Pangarkar and Deshmukh [50] developed a multi-effect air gap membrane distillation (ME-AGMD) module for water treatment. They applied a mathematical model of the single stage AGMD system for four stages ME-AGMD. They presented the performance of the single effect AGMD and multi effect -AGMD process at various operating conditions such as temperature and flow rate for feed and coolant solutions, also the air gap thickness. The results showed that, (1) The maximum permeate flux of ME-AGMD is about 166.38 L/m^2 h at 80 ^oC feed temperature, 1.5 L/min feed flow rate, 20 ^oC cold water temperature, cold water flow rate in each cooling channel of 0.75 L/min and 5 mm air gap thickness, (2) The flux of ME-AGMD module is about 3.2–3.6 times the flux of single stage AGMD module, (3) The efficiency of the ME-AGMD system is higher than efficiency of the single effect AGMD system.

Lienhard et al. [51] evaluated the performance of a multi-stage vacuum membrane distillation (MS-VMD) system which is thermo-dynamically comparable to a multi-stage

flash (MSF) for water desalination. They applied Pitzer's equations for NaCl-solution properties in order to model a wide range of NaCl concentrations. Also, they used the specific membrane area, second law efficiency, and energy efficiency (gained output ratio or GOR) to determine the performance of the system. They found that, (1) Increasing the boiling point elevation (BPE) of the feed water at high salinities resulted in higher heating requirements, lower GOR values, and lower fluxes. (2) When the feed salinity increases the separation least heat increases faster than the specific energy consumption for the system. (3) By using different feed concentrations, and reasonable membrane areas, the MSVMD systems will be as efficient as the multi-stage flash system.

Xing et al. [52] integrated a multi-effect membrane distillation (MEMD) with 2 t/d desalination plant by using poly-tetra-fluoro-ethylene (PTFE) hollow fiber membranes. They analyzed the effect of operating conditions on the performance of the plant. They found that, the GOR and water production are affected by temperature difference between effects and operating temperature. Results showed that (1) The plant gained output ratio (GOR) is 2.76. (2) When the operating temperature increases from 60°C to 80°C the productivity increasing by 12.7%, and it is 9.5% for 4.5°C to 8°C temperature increasing. (3) Vacuum degree and the feed temperature have strong effects on the productivity. (4) The water production increasing by 55%, and permeate flux increases from 3.95 kg/m^2·h to 6.12 kg/m^2·h when feed temperature increased from75°C to 90°C. (5) The productivity increased linearly by 25% as vacuum degree increases from 70 kPa to 82 kPa. (6) The feed salinity and feed flow have lower effects on performance.

Li et al. [53] investigated a multi-stage (4-stage) air gap membrane distillation system for more concentrating reverse osmosis brine gaining a higher water recovery. They performed

one-stage air gap membrane distillation system by utilizing the reverse osmosis brine as feed. They found that, the maximum value of the gained output ratio and the permeate flux could reach 7.1 and 6.8 kg/m^2 h respectively.

Luan et al. [54] optimized vacuum membrane distillation (VMD) system. Then, the possibility of using VMD for the treatment of waste-water produced by natural gas exploitation was studied under optimized operation conditions.

2.11 Solar desalination

Fane et al. [55] examined the feasibility of a solar powered MD system to get fresh water in rural areas. They used conventional heat-exchange devices for recovering large amounts of the latent heat of vaporization. They used computer simulation data for designing and constructing their system. They also used the economic sensitivity analysis to select the optimum heat recovery. They found that the solar powered membrane distillation to be technically feasible. A simulation model has been developed which successfully combined programs for the simulation of the separate MD and solar components. They used the simulator to predict actual performances reasonably well. The simulator has also been used to analyze the effect of design strategies on actual productivity. The capital cost of the unit was very sensitive to the extent to which heat is recovered, especially above a heat recovery factor of about 0.8. They got low MD fluxes, and they expected that high feed temperatures will increase the flux and proportionally reduce energy lost by conduction. They concluded that, for plant capacity of 50kg/day the optimum configuration appears to be 0.7 m^2 heat exchange area, membrane area of 1.8 m^2, and 3 m^2 solar collector area. They estimated the capital cost for the unit to be $3500.

Qtaishat and Banat [56] tested many lab scale and small solar powered MD plants for desalination. The process is considered suitable to integrate with solar energy for small capacities. The initial investment had the main cost. However, the energy has low or even no cost once the system is operational.

Ghaffour et al. [57] carried out an overview of desalination technologies driven by Renewable Energy (RE), they focused on integrated systems, their current technological and economic limitations, as well as their advancement and possible applications. They showed that: (1) the cost of solar energy can be reduced through research on Renewable Energy techniques and mass production of these systems, (2) Geothermal energy has low-cost, so it can be used effectively for desalination, (3) New boundaries in the use of RE technique can be established by technical enhancement of innovative and energy efficient desalination techniques such as Adsorption Desalination (AD) and Membrane Distillation (MD), (4) A combination of geothermal and solar system for desalination can provide the most effective use of RE.

Salata, and Coppi [58] studied the possibility of reaching temperatures above 100 ^{o}C, by using heat transformers and solar ponds, for producing fresh water and the surface area of solar ponds needed. They found that it is possible to get temperatures above 100 ^{o}C through the solar energy, the pond area between 1000 and 4000 m^2 is needed to produce 1 m^3/day of desalinated water.

Al-Zahrani et al. [59] improved an integrated solar-driven MD desalination system for drinkable water production. The system included both water and energy sources. They combined evacuated tubes solar collectors and solar photovoltaic (PV) for their system

operation. They prepared the system to be stand-alone system in areas where potable water and electricity are not easily available. The main components of the system were: the photovoltaic (PV) system, solar-thermal system, and multistage vacuum MD system. They found that the system could be sustainable for water desalination because it is more efficient and environmentally friendly.

Schwantes et al. [60] introduced three different plants using a parallel multi-stage MD system. Two of the plants were powered by solar collectors, and the third one was waste heat driven plant. They examined the effect of some variables (such as feed concentration, feed flow rate, process temperature, and operating time) on the values of specific thermal heat demand and Gain Output Ratio and compared their results with laboratory experiments.

CHAPTER 3

MATHEMATICAL MODELING FOR WGMD SYSTEM

In this chapter, the mathematical model of a single stage water gap membrane distillation (WGMD) system is developed. Different operating variables such as feed temperature, coolant temperature, feed flow rate, and coolant flow rate are considered. In addition, the calculation of evaporation efficiency, gain output ratio, temperature polarization coefficient, and concentration polarization coefficient are presented. Furthermore, the model results are validated against the experimental data for the same module design. It should be mentioned that heat transfer area is not constant across the module because of the internal design of the module under consideration. The area of permeation is equal to the total area of holes in perforated support plate while the area of feed side, coolant side, and condensation plate are different. Finally, it is important to mention that the mathematical model for AGMD system is available in literature by Khayet and Cojocaru [35] and Khalifa et al. [40], that is why we developed the mathematical model for WGMD which is not available in details in literature.

3.1 Heat transfer model

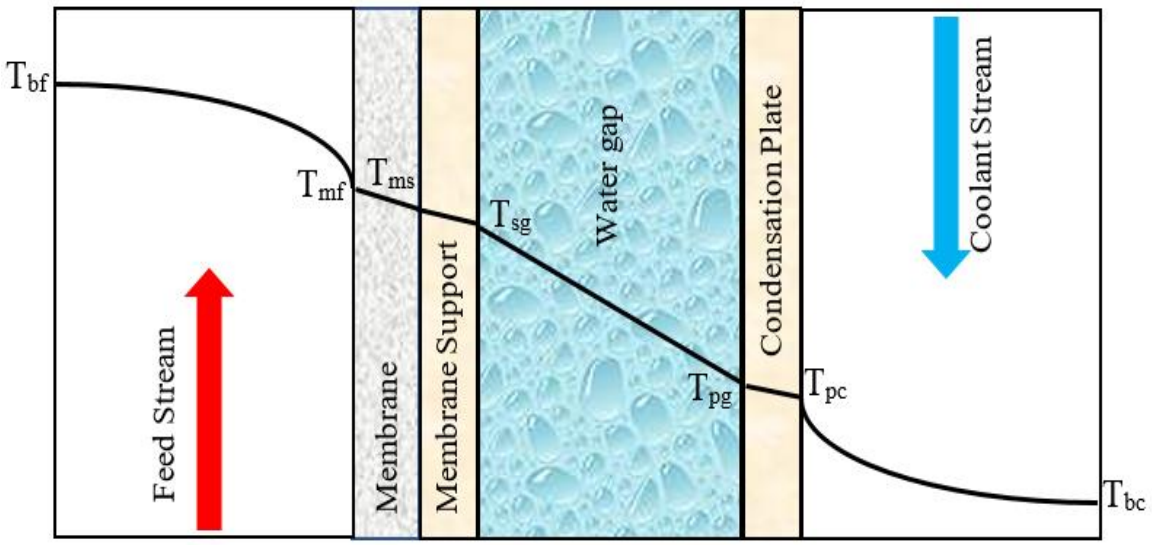

Figure 3.1: Schematic for the heat and mass transfer inside the WGMD module

Referring to Figure 3.1, the heat transfer rate from the feed stream to the coolant stream in the water gap membrane distillation (WGMD) module can be explained as follow:

1. Heat transfer by convection from the hot feed water to the membrane surface. This heat transfer can be calculated using Newton's law of cooling [28, 62, 63]

$$Q_f = h_f * (T_{bf} - T_{mf}) * A_f \tag{3.1}$$

Where h_f is the convective heat transfer coefficient in the feed side, that can be calculated using different correlations depending on the flow type (laminar or turbulent). T_{bf} and T_{mf} are the water bulk and membrane surface temperatures in the feed side. A_f is the heat transfer area in the feed side.

2. Heat transfer through membrane matrix, which consists of two parts, evaporative heat transfer through the membrane pores and conductive heat transfer through the membrane material [40]

$$Q_{mem} = (Q_{cm} + Q_v) * A_m \tag{3.2}$$

Where, A_m is the heat transfer area through the membrane. Q_{cm} is the heat transfer by conduction through the membrane material. It can be given using Fourier's law of conduction [40] as:

$$Q_{cm} = (\frac{k_m}{\delta}) * (T_{mf} - T_{ms}) \tag{3.3}$$

Where k_m is thermal conductivity of membrane matrix, δ is the thickness of membrane respectively. T_{mf} and T_{ms} are membrane surface temperatures in feed and support side. The thermal conductivity of membrane matrix k_m is represented by the following relation [28, 45]

$$k_m = [(\frac{\varepsilon}{k_{gas}}) + (\frac{1-\varepsilon}{k_{mem}})]^{-1} \tag{3.4}$$

Where k_{gas} and k_{mem} are the thermal conductivity of the gas entrapped in membrane pores and membrane material respectively and ε is the membrane porosity. The evaporative heat transfer rate through the membrane pores Q_v is written as [40]:

$$Q_v = J_w * \Delta H_v \tag{3.5}$$

Where J_w is the permeate flux, ΔH_v is the enthalpy of vaporization of water, that can be written as [63]:

$$\Delta H_v = \left(1.7535 * T_m\right) + 2024.3 \text{ [kJ/kg]} \tag{3.6}$$

3. The conductive heat transfer through the support plate, that can be calculated using Fourier's law of conduction as:

$$Q_{\text{support}} = \left(\frac{k_{\text{support}}}{\delta_{\text{support}}}\right) * \left(T_{ms} - T_{sg}\right) * \mathrm{A}_{\text{support}} \tag{3.7}$$

Where k_{support} and δ_{support} are thermal conductivity and thickness of the support plate, respectively. $\mathrm{A}_{\text{support}}$ the heat transfer area of support plate, and T_{sg} is the support plate surface temperature in the gap side.

4. The heat transfer through the water gap is considered to be pure conduction since the water inside the gap is stagnant and natural convection can be neglected. The heat transfer through the water gap can be calculated as:

$$Q_{gap} = \left(\frac{k_{gap}}{\delta_{gap}}\right) * \left(T_{sg} - T_{pg}\right) * \mathrm{A}_{gap} \tag{3.8}$$

Where k_{gap} and δ_{gap} are thermal conductivity and thickness of the water gap respectively. A_{gap} the heat transfer area through the gap. And T_{pg} is the condensation plate surface temperature in the gap side.

5. The conductive heat transfer through the condensation plate, that can be written as:

$$Q_{plate} = (\frac{k_{plate}}{\delta_{plate}}) * (T_{pg} - T_{pc}) * A_{plate} \quad (3.9)$$

Where k_{plate} and δ_{plate} are thermal conductivity and thickness of the condensation plate, respectively. A_{plate} the heat transfer area in the condensation plate, and T_{pc} is the condensation plate surface temperature in the coolant side.

6. Convective heat transfer from the condensation plate to coolant water can be given as [40]:

$$Q_c = h_c * (T_{pc} - T_{bc}) * A_c \quad (3.10)$$

Where h_c is the convective heat transfer coefficient in the coolant side. It can be calculated by using different correlations depending on the flow type (laminar or turbulent). A_c is the heat transfer area in the coolant side, and T_{bc} is the bulk coolant temperature.

Under steady state condition, following conservation of energy, the heat transfer across the module is constant.

$$Q_f = Q_m = Q_{support} = Q_{gap} = Q_{plate} = Q_c \quad (3.11)$$

The convective heat transfer coefficients for feed and coolant streams can be calculated as [65, 66]:

$$h_f = Nu_f * \frac{k_{wf}}{D_{hf}} \quad (3.12)$$

$$h_c = Nu_c * \frac{k_{wc}}{D_{hc}} \tag{3.13}$$

Where Nu_f and Nu_c are dimensionless Nusselt number for feed and coolant streams. k_{wf} and k_{wc} are the thermal conductivity of feed and coolant water respectively. D_{hf} and D_{hc} are hydraulic diameters of feed and coolant flow channels.

If the flow is laminar, the Nusselt number can be given as [65, 66]

For feed side $$Nu_f = 1.86 * (Re_f * Pr_f * \frac{D_{hf}}{L})^{0.33} \tag{3.14}$$

For coolant side $$Nu_c = 1.86 * (Re_c * Pr_c * \frac{D_{hc}}{L})^{0.33} \tag{3.15}$$

For turbulent flow, the following equations for Nusselt number are considered:

- For hot feed flow [63, 23]

$$Nu_f = 0.027 * Re_f^{0.8} * Pr_f^{0.4} * (\frac{\mu_{bf}}{\mu_{mf}})^{0.14} \tag{3.16}$$

- For coolant flow [63, 23]

$$Nu_c = 0.027 * Re_c^{0.8} * Pr_c^{0.3} * (\frac{\mu_{bc}}{\mu_{pc}})^{0.14} \tag{3.17}$$

Where Re_f and Re_c are dimensionless Reynolds number values for feed and coolant flow. Pr_f and Pr_c are dimensionless Prandtl number values for feed and coolant flow. μ_{bf}, μ_{bc}, μ_{mf}, and μ_{pc} are dynamic viscosity bulk feed, bulk coolant, and membrane feed surface and plate coolant surface, respectively.

3.2 Mass transfer and Pressure model

The permeate mass flux in WGMD depends on equivalent mass transfer resistance (R_{MD}) and difference in vapor pressure (ΔP_m) due to the temperature difference across the membrane. The permeate mass flux can be given as [23]:

$$J_w = \frac{\Delta P_m}{R_{MD}} \tag{3.18}$$

Where ΔP_m is the vapor pressure difference across the membrane which can be written as:

$$\Delta P_m = P_{mf} - P_{ms} \tag{3.19}$$

If the effect of feed salinity is considered, equation 3.18 will modified to:

$$J_w = \frac{P_{mf} \cdot \gamma_{wf} \cdot X_{wf} - P_{ms}}{R_{MD}} \tag{3.20}$$

Where γ_{wf} is the activity coefficient and X_{wf} is the mole fraction of water in feed. Activity coefficient represents the variation of substances from their ideal behavior due to impurities, and mole fraction is the ratio of number of moles of any specie to the total number of moles present in solution. The activity coefficient for an aqueous solution of NaCl is given as [63, 67]

$$\gamma_{wf} = 1 - \left(0.5 \cdot X_{Nacl}\right) - \left(10 \cdot \left(X_{Nacl}\right)^2\right) \tag{3.21}$$

Where, X_{Nacl} is the mole fraction of NaCl in the feed solution.

The vapor pressures at the feed surface of the membrane and the support surface of the membrane can be calculated using the Antoine equation [67] as follows:

$$P_{mf} = exp\left(23.1964 - \left(\frac{3816.44}{T_{mf} - 46.13}\right)\right) \tag{3.22}$$

$$P_{ms} = exp\left(23.1964 - \left(\frac{3816.44}{T_{ms} - 46.13}\right)\right) \tag{3.23}$$

The partial pressure exerted by the water vapor inside the pores can be found out by using Antoine equation [68].

$$P_{v} = exp\left(23.1964 - \left(\frac{3816.44}{T_{m} - 46.13}\right)\right) \tag{3.24}$$

Where, T_m is the mean temperature across the membrane and can be taken as:

$$T_m = \frac{T_{mf} + T_{ms}}{2} \tag{3.25}$$

Considering air and water vapor filling the pores then the partial pressure of air inside the membrane pores can be taken as [40]:

$$P_{air,pore} = P_{pore} - P_v \tag{3.26}$$

P_v is the partial pressure of water vapors inside the pores and P_{pore} is the total pores pressure.

$$P_{pore} = 101325\ pa$$

(3.27)

The equivalent mass transfer resistance R_{MD} can be described by Knudsen diffusion, Molecular diffusion, and Poiseuille flow [70, 71, 72, 73]. R_{MD} can be written as:

$$R_{MD} = R_{km} + R_{Mm} \tag{3.28}$$

Where R_{km} is the Knudsen diffusion resistance that can be written as:

$$R_{km} = \left(\left(\frac{2 \cdot \varepsilon \cdot d_{pore}}{3 \cdot \delta \cdot \tau} \right) \cdot \left(\frac{8 \cdot M_w}{\pi \cdot R \cdot T_m} \right)^{0.5} \right)^{-1} \tag{3.29}$$

The Molecular diffusion resistance R_{Mm} can be written as:

$$R_{Mm} = \left(\frac{M_w \cdot \varepsilon \cdot PD_{w,a}}{R \cdot T_m \cdot \delta \cdot \tau \cdot P_{air,pore}} \right)^{-1} \tag{3.30}$$

Where M_w is the molar mass of water vapor molecule, τ is the membrane tortuosity, T_m is the mean temperature across the membrane, $P_{air,pore}$ is the air pressure inside the membrane pores, P is the total pressure of water vapor and air, and $D_{w,a}$ is the diffusion coefficient of the vapor through the air.

The membrane pore is filled with water vapor and air that is already entrapped in the pores. The product of the total pressure inside the membrane pores and ordinary diffusion of water vapor into air molecules [$PD_{w,a}$] affects the permeate flux. If the pressure of air inside the

pores increases, the permeate flux decreases. Diffusivity of water vapors produced through the static air inside the membrane pores can be used as [28, 45, 64]

$$PD_{w,a} = \left(0.00001895\right) \cdot T_m^{\,2.072} \tag{3.31}$$

Other similar equations that may be used instead of above equation are found in literature. To obtain the mass diffusivity ($D_{w,a}$) in above equation, the following relation may be considered [74, 75]

$$D_{w,a} = D^0 * \left(\frac{T_m}{298}\right)^{2.334} \tag{3.32}$$

The membrane tortuosity τ can be calculated as [28, 71]

$$\tau = \frac{(2-\varepsilon)^2}{\varepsilon} \tag{3.33}$$

Where another expression can also be used to calculate tortuosity as in [63, 76]

$$\tau = \frac{1}{\varepsilon} \tag{3.34}$$

Solving this set of equations simultaneously, we can predict the temperature at each point from which we can find the temperature difference across the membrane and consequently the pressure difference across the membrane. Then the permeate flux is calculated from equation 3.20. From the above model, the thermal evaporative efficiency, gain output ratio (GOR), temperature polarization coefficient, and concentration polarization coefficient can be calculated.

3.3 Model Validation

In order to validate the theoretical model, comparison is made between theoretical and experimental results [46] at various operating conditions. The validation of the theoretical model is shown in Figures 3.2 to 3.5. Figure 3.2 shows the variation of output flux with feed temperature at three different inlet coolant temperatures (5, 15, and 24^{o}C) for the PTFE 0.45 μm membrane, 1.5 L/min feed flow rate, 2 L/min coolant flow rate, and 140 mg/L feed concentration. The model shows good agreement with experimental measurements at any feed temperature with coolant temperatures of 5 and 15^{o}C, where the percentage of error is below 4 %. The maximum difference between the experimental and theoretical output flux is observed for the higher coolant temperature at maximum feed temperature of 90°C. The variation of permeate flux with feed flow rate is illustrated in Figure 3.3. The model is showing a good result compared to the experimental measurements at low flow rates and with about 10 % deviation compared to the experimental values at high flow rate values. Figure 3.4 presents the effect of coolant flow rate on the output flux for both theoretical and experimental investigations. The model is able to predict the output flux at different values of coolant flow rate, where the maximum percentage error is about 5 %. Figure 3.5 shows the effect of gap width on the output flux at different feed temperatures for both theoretical and experimental investigations. The model is showing a good

agreement with experimental data for 4 and 8 mm gap width, but for 2 mm gap width the percentage error reach about 28 % at feed temperature of 90^{o}C.

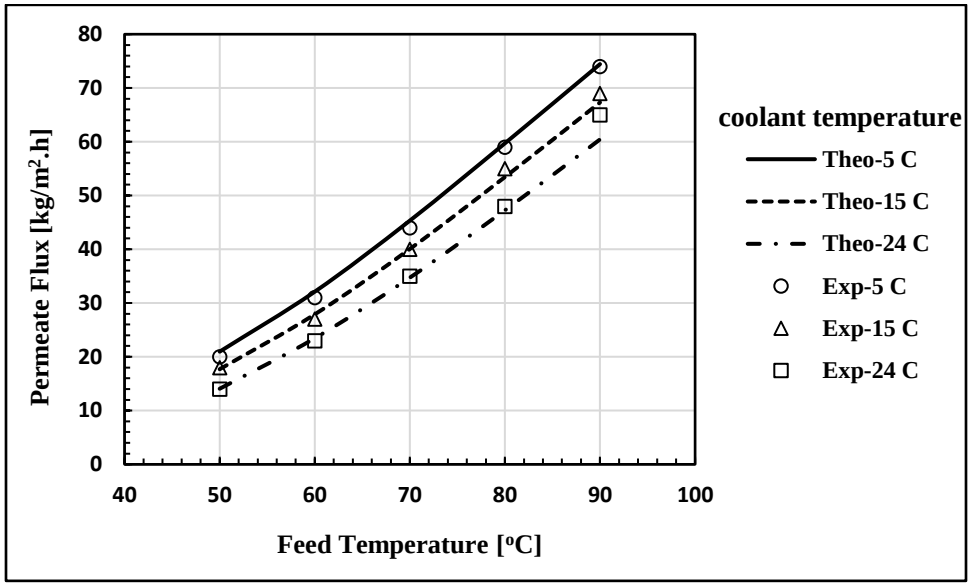

Figure 3.2: Model validation: Effect of feed temperature on permeate flux

Conditions: membrane PTFE 0.45 μm, 4 mm gap width, feed salinity of 140 mg/L, feed flow rate of 1.5 L/min, and coolant flow rate of 2 L/min.

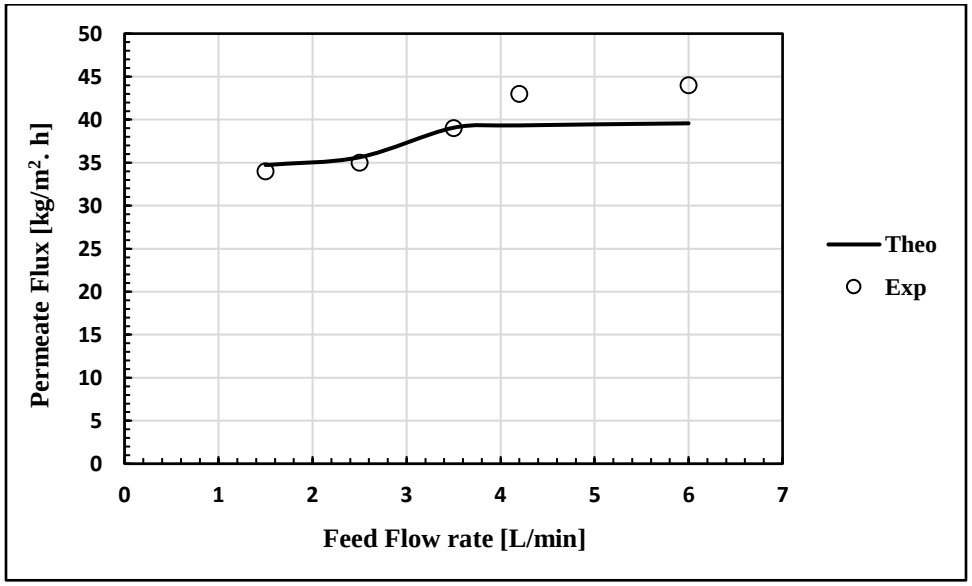

Figure 3.3: Model validation: Effect of feed flow rate on permeate flux

Conditions: membrane PTFE 0.45 μm, 4 mm gap width, feed salinity of 140 mg/L, feed temperature of 70°C, coolant temperature of 24°C, and coolant flow rate of 2 L/min.

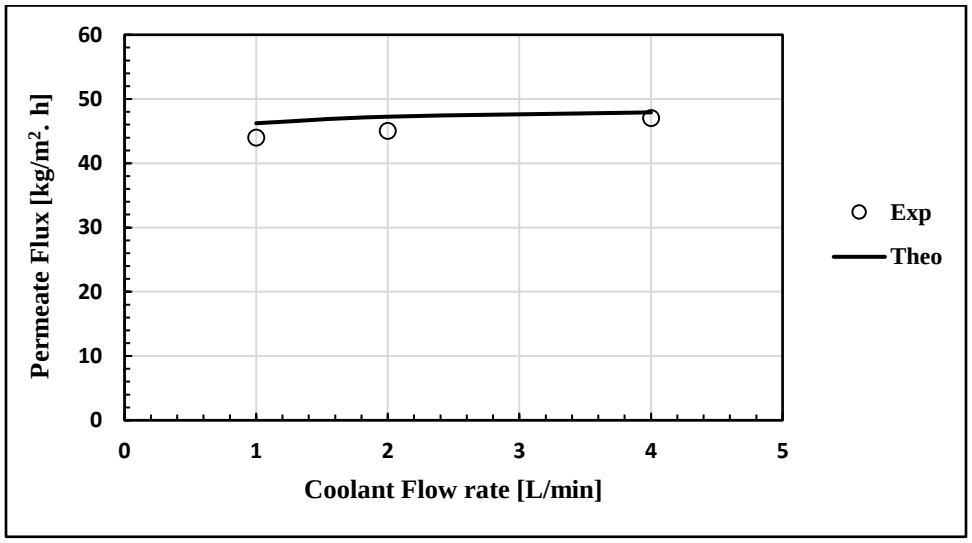

Figure 3.4: Model validation: Effect of coolant flow rate on permeate flux

Conditions: membrane PTFE 0.45 μm, 4 mm gap width, feed salinity of 140 mg/L, feed temperature of 80°C, coolant temperature of 24°C, and feed flow rate of 1.5 L/min.

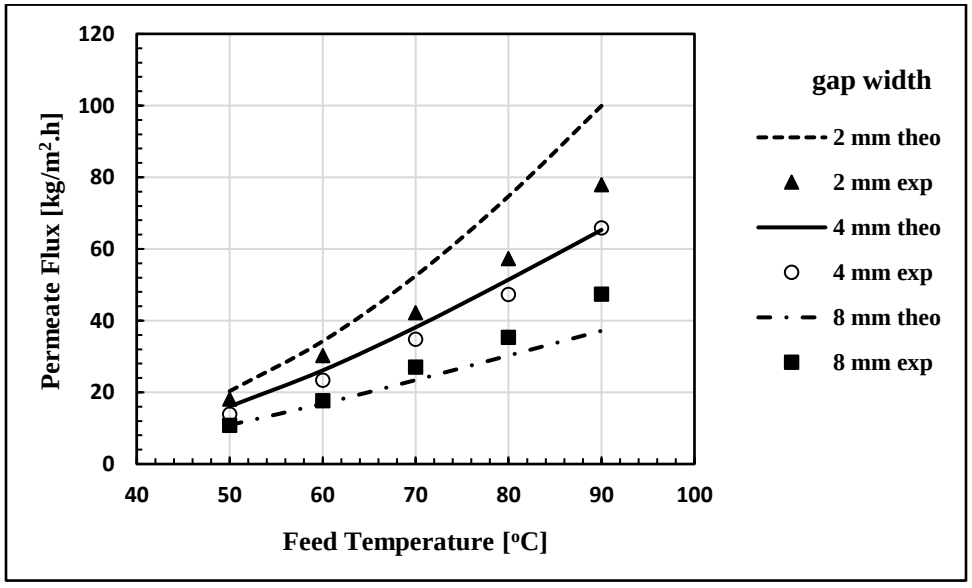

Figure 3.5: Model validation: Effect of gap width on permeate flux

Conditions: membrane PTFE 0.45 μm, feed salinity of 140 mg/L, feed flow rate of 2.3 L/min, coolant temperature of 20°C, and feed flow rate of 2.3 L/min.

3.4 Model Results

3.4.1 Effect of feed temperature

Figure 3.6 shows the variation of the output flux with feed temperature at different coolant temperatures. There is an increase in the output flux with increasing the feed temperature. Because a small increase in feed temperature can make significant different in the vapor pressure (the driving force in MD process), and that leads to a significant increase in the permeate flux. The percentage increase in the permeate flux at a given coolant temperatures when the feed temperature changes from 50°C to 90°C is calculated as well. Increasing the feed temperature increases the permeate flux at any coolant temperature, but the flux increases significantly at higher coolant temperature. The maximum percentage increase in flux (at 30°C coolant temperature) is about 401.9%. The highest value of output flux is about 75.4 kg/m^2 h at 90°C feed temperature, 50°C coolant temperature.

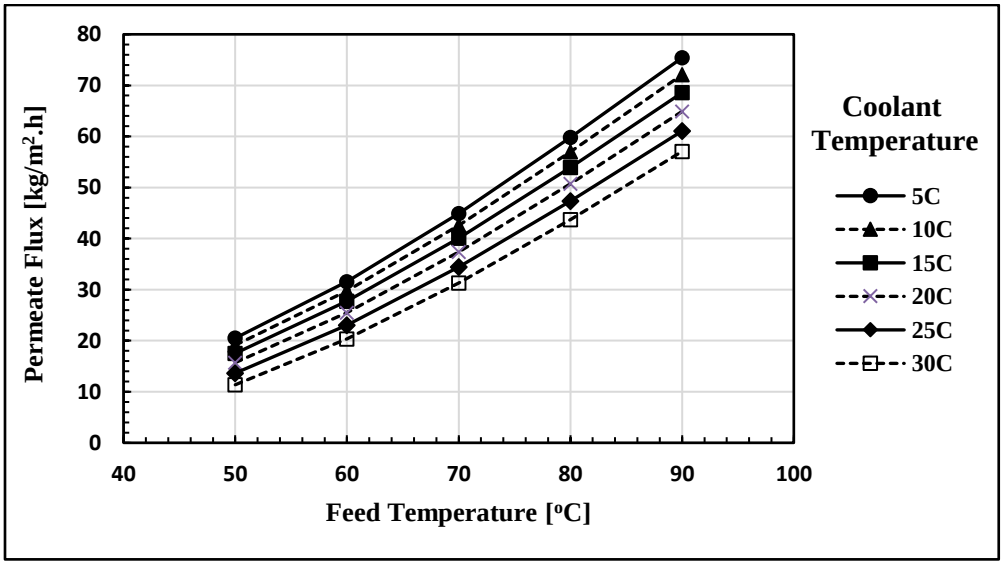

Figure 3.6: Effect of feed temperature on permeate flux at different coolant temperatures

Conditions: membrane PTFE 0.45 μm, feed salinity 140 mg/L, 4 mm gap width, 1.5 L/min feed flow rate, and 2 L/min coolant flow rate.

The effect of feed temperature on output flux at different feed flow rates is shown in Figure 3.7. It can be clearly seen that the permeate flux increases with increasing feed flow rate. Increasing the feed flow rate enhances the turbulence level, and that leads to higher values of the heat and mass transfer coefficients in the feed side of membrane. The permeate flux increases exponentially with feed temperature for feed flow rates of 1 and 6 L/min because the Reynolds number is in laminar flow range (less than 2000) for 1 L/min feed flow rate and within turbulent range (more than 2000) for 6 L/min feed flow rate. For 3 L/min feed flow rate there is significant increase in the permeate flux at feed temperatures of 80 and 90^{o}C because the flow rate is changed from laminar (at lower temperatures) to turbulent (at higher temperatures) as shown in Figure 3.8.

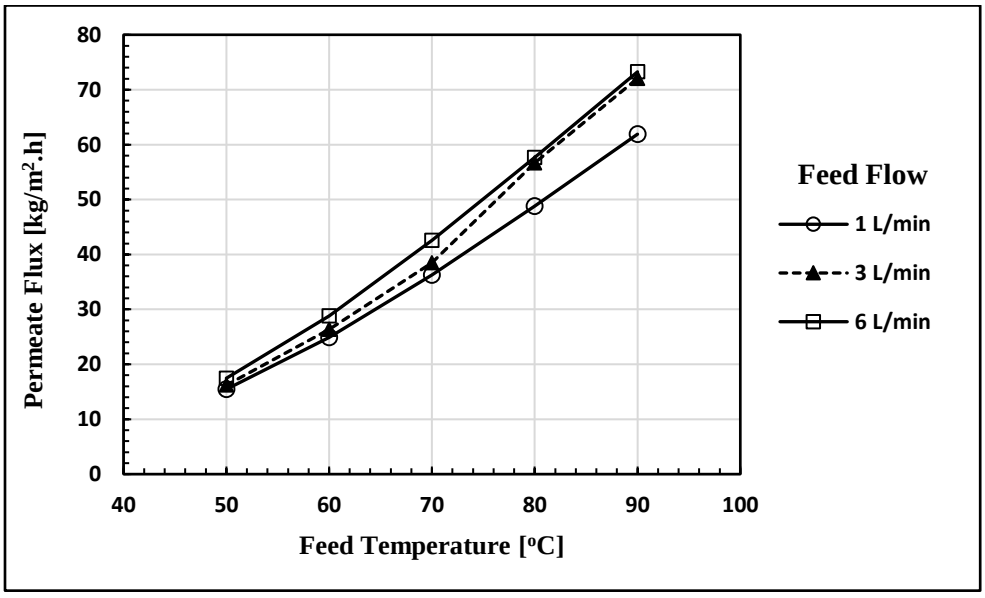

Figure 3.7: Effect of feed temperature on permeate flux at different feed flow rates

Conditions: membrane PTFE 0.45 μm, coolant temperature of 20^{o}C, feed salinity 140 mg/L, 4 mm gap width, and 2 L/min coolant flow rate.

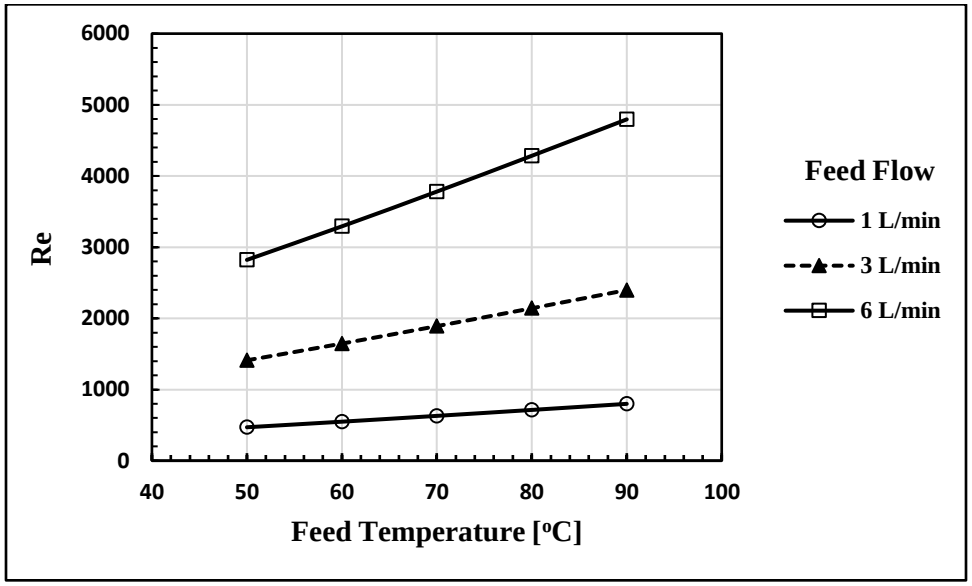

Figure 3.8: Effect of feed temperature on Reynolds number at different feed flow rates

Conditions: membrane PTFE 0.45 μm, coolant temperature of 20°C, feed salinity 140 mg/L, 4 mm gap width, and 2 L/min coolant flow rate.

Illustrated in Figure 3.9 is the influence of feed temperature on flux at different coolant flow rates. The output flux increases with increasing feed temperature for any value of coolant flow rate. The percentage increase in flux when the coolant flow rate is changed from 2 to 6 L/min is very low, and the maximum percentage change is observed at higher feed temperature and it is about 1.97 %. Therefore, increasing the coolant flow rate from 2 to 6 L/min has insignificant impact on the distillate flux.

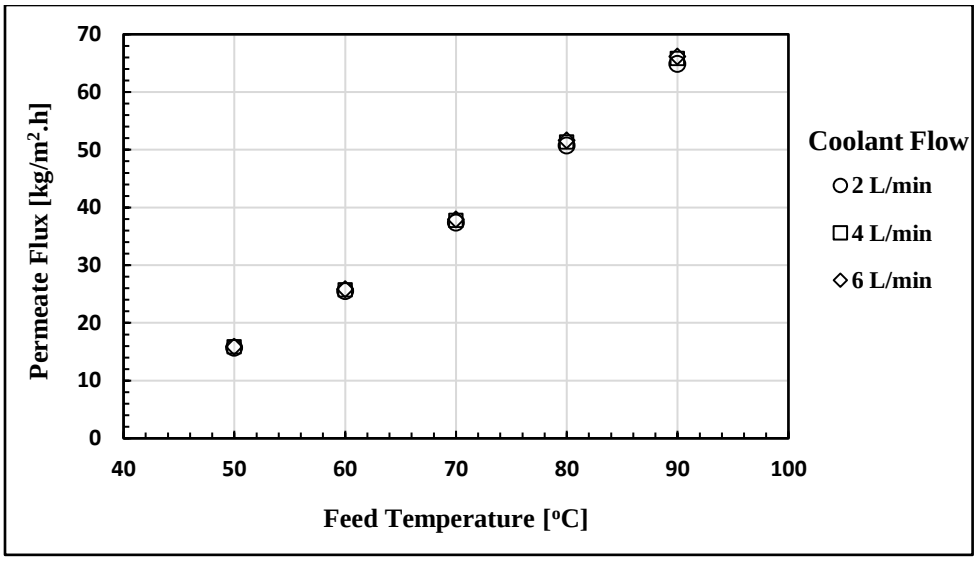

Figure 3.9: Effect of feed temperature on permeate flux at different coolant flow rates

Conditions: membrane PTFE 0.45 μm, coolant temperature of 20°C, feed salinity 140 mg/L, 4 mm gap width, and 1.5 L/min feed flow rate.

Figure 3.10 the effect of gap width on system output flux at different operating feed temperatures. Four different values of the gap width (2, 4, 6, and 8 mm) are used in order to investigate the influence of gap width on the flux, where the feed temperature is changed from 50 to 90°C. Increasing the gap width from 2 to 8 mm decreases the permeate flux at any feed temperature particularly at higher feed temperatures, because increasing the gap width means increasing the heat transfer resistance through the gap. The maximum percentage decrease in flux with increasing gap width is about 86.2 %, where the minimum value is 45.8 % at feed temperature of 50°C. So, the gap width effect decreases with decreasing the feed temperature.

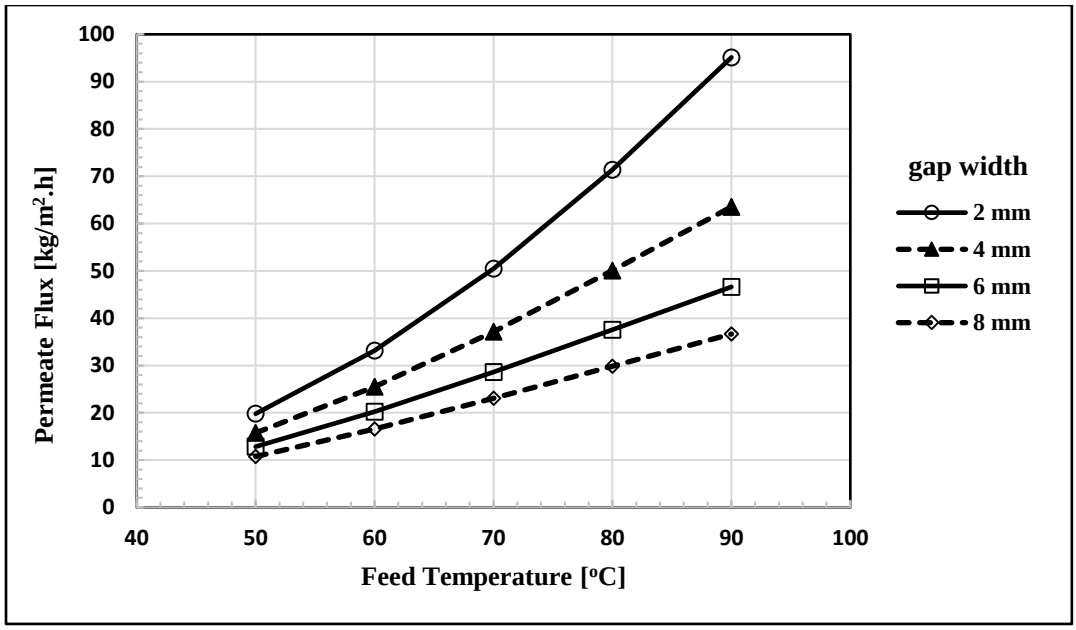

Figure 3.10: Effect of feed temperature on permeate flux at different gap thicknesses

Conditions: membrane PTFE 0.45 μm, coolant temperature of 20°C, feed salinity 140 mg/L, 2 L/min coolant flow rate, and 1.5 L/min feed flow rate.

3.4.2 Effect of coolant temperature

The effect of coolant temperature on distillate flux at different feed temperatures is shown in Figure 3.11. In this investigation, the coolant temperature changes from 5 to 25°C. The permeate flux Increases with decreasing the coolant temperature at a given feed temperature, because decreasing the coolant temperature increases the trans-membrane vapor pressure difference. The maximum percentage increase in permeate flux when the coolant temperature decreases from 25 to 5°C occurs at lower feed temperature (50°C) and it is about 50.3 %. Compared to feed temperature and gap width, the coolant temperature has less effect on the output flux.

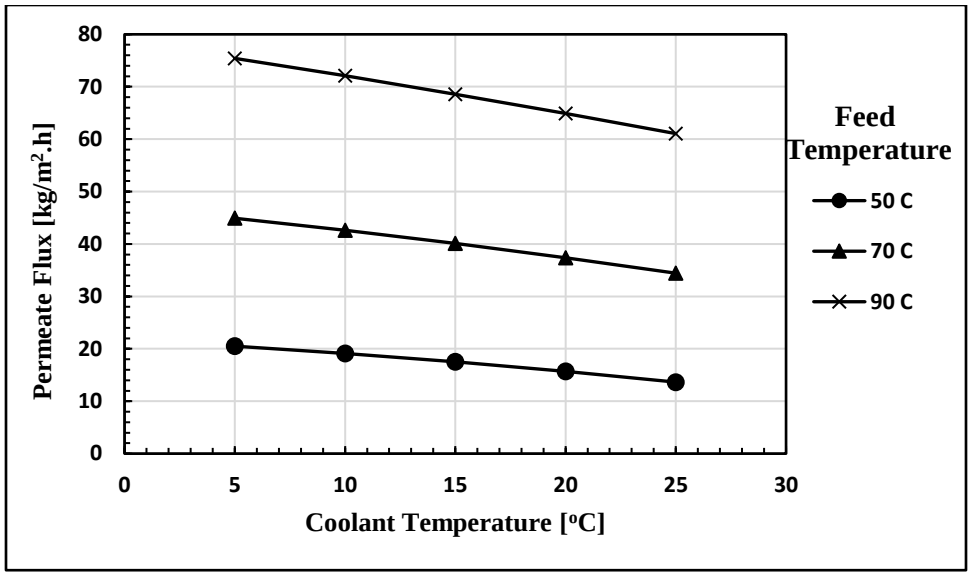

Figure 3.11: Effect of coolant temperature on permeate flux at different feed temperatures

Conditions: membrane PTFE 0.45 μm, 4 mm gap width, feed salinity 140 mg/L, 2 L/min coolant flow rate, and 1.5 L/min feed flow rate.

3.4.3 Effect of feed flow rate

The influence of feed flow rate on permeate flux at different coolant flow rates is shown in Figure 3.12. In this part, the feed flow rate is changed from 1 to 5 L/min at constant feed temperature of 70°C and 20°C coolant temperature where three different values for coolant flow rate are used. The percentage increase in permeate flux is calculated for increasing both feed and coolant flow rate. The percentage increase in flux varies from 24.42 % at low coolant flow rate to 25.12 % at high coolant flow rate when the feed flow rate is increased from 1 to 5 L/min, where it changes from 1.48 to 2.06 % when the coolant flow rate is changed from 2 to 6 L/min. That means the feed flow rate has a higher effect on permeate flux than the coolant flow rate.

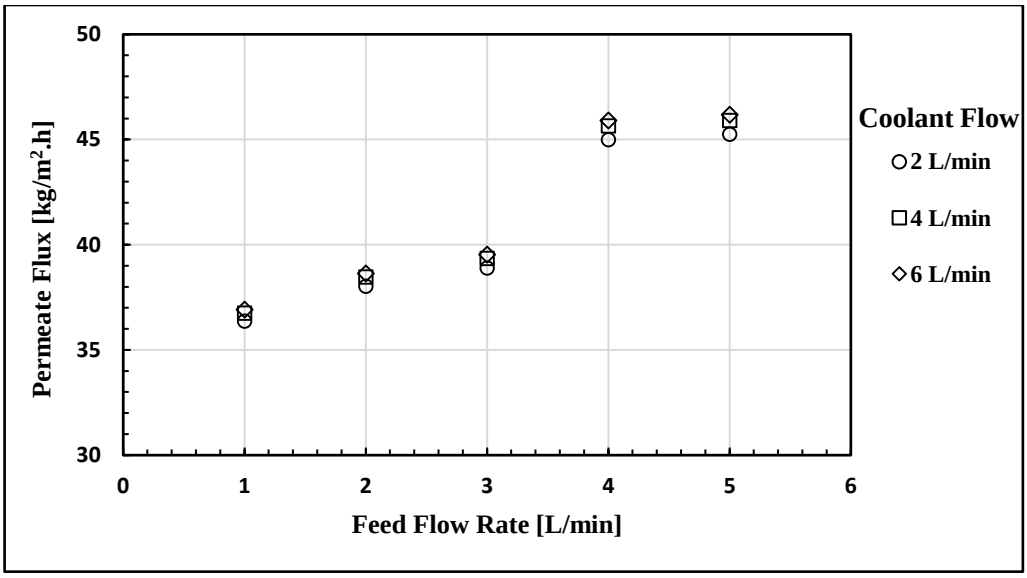

Figure 3.12: Effect of feed flow rate on permeate flux at different coolant flow rates

Conditions: membrane PTFE 0.45 μm, 4 mm gap width, feed salinity 140 mg/L, 20°C coolant temperature, and 70°C feed temperature.

3.4.4 Effect of feed concentration

Figure 3.13 represents the effect of feed concentration on permeate flux at different feed temperatures. Four different concentrations of the feed (0.14 g/L, 12 g/L, 30 g/L, and 100 g/L) are used to study the effect of salinity. On the other hand, three different feed temperatures (50°C, 70°C, and 90°C) are considered. The permeate flux decreases as the feed concentration increases, because as the feed concentration increases the salt precipitation on the membrane feed surface also increases and that prevents the passage of water vapor through the membrane. A drop of about 43.7 % in permeate flux is observed when the feed salinity increases from 0.14 to 100 g/L at a feed temperature of 50°C, and about 19.6 % at a feed temperature of 90°C. That means increasing the feed concentration has significant impact on flux at lower feed temperatures.

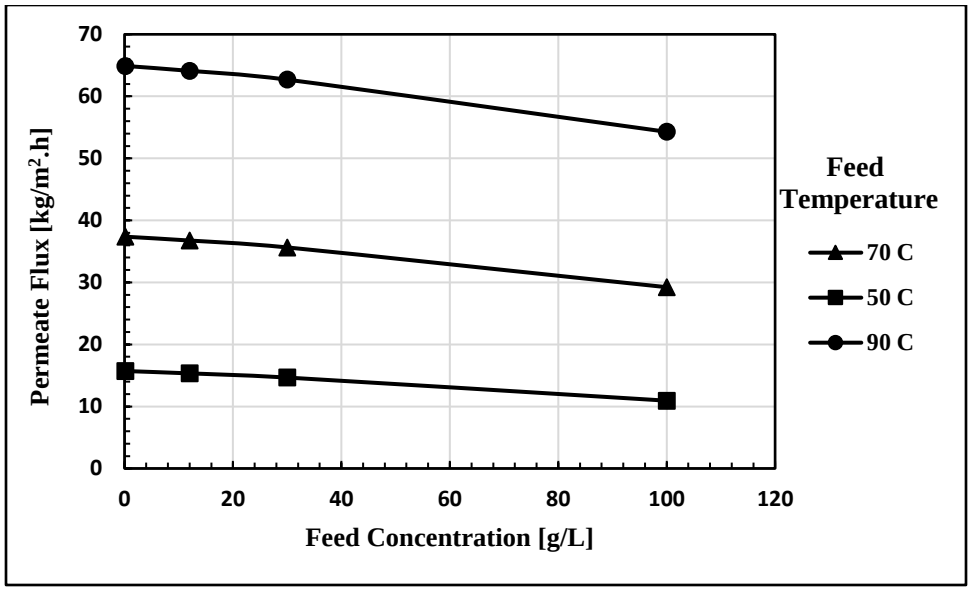

Figure 3.13: Effect of feed concentration on permeate flux at different feed temperatures

Conditions: membrane PTFE 0.45 μm, 4 mm gap width, feed flow rate of 1.5 L/min, coolant flow rate of 2 L/min, and 20°C coolant temperature.

3.5 Performance Measurements

3.5.1 Thermal (Evaporative) Efficiency

The evaporative efficiency is defined as the ratio of evaporative heat transfer (latent heat required to evaporate the water at the liquid/vapor interface in the feed side) to the total heat transfer to the membrane, and is given as [76]:

$$EE\ (\%) = (\frac{Q_v}{Q_{mem}})*100 \tag{3.35}$$

Where Q_{mem} and Q_v are given in equations 3.2 and 3.5, respectively. Figure 3.14 represents the effect of feed temperature on the thermal (evaporation) efficiency at different feed flow rates for the model under the following operating conditions: 20°C coolant temperature, 2

L/min coolant flow rate, 4 mm gap width, and 0.14 g/L feed concentration. The evaporation efficiency increases as the feed temperature increases, because of the enhancement in evaporation rate and vapor pressure. Increasing the feed temperature from 50 to 90°C increases the evaporation efficiency by a maximum of 21.4 %. Also, increasing the feed flow rate from 1.5 to 6 L/min increases the evaporation efficiency by a maximum of 2.8 %. Therefore, the evaporation efficiency is more sensitive to the feed temperature than feed flow rate.

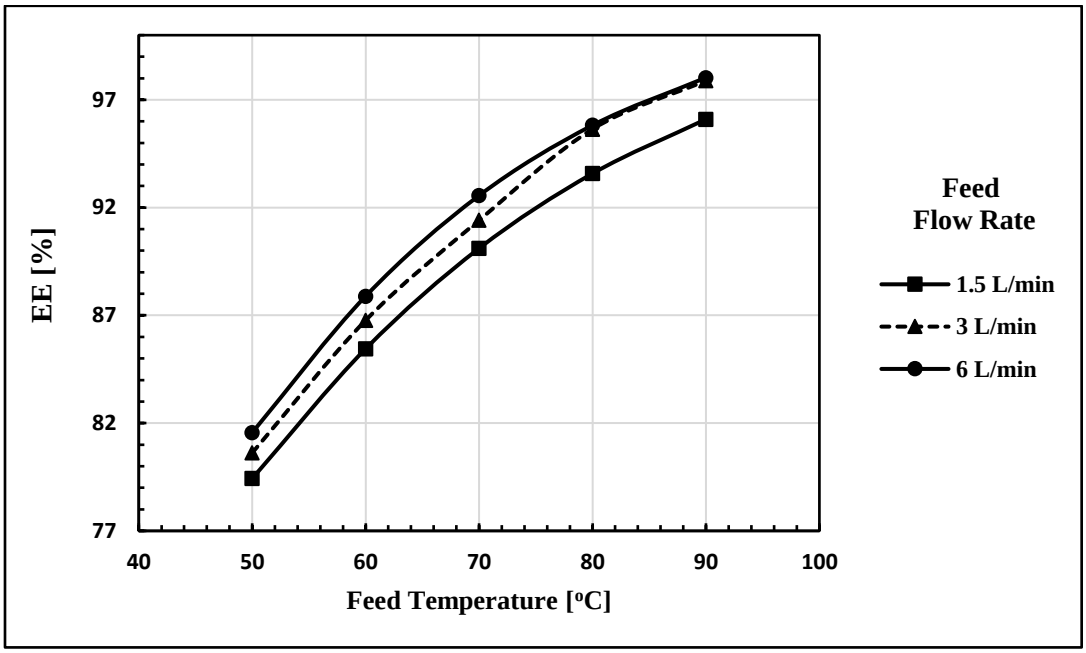

Figure 3.14: Effect of feed temperature on the evaporation efficiency

Conditions: membrane PTFE 0.45 μm, 4 mm gap width, feed salinity of 140 mg/L, coolant flow rate of 2 L/min, and 20°C coolant temperature.

3.5.2 Temperature Polarization

Temperature polarization, denoted by (θ), is considered as one of the disadvantage of membrane distillation. The temperature polarization coefficient is used as the baseline for

the energy efficiency. It is mainly used for measuring the ratio of the heat transfer resistance through the membrane to the total heat transfer resistance. Temperature polarization is the ratio of temperature difference across the membrane to temperature difference between bulk feed and bulk coolant streams. It can be expressed as:

$$\theta = \frac{T_{mf} - T_{ms}}{T_{bf} - T_{bc}} \tag{3.36}$$

Figure 3.15 shows the effect of feed temperature on the temperature polarization coefficient for the model under the following operating conditions, 20°C coolant temperature, 2 L/min coolant flow rate, 4 mm gap width, and 0.14 g/L feed concentration. The feed temperature is changed from 50°C to 90°C. The temperature polarization coefficient decreases as the feed temperature increases. In addition, the feed flow rate has insignificant effect on the temperature polarization coefficient. The higher value of the temperature polarization coefficient is achieved at feed temperature of 50°C and feed flow rate of 1.5 L/min which is about 0.38.

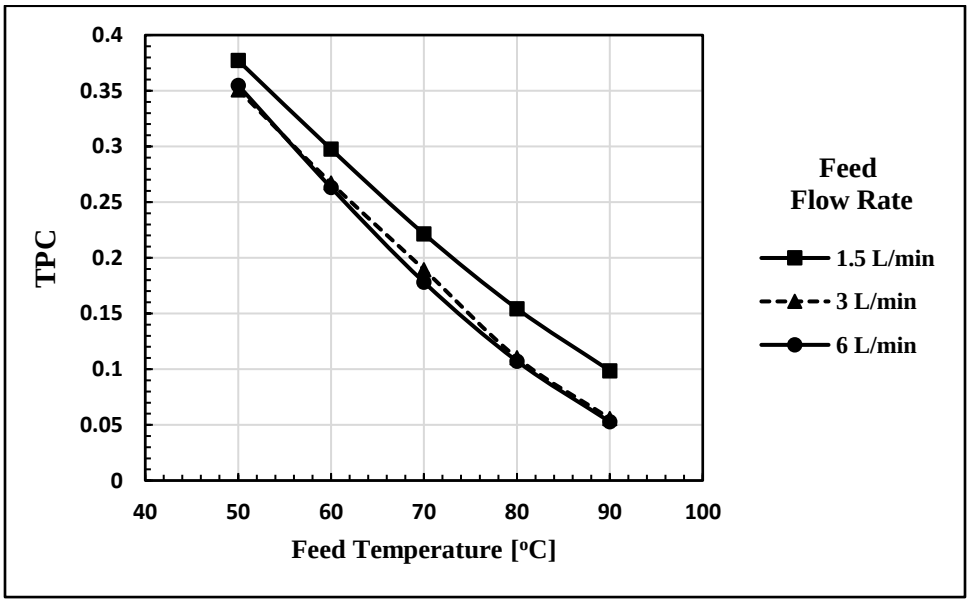

Figure 3.15: Effect of feed temperature on the temperature polarization coefficient

Conditions: membrane PTFE 0.45 μm, 4 mm gap width, feed salinity of 140 mg/L, coolant flow rate of 2 L/min, and 20°C coolant temperature.

3.5.3 Concentration Polarization

As the concentration of salts in feed stream is different from the concentration of salts at the feed membrane surface, another parameter 'concentration polarization coefficient' is defined as the ratio of concentration of salt at the feed surface of membrane to the concentration of salt in the bulk feed that can be given as [62]:

$$\beta = \frac{C_{mf}}{C_{bf}} \tag{3.37}$$

Where C_{mf} is the concentration at membrane feed surface and it is calculated as [45] [63]:

$$C_{mf} = C_{bf} * exp\ \left(\frac{J_w}{k_s * \rho_{bf}}\right) \tag{3.38}$$

Where, ρ_{bf} is the density of bulk feed and k_s is the mass transfer coefficient through the concentration boundary layer in the feed side and can be calculated as:

$$k_s = Sh * \frac{D_e}{D_h} \quad \text{and} \quad D_e = \frac{1}{R_{MD}} \tag{3.39}$$

Where D_e is the diffusion coefficient, D_h is hydraulic diameter of feed channel and Sh is the dimensionless Sherwood number. Sherwood number represents the ratio of diffusive to convective mass transfer. Sherwood Number is a function of Schmidt number and Reynolds number [45]. For Laminar Flow Sherwood number is given as [63] [64] which is Graetz–Lévêque equation:

$$Sh = 1.86 * \left(Re * Sc * \frac{D_h}{L}\right)^{1/3} \tag{3.40}$$

Where L is the channel length, D_h is the hydraulic diameter, and Sc is Schmidt number which is the ratio of momentum to the mass diffusivity and can be written as [63]:

$$Sc = \frac{\mu_{mf}}{D_e * \rho_{bf}} \tag{3.41}$$

For Turbulent Flow Sherwood number is calculated by using Dittus–Boelter equation [63]:

$$Sh = 0.023 * Re_f^{0.8} * Sc^{0.33} \tag{3.42}$$

Figure 3.16 shows the effect of feed temperature on the concentration polarization coefficient at different feed flow rates for the model under the following operating conditions, 20^{o}C coolant temperature, 2 L/min coolant flow rate, 4 mm gap width, and 0.14 g/L feed concentration. The feed temperature is changed from 50^{o}C to 90^{o}C while three feed flow rates (1.5, 3, and 6 L/min) are used. The concentration polarization coefficient increases as the feed temperature increases where it decreases as the feed flow rate increases. The maximum value of the concentration polarization coefficient is achieved at feed temperature of 90^{o}C and feed flow rate of 1.5 L/min and it is about 1.024.

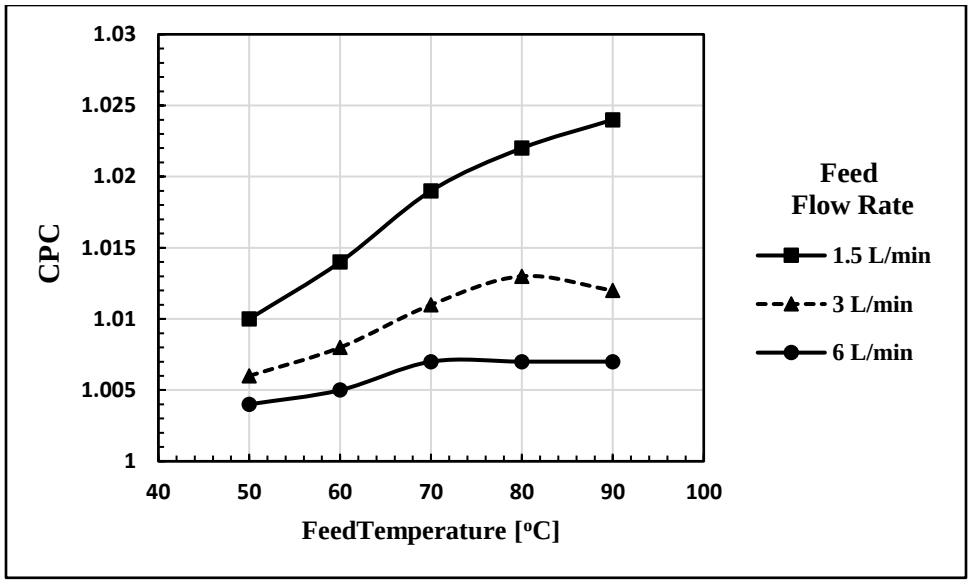

Figure 3.16: Effect of feed temperature on the concentration polarization coefficient

Conditions: membrane PTFE 0.45 μm, 4 mm gap width, feed salinity of 140 mg/L, coolant flow rate of 2 L/min, and 20°C coolant temperature.

3.5.4 Gain Output Ratio (GOR)

The gain output ratio (GOR) represent the ratio between the energy used to produce the permeate (evaporation) to the energy consumed by the MD system. GOR is defined as:

$$GOR = \left(\frac{J_w * \Delta H_v}{Q_{in}}\right) * A_m \tag{3.43}$$

Where J_w is the permeate flux, ΔH_v is enthalpy of vaporization of water, A_m is the effective membrane Area, and Q_{in} is the total heat supply to the MD module and it can be expressed as:

$$Q_{in} = m^{\cdot}_f * Cp_f * \left(T_{f,in} - T_{f,out}\right) \tag{3.44}$$

Where $m^{\cdot}_f$ is the mass flow rate of the feed water, Cp_f is the specific heat capacity of the feed water, while $T_{f,in}$ and $T_{f,out}$ are the bulk feed inlet and outlet temperatures, respectively.

Another expression that can be used to calculate the total heat supply to the system as:

$$Q_{in} = Q_{mem} + Q_{loss} \tag{3.45}$$

Where Q_{loss} is the heat loss from MD module to the surrounding, and can be written as:

$$Q_{loss} = \left(\frac{k_{\text{module}}}{\delta_{\text{module}}}\right) * \left(T_{bf} - T_{amb}\right) * \mathrm{A}_{f} \tag{3.46}$$

Where k_{module} and δ_{module} are thermal conductivity and thickness of the module material respectively. T_{amb} is the ambient temperature.

Figure 3.17 shows the effect of feed temperature on the gain output ratio (GOR) at different feed flow rates for the model under the following operating conditions, 20^{o}C coolant temperature, 2 L/min coolant flow rate, 4 mm gap width, and 0.14 g/L feed concentration. The Gain Output Ratio increases with increasing both feed temperature and feed flow rate. Because increasing the feed temperature increases the evaporation rate while increasing the feed flow rate enhances the turbulence level, and that leads to higher values of the heat and mass transfer coefficients in the feed side of membrane and that leads to higher values of permeate flux and higher GOR as well.

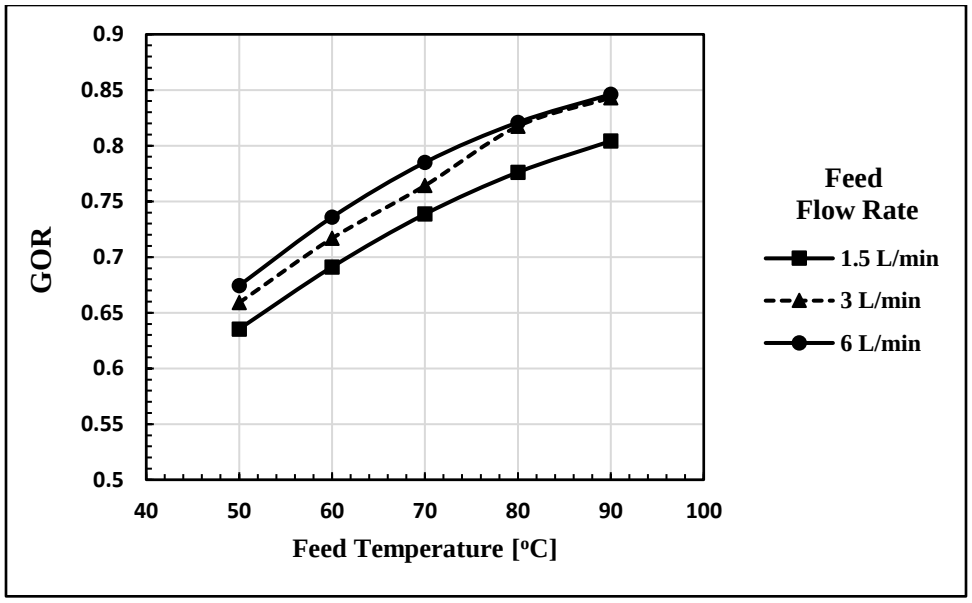

Figure 3.17: Effect of feed temperature on the gain output ratio (GOR)

Conditions: membrane PTFE 0.45 μm, 4 mm gap width, feed salinity of 140 mg/L, coolant flow rate of 2 L/min, and 20°C coolant temperature.

CHAPTER 4

EXPERIMENTAL SETUP

In this chapter the experimental setup of the multistage water gap and the multistage air gap membrane distillation systems are presented by describing the materials and components of each design, assembling the module, the instrumentation used in the experiments, and assembling the multistage system. This chapter also illustrates different type of connections (parallel, series, and mixed) for the multistage air gap membrane distillation, and the multistage water gap membrane distillation systems and the working principle for each type. The objectives and methodology of experiments are outlined as well.

4.1 System description

The layout of multistage MD system is illustrated in Figure 4.1. The system consists of two water closed cycles, hot and cold, connected to each of the MD modules (stages). An electric heater is used to deliver constant temperature and constant flow rate for the feed water (Figure 4.2.a). A water chiller operated by a controlled head is used to deliver constant temperature and constant flow rate for the coolant stream (Figure 4.2.b).

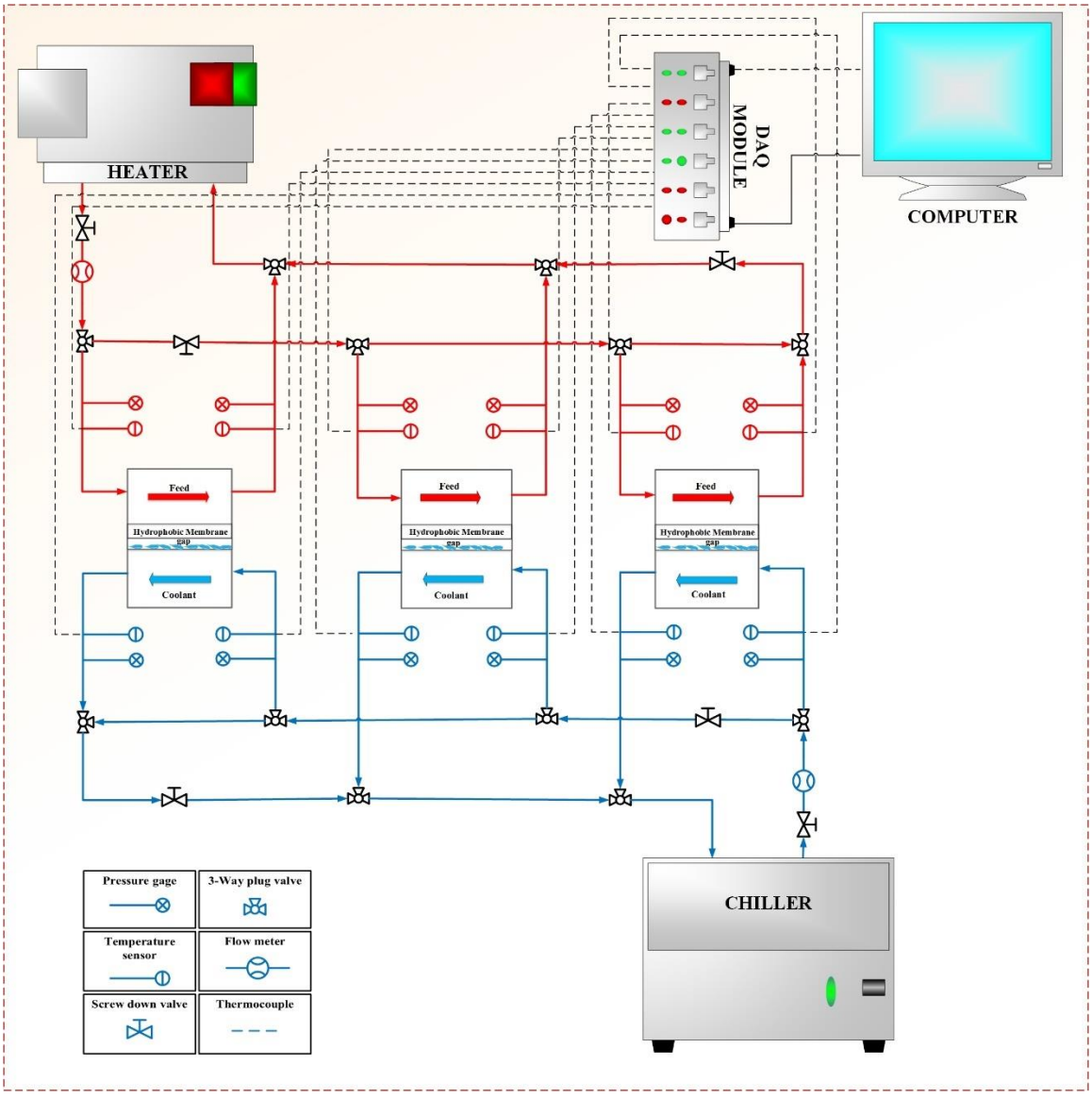

Figure 4.1: The layout of the system

The cold-water cycle pipelines are made of Poly-Vinyl Chloride (PVC) pipes, on the other hand the hot water cycle pipelines are made of Chlorinated Poly-Vinyl Chloride (CPVC) which is significantly more flexible and can withstand higher temperatures (more than 90^{o}C) than the Poly-Vinyl Chloride (PVC) pipes. Each cycle has some valves in order to control the water flow rate and to change the flow arrangement from series to parallel. The complete setup is shown in Figure 4.3.

(a) The electric heater

(b) The electric chiller

Figure 4.2: The electric heater and chiller

Figure 4.3: The experimental setup

4.2 Module design

The multistage system consists of three MD modules. The modules are fabricated from 2 High-Density-Poly-ethylene (HDPE) sheets with total dimensions of 200 mm width, 225 mm length, and 30 mm thickness. One chamber is used for hot feed water stream and another one is used for cooling water stream. Each chamber has two headers for inlet and outlet water flow, and two rectangular flow channel with 60 mm width, 120 mm length, and 5 mm depth as shown in Figure 4.4.a and Figure 4.4.b. In this system, the separation process occurs by the transfer of the water vapor through the membrane that is fitted inside the module, a perforated brass plate with 1.5 mm thickness is used to support the membrane as shown in figure 4.4.c. In order to prevent external and internal leakage, a rubber sheet

with 2 mm thickness is used as gasket. Due to the vapor pressure difference across the membrane, the vapor permeates across the membrane to the cold side and condenses inside each MD module on a condensation brass plate with 1.5 mm thickness as shown in figure 4.4.d.

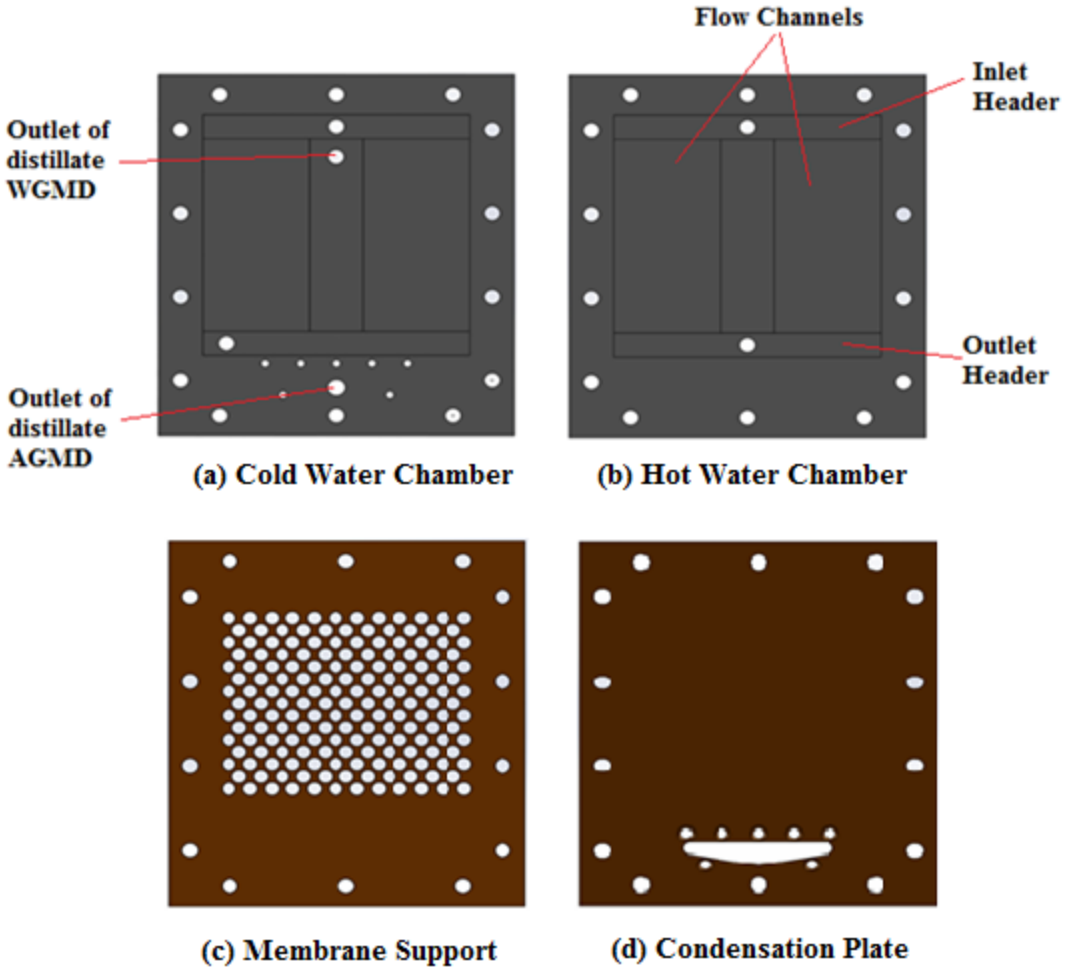

Figure 4.4: MD module components

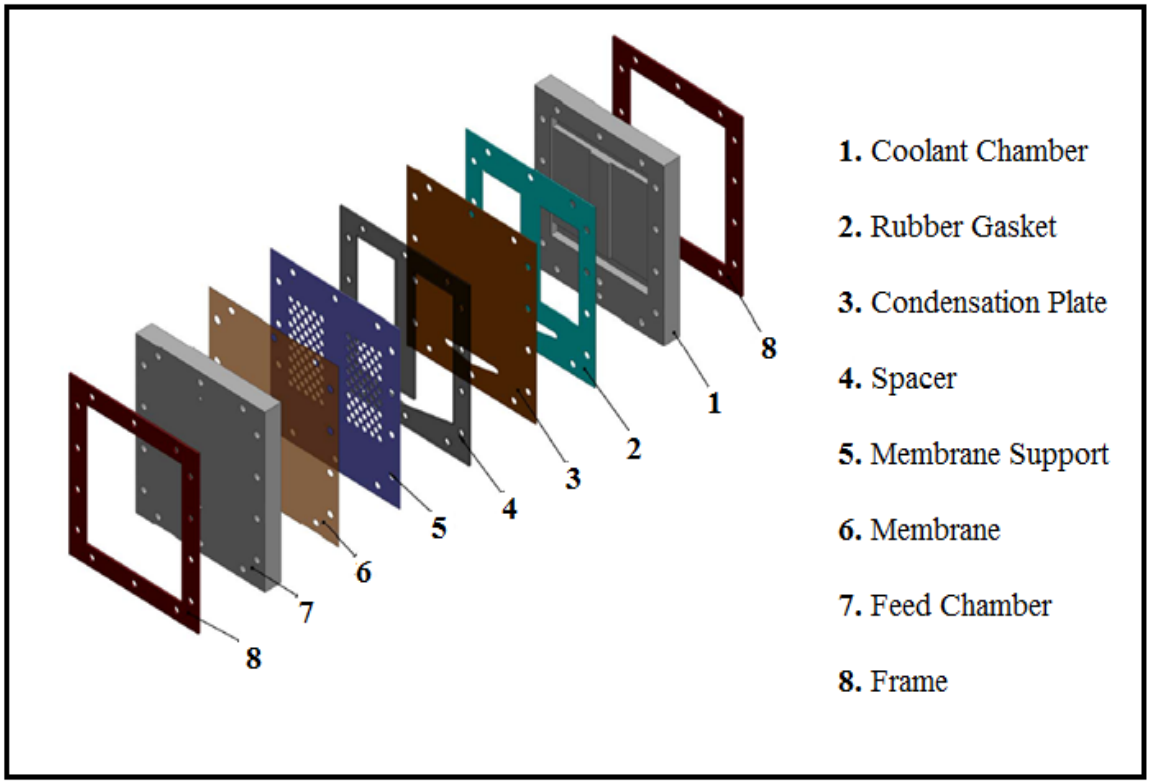

Figure 4.5: Assembly of the MD module

4.3 Membrane characterization

Most hydrophobic membranes are made of poly-ethylene (PE), poly-propylene (PP), poly-vinylidene-fluoride (PVDF), and poly-tetra-fluoroethylene (PTFE). In general, the membrane used in the MD process should have lower mass transfer resistance and lower thermal conductivity to avoid heat loss through the membrane. Furthermore, the membrane should have higher resistance to chemicals and high thermal stability with higher temperatures [28]. The commercial membrane used in this work is poly-tetra-fluoroethylene (PTFE) with pore size of 0.45 μm as in Table 4.1.

Table 4.1: Membrane Characterization

Thickness of active layer (μm)	6.9 ± 2.0
Thickness of support layer (μm)	141.4 ± 15.8
Total membrane thickness (μm)	153.9 ± 13.6
D_p (μm)	0.45
ε (%)	79.7 ± 8.7
θ (º) active layer	139.0 ± 2.8
θ (º) support layer	119.3 ± 1.0

4.4 Measuring Devices and Instrumentations

For measurements purposes, a turbine flow meter (OMEGA Type) is employed to measure the coolant flow rate (Figure 4.6). Rotameter (OMEGA FL 50000) is employed to measure feed flow rate (Figure 4.6). A conductivity meter is used to measure salinity of feed, coolant, and permeate water (Figure 4.6). The temperatures and pressures of the feed and coolant streams are measured by connecting thermocouples and pressure gages at the inlet and the exit of each MD module. In addition, a LabVIEW code is developed and the thermocouples are connected to data acquisition system to record temperature readings at inlet and exit of each module. By collecting a volume (or mass) of distilled water from the MD system, and measuring the time for sample collection, the permeate flux can be calculated for the effective area of membrane. In addition, the salt rejection factor can be calculated by measuring the salinity (concentration) of the feed and the permeate.

Figure 4.6: Measuring Devices and Instrumentations

4.5 System Operation

The feed water is heated up by the heater and pumped to the inlet of the MD module. The feed water comes into the MD module through the header and then enters the flow channels. After the passage through the channel, it is collected again into the outlet header, then it comes out of the MD module after vapor production. After the feed water exits from the last stage MD module, it returns to the feed bath for reheating and recirculation. The cold water is pumped from the chiller to the inlet of the coolant chamber in MD module. The cold water comes into the MD module through the header and then disseminated into the cold-water channels to cool down the condensation plate and it passes through the coolant channels to the outlet header, to the exit of the MD module. After the cold water leaves the last stage MD module, it returns to the coolant bath for cooling and recirculation. The temperatures of the feed and coolant streams are measured by connecting thermocouples at the inlet and the exit of each of the three MD modules. Also, flow meters are utilized to measure the flow rate of feed and coolant streams.

In case of air gap, vapor permeated through the membrane pores is condensed on the condensation plate surface and collected from a lower portion in the gap. In case of water gap, vapor permeated through the membrane pores and condenses inside the gap directly and taken from a bore in the upper of the gap. By collecting a volume of distilled water from the MD system at specific time period, the permeate flux can be calculated.

4.6 System Flow Arrangements

In this part four different flow arrangements for feed and coolant streams are experimentally investigated as follows:

4.6.1 Parallel flow arrangement

In parallel flow arrangement (Figure 4.7), the feed water is pumped from the heated feed bath to each of the MD modules in parallel, at the same temperature. The feed water exits from each MD module, it returns to the feed bath for reheating and recirculation. On the other hand, the cold water is pumped from the chiller to enter each MD module in parallel, at the same temperature.

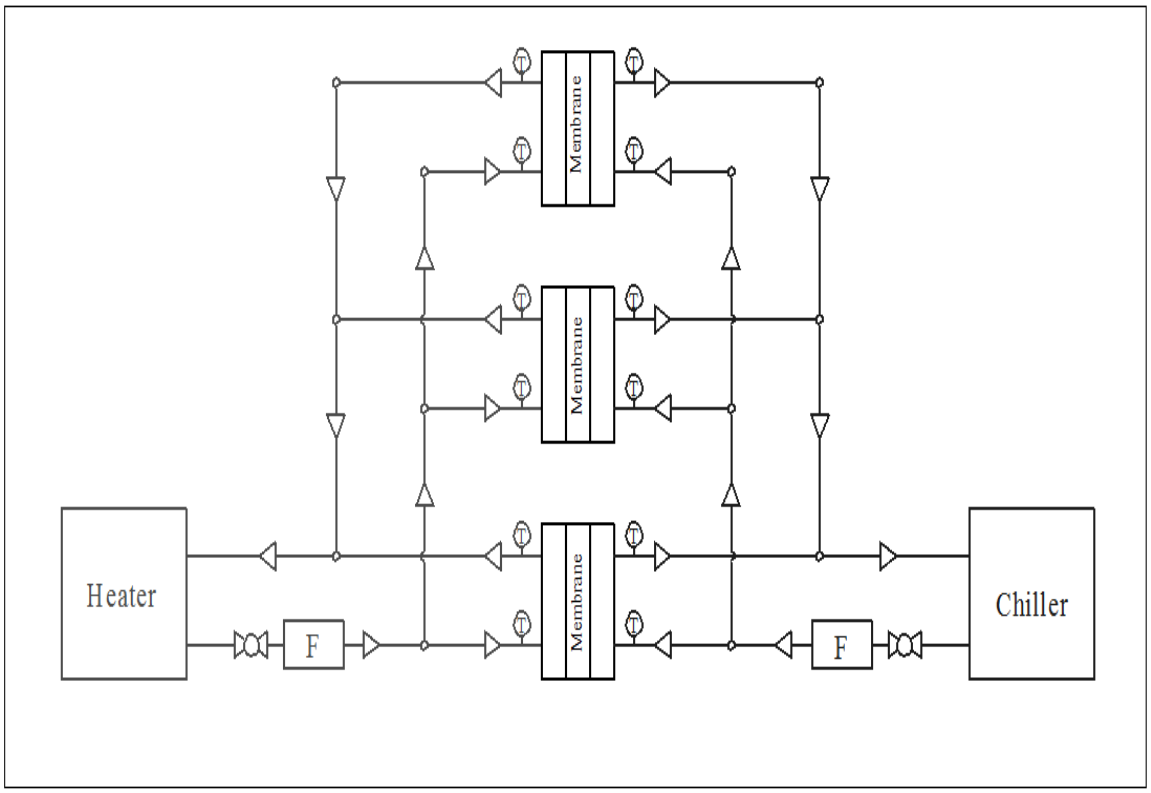

Figure 4.7: Parallel flow arrangement

4.6.2 Series flow arrangement

In series flow arrangement (Figure 4.8), the feed water is pumped from the heater to the feed bath and then enters the feed chamber of the first module. The water comes out from the first module enters the second MD module through the module header. After the feed water exits from the feed chamber of the last module, it returns to the feed bath for reheating and recirculation. The cold water is pumped from the chiller to the inlet of the coolant chamber in the first MD module. The water comes out from the first module enters the second MD module. After the cold water leaves the coolant chamber of the last module, it returns to the coolant bath for cooling and recirculation.

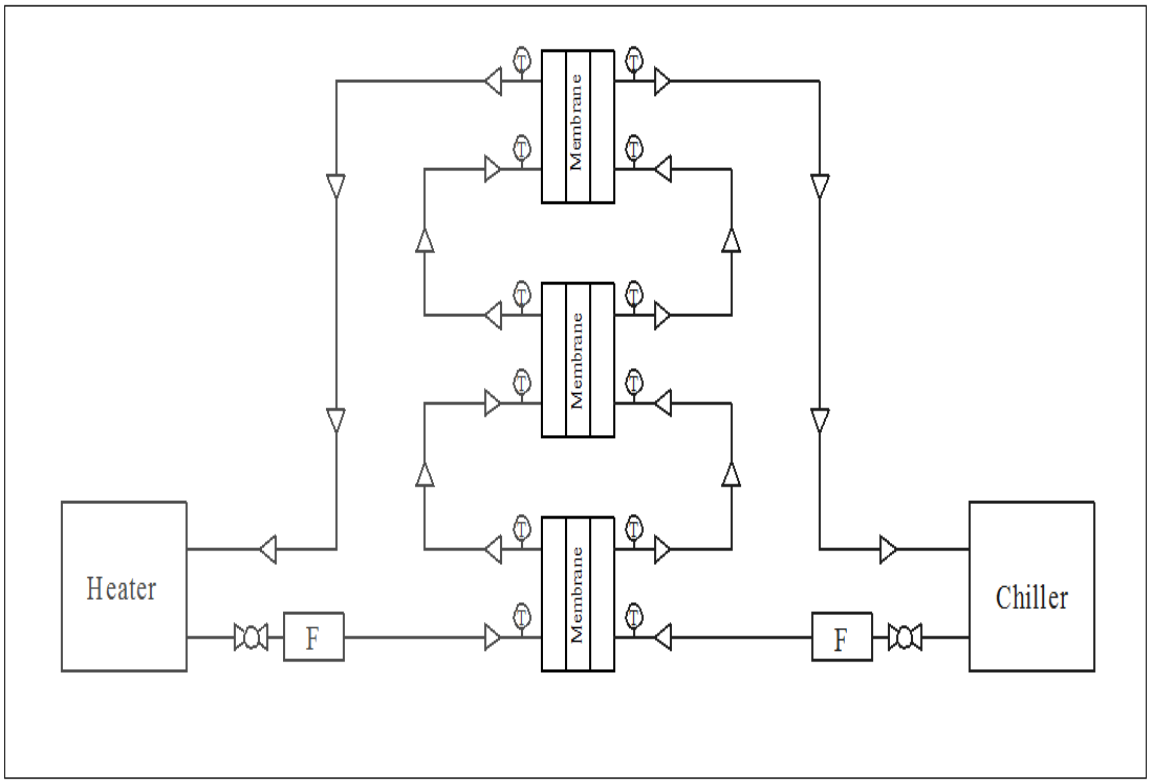

Figure 4.8: Series flow arrangement

4.6.3 Mixed flow arrangement

In this case, there are two types of connections as the following:

4.6.3.1 Parallel feed connection - series coolant connection

In parallel feed-series coolant flow arrangement (Figure 4.9-a), the feed water is pumped from the heater to the feed bath and then enters all the three MD modules in parallel, at the same temperature. The feed water exits from each MD module, it returns to the feed bath for reheating and recirculation. On the other hand, the cold water is pumped from the chiller to the inlet of the coolant chamber in the first MD module. The water comes out from the first module enters the second MD module. After the cold water leaves the coolant chamber of the last module, it returns to the coolant bath for cooling and recirculation.

4.6.3.2 Series feed connection - parallel coolant connection

In parallel feed-series coolant flow arrangement (Figure 4.9-b), the feed water is pumped from the heater to the feed bath and then enters the feed chamber of the first module. The water comes out from the first module enters the second MD module. After the feed water exits from the feed chamber of the last module, it returns to the feed bath for reheating and recirculation. For the coolant side, the cold water is pumped from the chiller to the coolant bath and then enter all the three MD modules in parallel, at the same temperature.

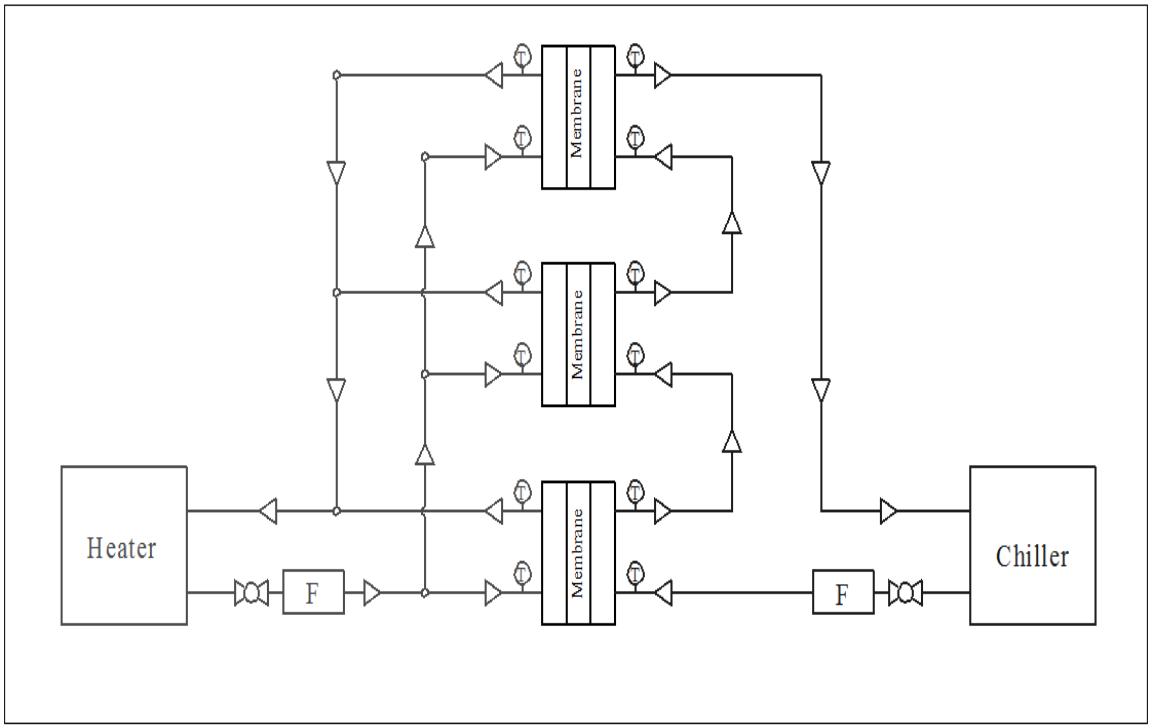

(a) Parallel feed connection - series coolant connection

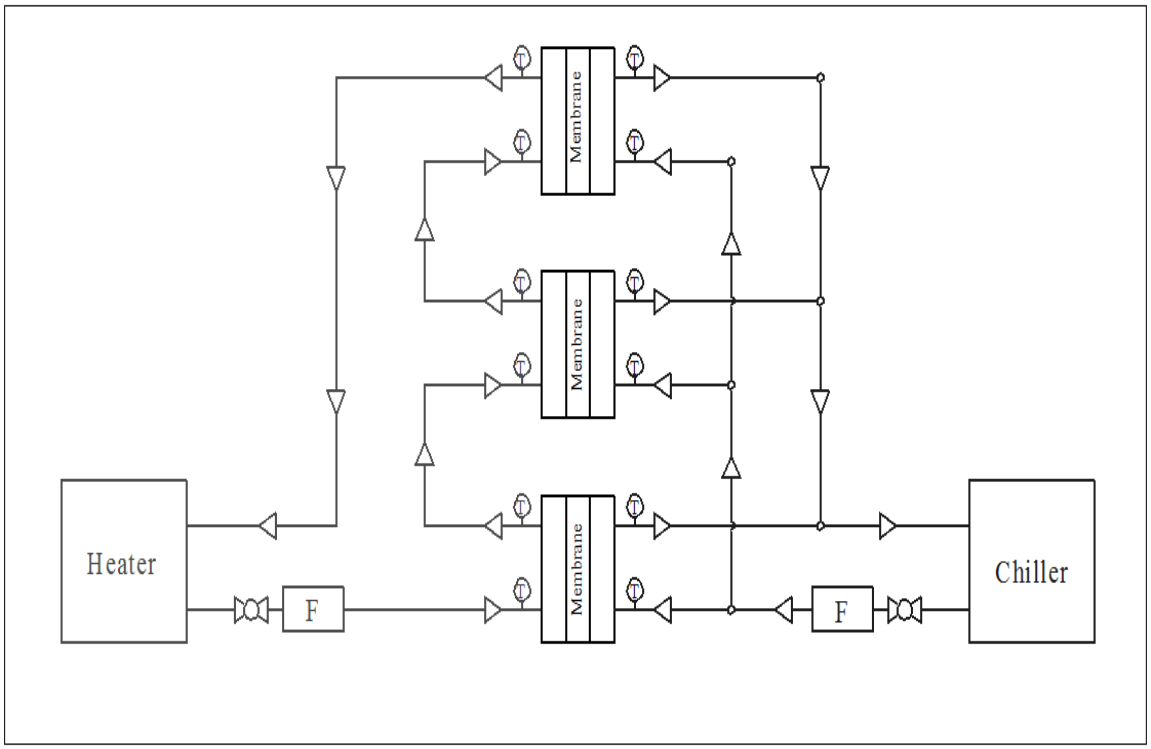

(b) Series feed connection - parallel coolant connection

Figure 4.9: Mixed flow arrangement

4.7 Experimental work plan

A parametric study on different operating variables is carried out to study the effect of these variables on the permeate flux. This is done by varying one operating variable while keeping the others constant. The investigated operating parameters are the feed flow rate, feed temperature, coolant flow rate, coolant temperature, and feed concentration. The effect of changing the arrangement on permeate flux is also investigated. The experimental work plan is shown in Table 4.2.

Table 4.2: Experimental work plan

No	Variable	Range
1	Feed Temperature	50 ^{o}C – 90 ^{o}C
2	Coolant Temperature	10 ^{o}C - 25 ^{o}C
3	Flow Rate of Feed (Parallel)	5 L/min - 7 L/min
4	Flow Rate of Feed (Series)	1.3 L/min – 3.3 L/min
5	Flow Rate of Coolant (Parallel)	5 L/min - 7 L/min
6	Flow Rate of Coolant (Series)	1.3 L/min – 3.3 L/min
7	Gap width	2mm, 4 mm, and 8 mm
8	Feed Concentration	0.15 g/L, 3 g/L, and 35 g/L

CHAPTER 5

RESULTS AND DISCUSSION

In this chapter the effect of operating conditions such as feed temperature, coolant temperature, feed flow rate, coolant flow rate, gap width, and feed concentration on the permeate flux for multistage air gap membrane distillation system and multi-stage water gap membrane distillation system are presented and discussed for different flow arrangements (parallel, series, and mixed).

5.1 Effect of feed temperature

The effect of feed temperature on permeate flux (Figure 5.1) is investigated for multistage air gap and multi-stage water gap membrane distillation systems with parallel and series flow arrangements. The feed temperature is changed from 50^{o}C to 90^{o}C with 10^{o}C increment. The variation of permeate flux with feed temperature is measured at constant coolant temperature of 20^{o}C, 4 mm gap width, and 150 mg/L feed concentration. The feed flow rate is 7 L/min (the total flow rate for the three modules such that each module receives 2.3 L/min) in case of parallel flow arrangement, and 2.3 L/min for series flow arrangement, the coolant flow rate is also 7 L/min (total flow rate for the three modules such that each module receives 2.3 L/min) in case of parallel flow arrangement, and 2.3 L/min for series flow arrangement. The output flux of the multistage system is also compared with that for a single stage system and the permeate flux ratio for both processes is calculated as well.

Figure 5.1 shows the variation of permeate flux with feed temperature for MS-AGMD and MS-WGMD systems with parallel and series flow arrangements. It is clear that the permeate flux increases with increasing the feed temperature for both systems because increasing the feed temperature increases the evaporation rate in the feed side and increases the vapor pressure difference across the membrane. The permeate flux for parallel flow arrangement is slightly higher than that for the series one. The higher value of the system permeate flux (total permeate flux from three modules) is achieved at feed temperature of 90^{o}C, and it is about:

- 96.43 kg/m^2.h for multistage air gap membrane distillation system with parallel flow arrangement.
- 197.76 kg/m^2.h for multistage water gap membrane distillation system with parallel flow arrangement.
- 83.7 kg/m^2.h for multistage air gap membrane distillation system with series flow arrangement.
- 167.82 kg/m^2.h for multistage water gap membrane distillation system with series flow arrangement.

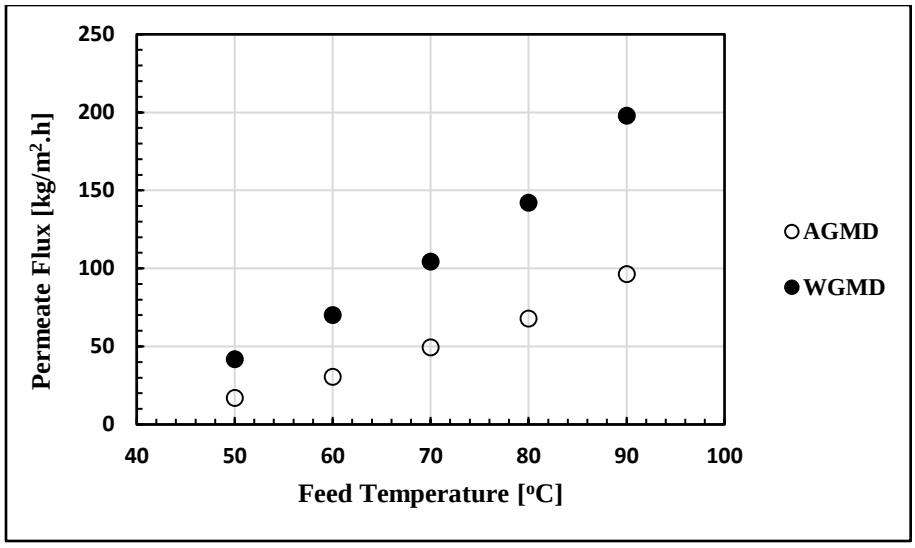

(a) Effect of feed temperature on the permeate flux for parallel AGMD & parallel WGMD

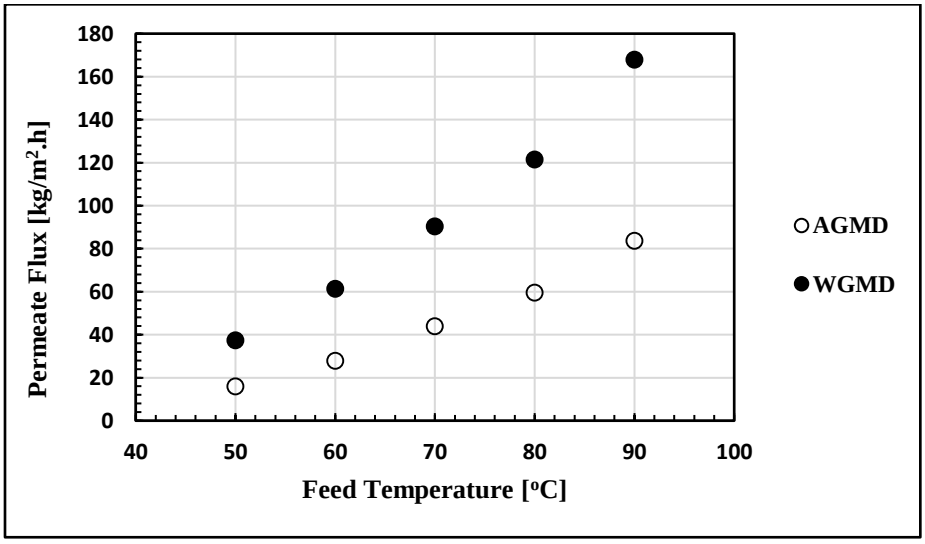

(b) Effect of feed temperature on the permeate flux for series AGMD & series WGMD

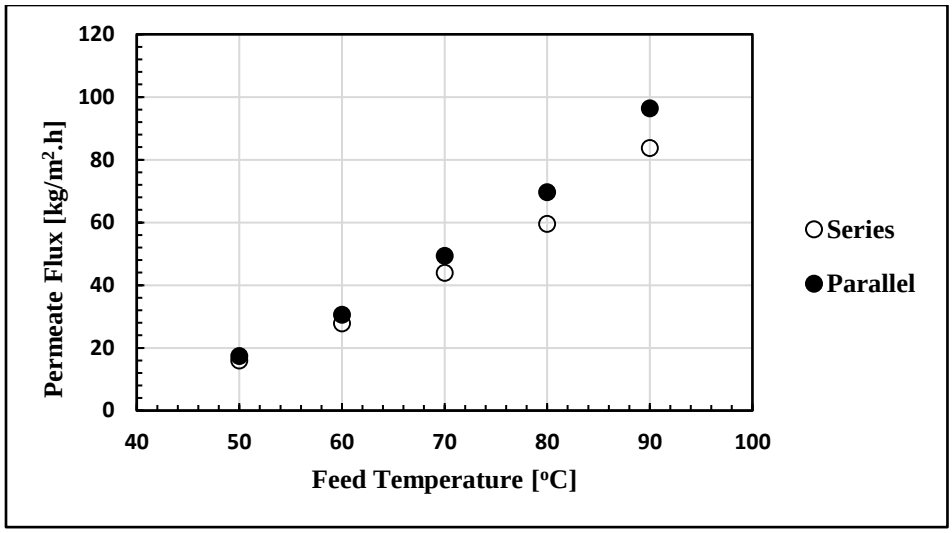

(c) Effect of feed temperature on the permeate flux for parallel & series AGMD system

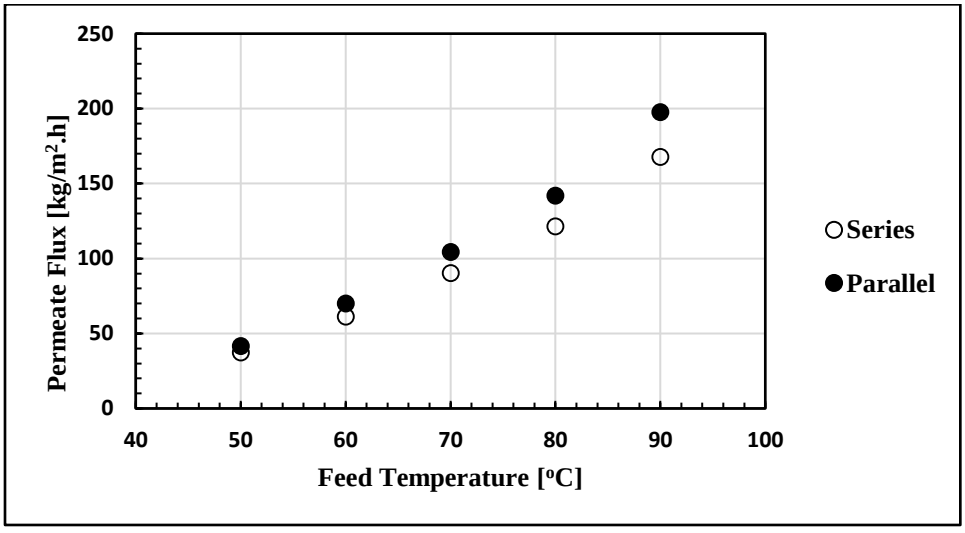

(d) Effect of feed temperature on the permeate flux for parallel & series WGMD system

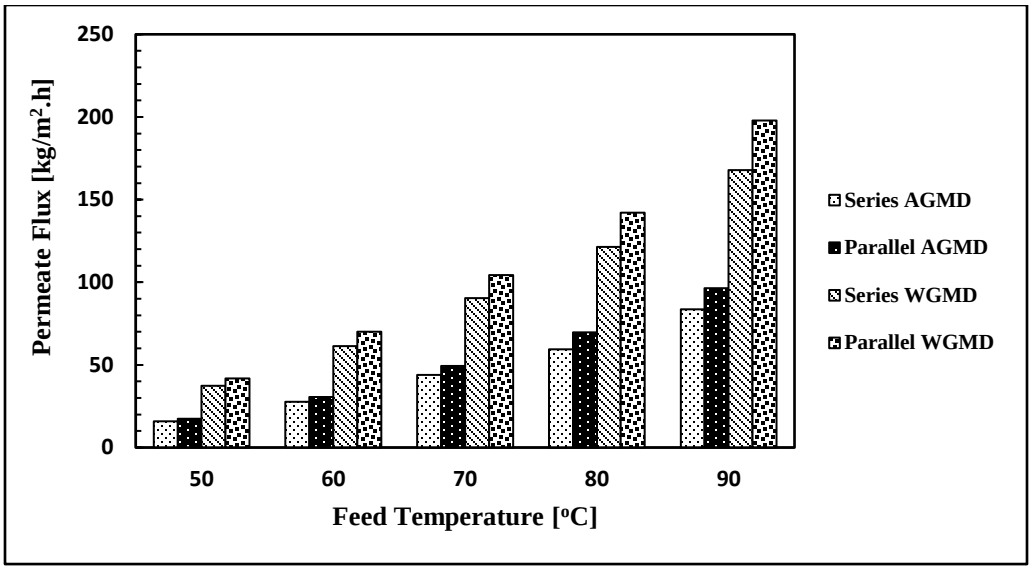

(e) Effect of feed temperature on the permeate flux for parallel and series AGMD & WGMD

Figure 5.1: Effect of feed temperature on permeate flux for multistage MD systems

Conditions: membrane PTFE 0.45 μm, coolant temperature 20°C, feed salinity 150 mg/L, 4 mm gap width, feed and coolant flow rates of 2.3 L/min for each module.

From Figure 5.1 it can be clearly seen that, the output flux for water gap system is higher than that for air gap design because the water has higher heat capacity than air and that reduces the mass transfer resistance in the gap in case of WGMD. So, the ratio of the water gap to air gap permeate flux is calculated at different feed temperatures as illustrated in Figure 5.2. The ratio of the water gap flux to air gap flux varies from 2.05 to 2.45 for parallel arrangement, and from 2.005 to 2.33 in case of series connection.

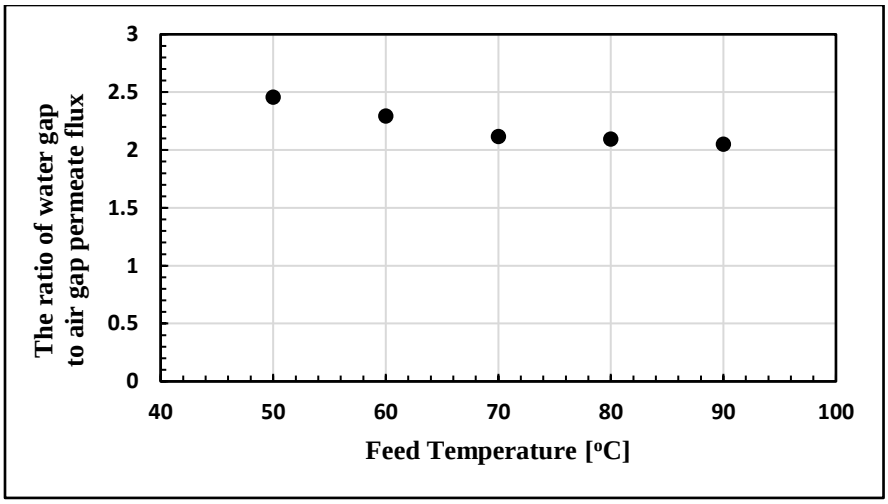

(a) The ratio of water gap to air gap permeate flux for parallel arrangement

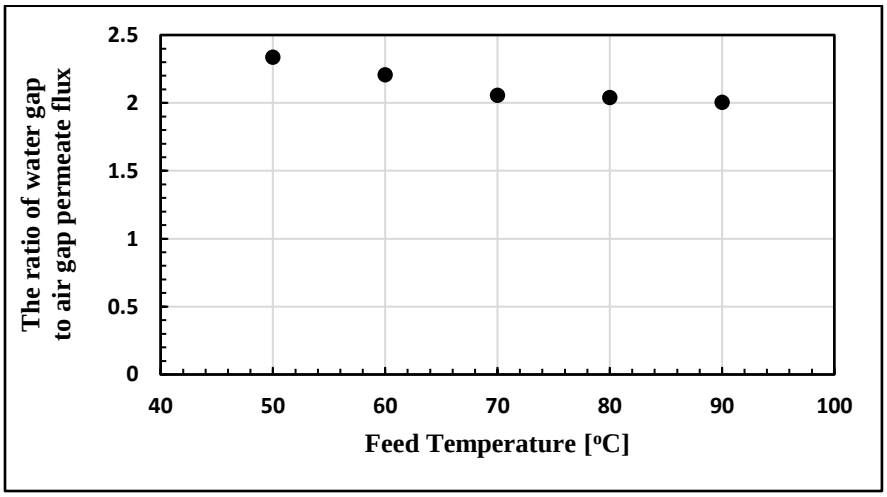

(b) The ratio of water gap to air gap permeate flux for series arrangement

Figure 5.2: The ratio of water gap to air gap permeate flux

Conditions: membrane PTFE 0.45 μm, coolant temperature 20°C, feed salinity 150 mg/L, 4 mm gap width, feed and coolant flow rates of 2.3 L/min for each module.

The stage permeate flux is illustrated in Figure 5.3. In case of parallel flow arrangement for both water gap and air gap systems, the feed water and coolant water enter each of MD modules in parallel, at the same temperature and flow rate. Therefore, the three MD

modules produced almost the same output flux. In case of series flow arrangement, the water comes out from one stage is used as inlet to the next stage. Therefore, the three MD modules are not operating at the same temperature and hence produce different output fluxes.

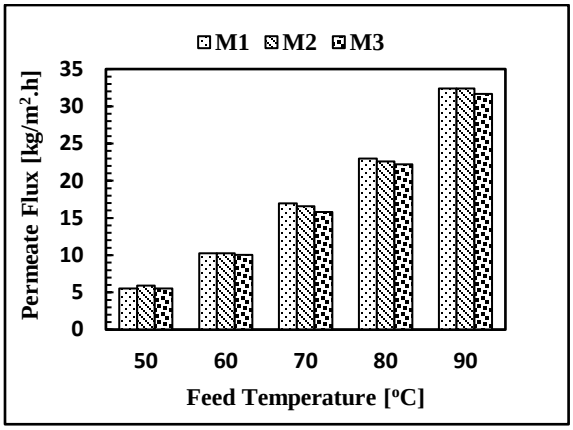

(a) Stage permeate flux for parallel-AGMD

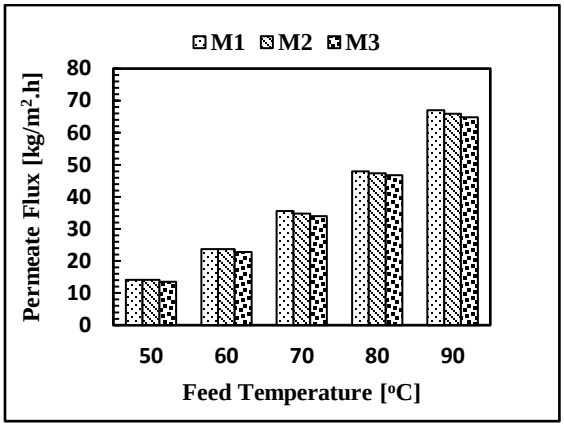

(b) Stage permeate flux for parallel-WGMD

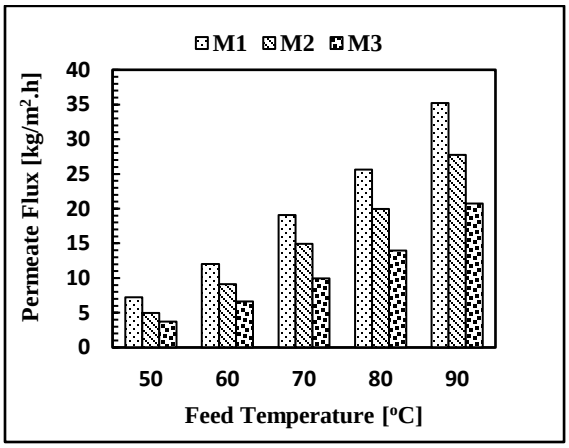

(c) Stage permeate flux for series-AGMD

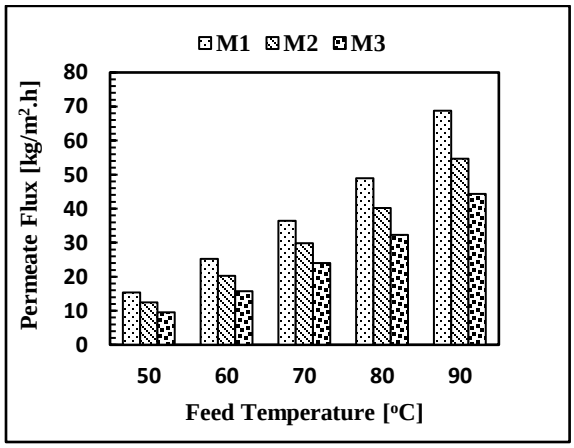

(d) Stage permeate flux for series-WGMD

Figure 5.3: Stage permeate flux for air gap and water gap systems

Conditions: membrane PTFE 0.45 μm, coolant temperature 20°C, feed salinity 150 mg/L, 4 mm gap width, feed and coolant flow rates of 2.3 L/min for each module.

In order to see the effect of changing the flow arrangement on permeate flux, the percentage increase in flux when the flow arrangement is changed from series to parallel is calculated as shown in Figure 5.4. Because of decreasing feed temperature and increasing coolant temperature at each stage, changing the flow arrangement from series to parallel increases the permeate flux by a small amount at a given feed temperature. The percentage increase in flux changes from 5.99 % to 13.2 % for air gap, and from 10.6 % to 15.1 % for water gap.

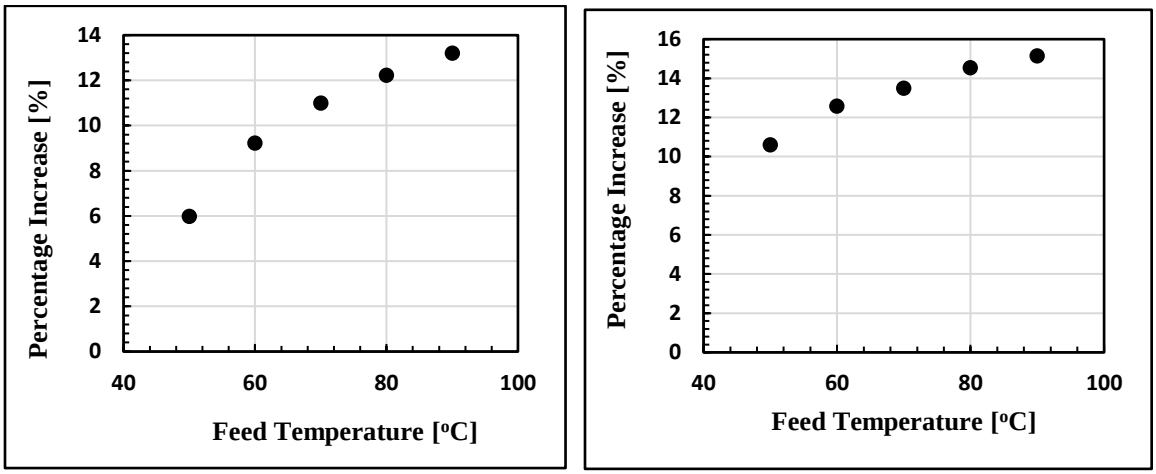

(a) Percentage increase in flux for AGMD (b) Percentage increase in flux for WGMD

Figure 5.4: Percentage increase in flux when the connection is changed from series to parallel

Conditions: membrane PTFE 0.45 μm, coolant temperature 20°C, feed salinity 150 mg/L, 4 mm gap width, feed and coolant flow rates of 2.3 L/min for each module.

In order to compare the productivity of multistage and single stage systems, the ratio of multistage to single stage permeate flux is calculated as shown in Figure 5.5. The single module permeate flux for parallel is used as reference value of comparison. The flux ratio for AGMD varies from 2.58 to 2.69 for series flow arrangement, and between 2.86 and 3 for parallel flow arrangement, where the flux ratio for WGMD varies from 2.59 to 2.65 for series flow arrangement, and between 2.96 and 3 for parallel flow arrangement. Feed temperature has no effect on this ratio because the feed temperature is used as reference in calculation.

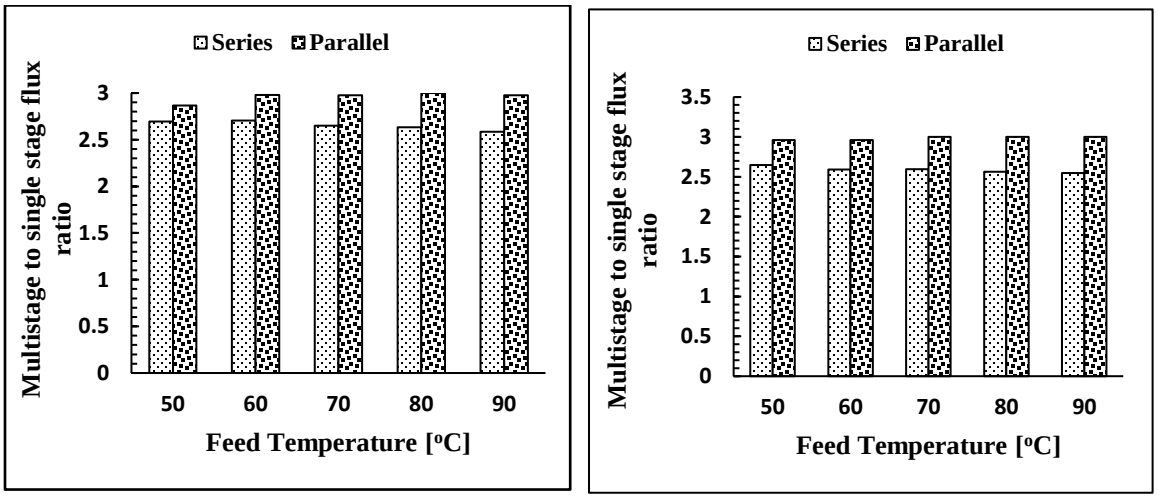

(a) AGMD (b) WGMD

Figure 5.5: The ratio of multistage to single stage permeate flux

Conditions: membrane PTFE 0.45 μm, coolant temperature 20°C, feed salinity 150 mg/L, 4 mm gap width, feed and coolant flow rates of 2.3 L/min for each module.

The variation of total temperature difference (temperature difference between inlet of first module and outlet of last module) with the feed temperature for parallel and series flow arrangements is shown in Figure 5.6. The cold water enters the first module at constant temperature of 20^{o}C, where the feed and coolant flow rates are 7 L/min (total flow rate for the three modules) in case of parallel connection and 2.3 L/min in case of series connection. The temperatures at inlets and outlets of the feed and coolant streams are observed using thermocouples connected with data acquisition system and LabVIEW code. For air gap and water gap systems, the temperature difference between inlet and outlet of the multistage MD system increases with increasing the feed temperature for both feed and coolant streams. For air gap the temperature change in the feed side varies from -0.5^{o}C to -1.87^{o}C for parallel flow arrangement, and from -1.27^{o}C to -6.63^{o}C for series flow arrangement. The cold-water temperature increases by 0.26^{o}C to 1.12^{o}C for parallel flow arrangement, where it increases by 0.48^{o}C to 1.47^{o}C for series flow arrangement. For water gap the hot water temperature change by -1.18^{o}C to -2.38^{o}C for parallel flow arrangement, and from -2.14^{o}C to -7.41^{o}C for series flow arrangement. The temperature difference in the cold side varies from 0.48^{o}C to 1.47^{o}C for parallel flow arrangement, where it increases by 2.34^{o}C to 4.96^{o}C for series flow arrangement. From the above results, it is clear that, the temperature difference for series arrangement is higher than that for parallel for both air gap and water gap processes. Also, the temperature difference between outlet and inlet for water gap is higher than that of the air gap.

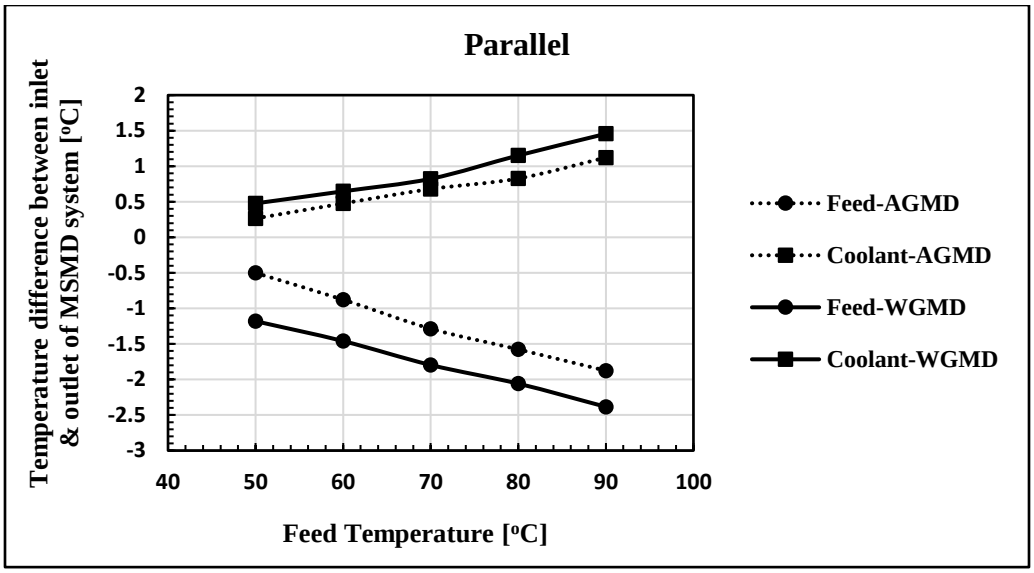

(a) The variation of temperature differences with feed temperature for parallel connection

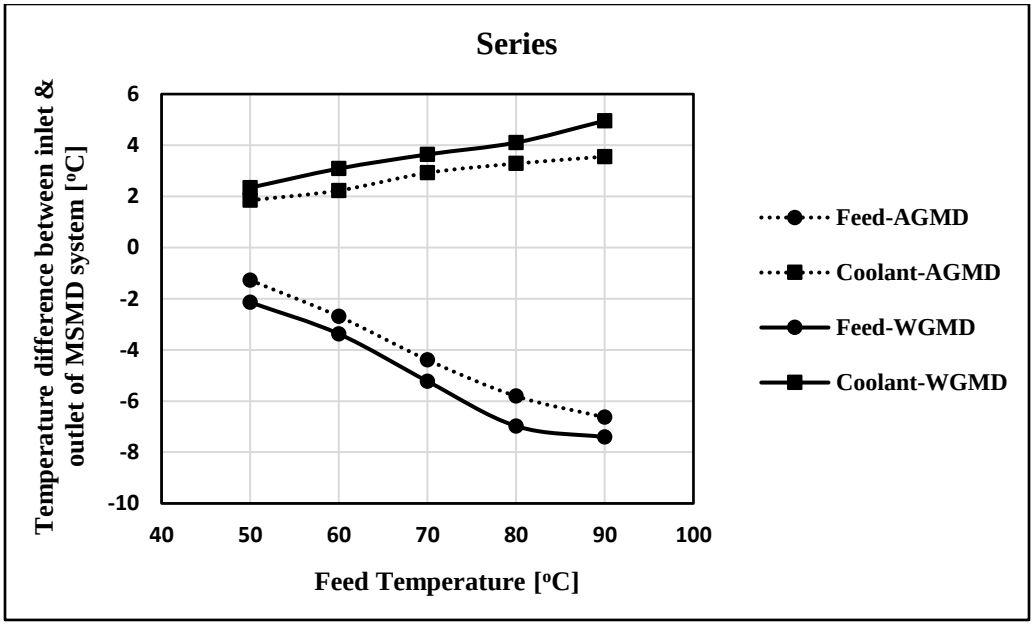

(b) The variation of temperature differences with feed temperature for series connection

Figure 5.6: The variation of temperature differences with feed temperature

Conditions: membrane PTFE 0.45 μm, coolant temperature 20°C, feed salinity 150 mg/L, 4 mm gap width, feed and coolant flow rates of 2.3 L/min for each module.

5.2 Electric Power Consumption

Power transducers connected to the data acquisition system are used to measure the electric power consumed by the water heater and water chiller. The variation of the power consumed by heater and chiller with feed temperature for AGMD and WGMD with parallel and series flow arrangements is illustrated in Figure 5.7. The feed and coolant flow rates are 7 L/min (the total flow rate for the three modules) in case of parallel flow arrangement, and 2.3 L/min for series flow arrangement.

From Figure 5.7, the following conclusions can be made:

- The power consumed by the heater and chiller (under steady operation) increase with increasing the feed temperature. Because the heat transfer (heat losses) from MD modules to surrounding increases with increasing the feed temperature.
- From figures 5.7 (a), (b), (c), and (d), it is obvious that the power consumption for heater is higher than chiller power consumption for both AGMD and WGMD with parallel and series flow arrangements because of higher temperature difference in the feed stream than that for coolant stream.
- Although the feed and coolant flow rates in parallel connection are higher than series flow rates the power consumption for series connection is higher than that for parallel connection, and that because of higher total temperature difference (temperature difference between inlet of first module and outlet of last module) in case of series flow arrangement.
- The power consumed by the heater and chiller for water gap system is higher than power consumption for air gap system because the heat losses between the feed and coolant streams for WGMD is higher.

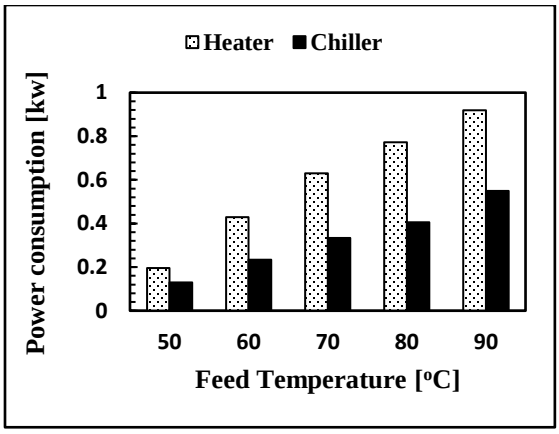

(a) Power consumption for parallel-AGMD

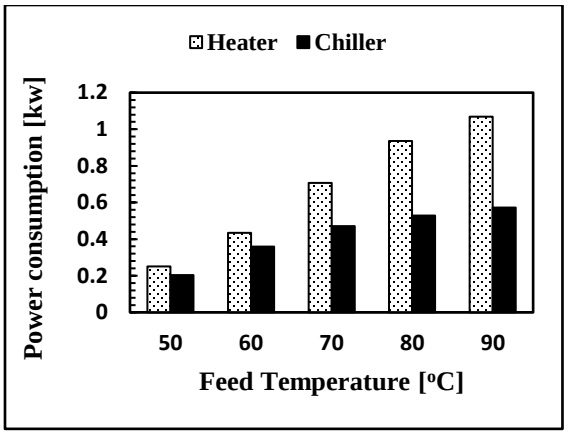

(b) Power consumption for series-AGMD

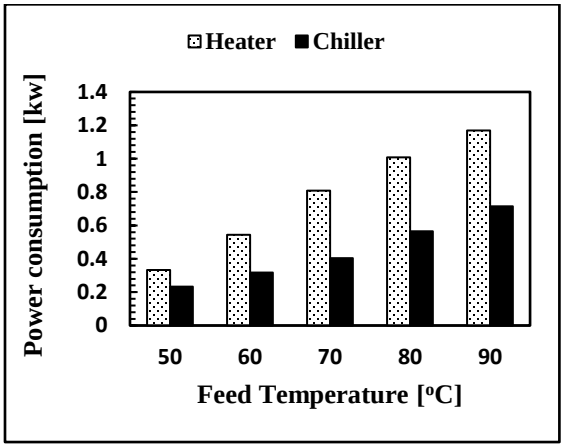

(c) Power consumption for parallel-WGMD

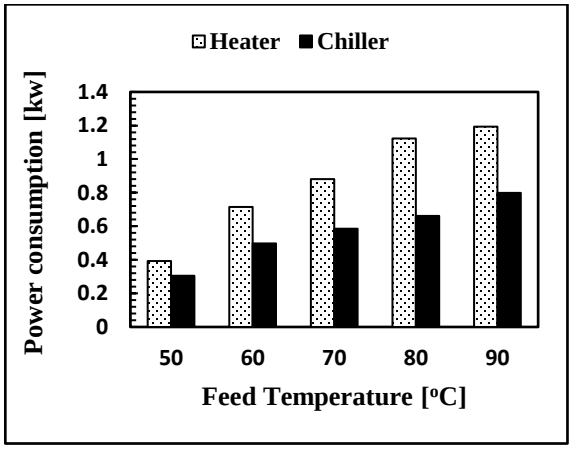

(d) Power consumption for series-WGMD

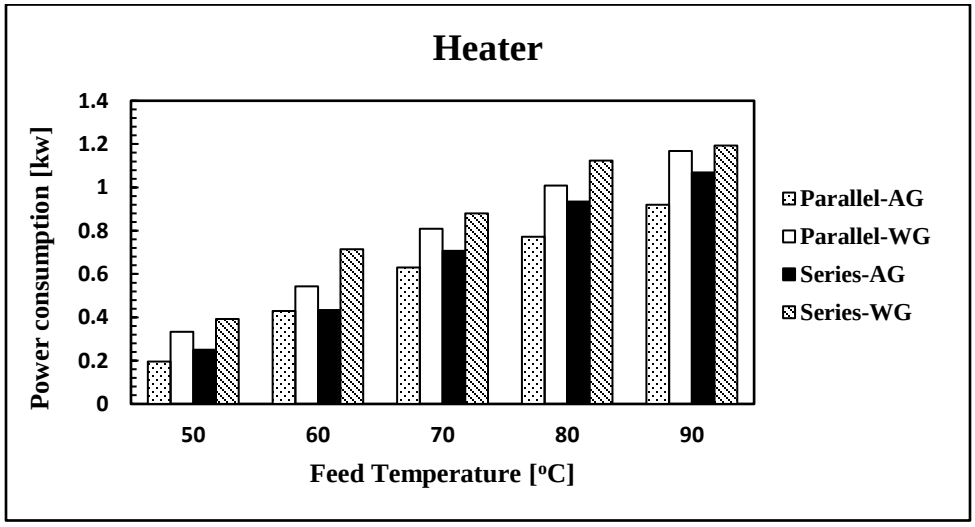

(e) Heater power consumption for AG & WG with parallel and series flow arrangements

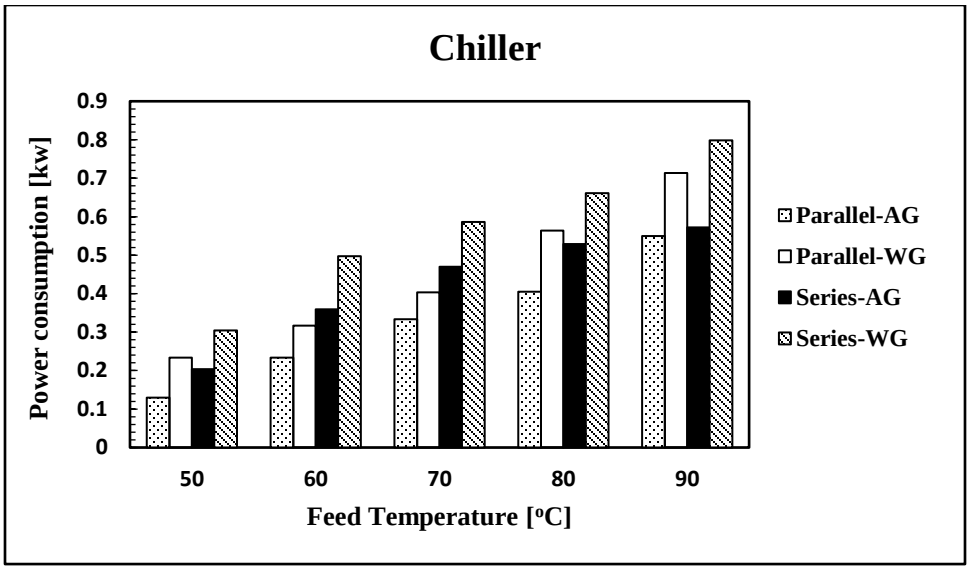

(f) Chiller power consumption for AG & WG with parallel and series flow arrangements

Figure 5.7: Electric power consumption variation with feed temperature

Conditions: membrane PTFE 0.45 μm, coolant temperature 20°C, feed salinity 150 mg/L, 4 mm gap width, feed and coolant flow rates of 2.3 L/min for each module.

5.3 Effect of coolant temperature

Figure 5.8 shows the variation of the permeate flux with coolant temperature for both MS-AGMD and MS-WGMD systems. The coolant temperature is varied from 10°C to 25°C with 5°C step increase. The variation in the permeate flux with cold water temperature is observed at fixed feed temperature of 70°C, 150 mg/L feed concentration, and 4 mm gap width. The total inlet feed and coolant flow rates are 7 L/min (total flow rate for the three modules) in case of parallel flow arrangement, and 2.3 L/min for series flow arrangement. From Figure 5.8, the permeate flux decreases with increasing the coolant temperature for AGMD and WGMD systems because increasing the coolant temperature decreases the

temperature difference and pressure difference across the membrane and the condensation rate decreases as well. The permeate flux for water gap system is higher than that for air gap design. The permeate flux for parallel arrangement is slightly higher than that for the series one for both systems. The maximum flux is achieved at the lowest coolant temperature, and it is about:

- 62.5 kg/m^2.h for multistage air gap membrane distillation system with parallel flow arrangement.
- 163.3 kg/m^2.h for multistage water gap membrane distillation system with parallel flow arrangement.
- 53.5 kg/m^2.h for multistage air gap membrane distillation system with series flow arrangement.
- 145 kg/m^2.h for multistage water gap membrane distillation system with series flow arrangement.

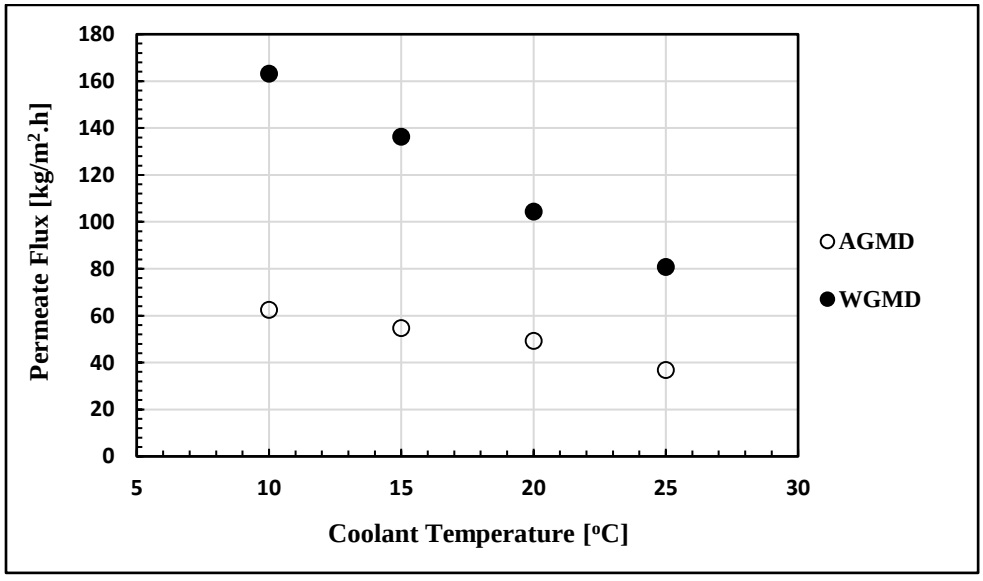

(a) Effect of coolant temperature on the permeate flux for parallel AGMD & parallel WGMD

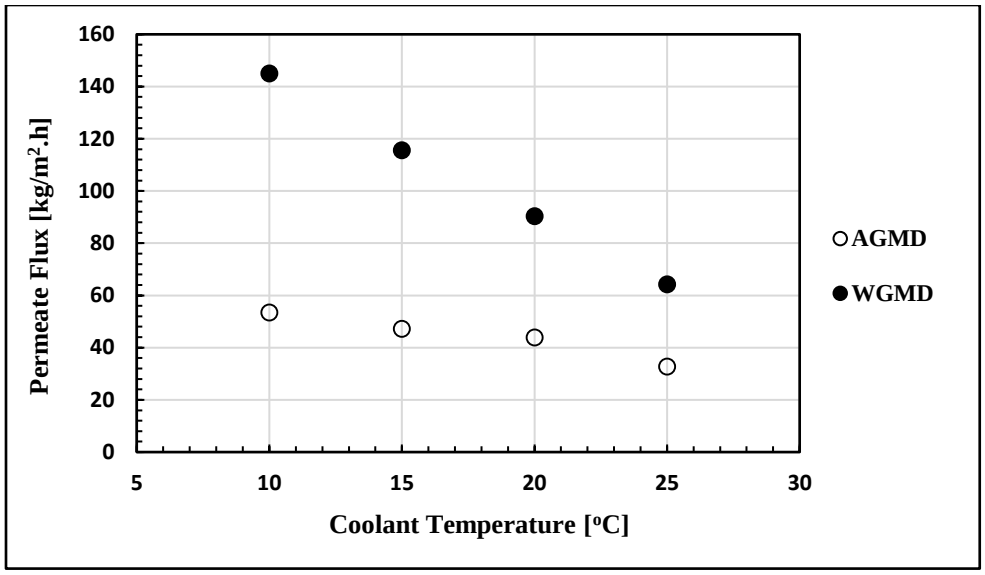

(b) Effect of coolant temperature on the permeate flux for series AGMD & WGMD

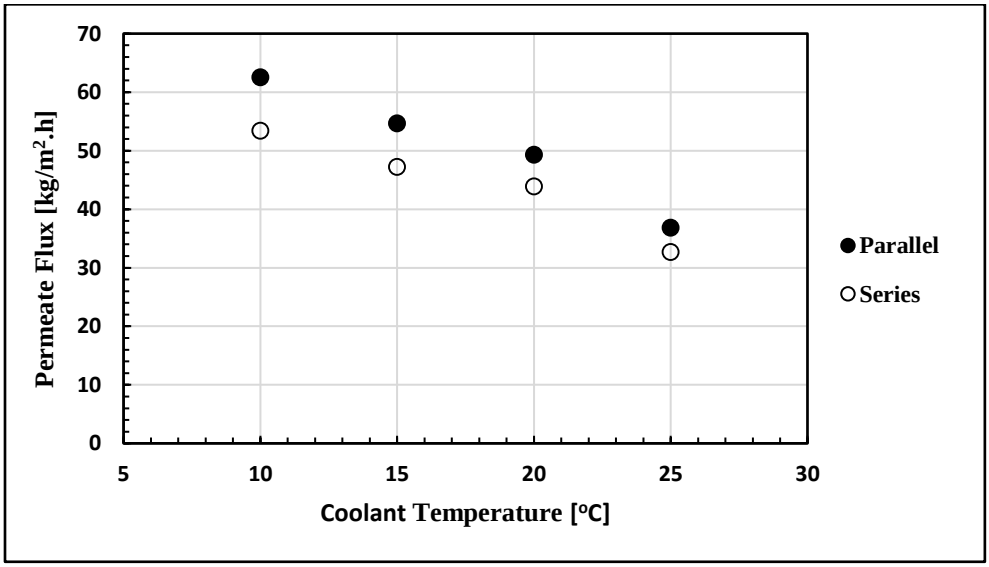

(c) Effect of coolant temperature on the permeate flux for parallel & series AGMD

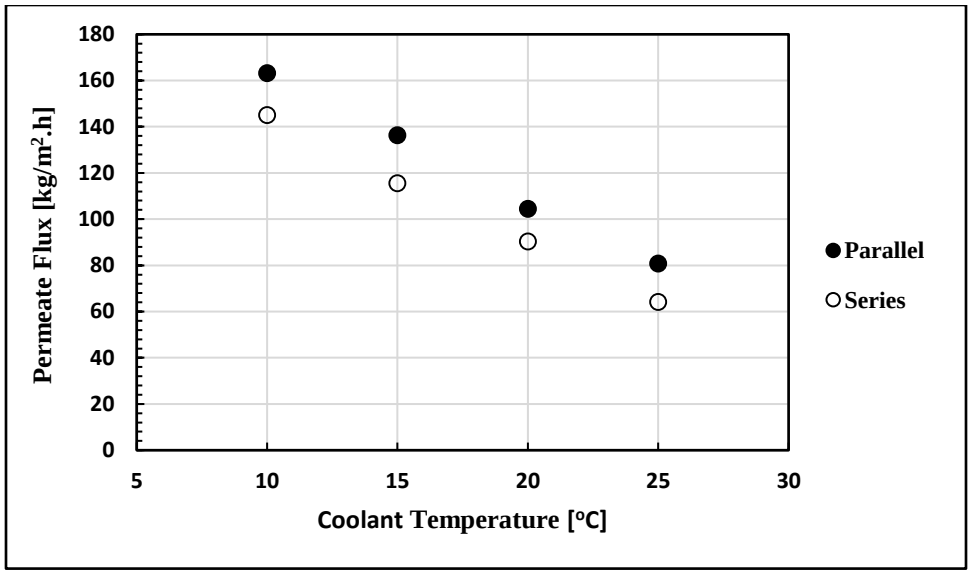

(d) Effect of coolant temperature on the permeate flux for parallel & series WGMD

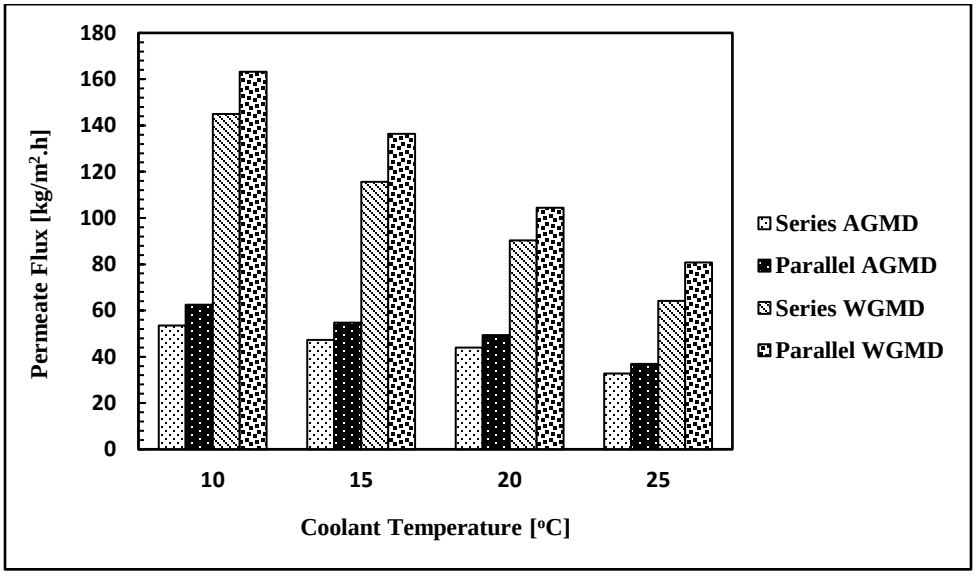

(e) Effect of coolant temperature on the permeate flux for parallel and series AGMD & WGMD

Figure 5.8: Effect of coolant temperature on permeate flux for multistage systems

Conditions: membrane PTFE 0.45 μm, feed temperature 70°C, feed salinity 150 mg/L, 4 mm gap width, feed and coolant flow rates of 2.3 L/min for each module.

The stage permeates flux variation with cooling water temperature is shown in Figure 5.9. In case of parallel connection, the feed and coolant water enter each MD module at constant temperatures so, the three MD modules produced almost the same output flux. On the other hand, in case of series flow arrangement the three MD modules produced different output fluxes and that because of decreasing feed temperature and increasing coolant temperature from the first stage to the last stage.

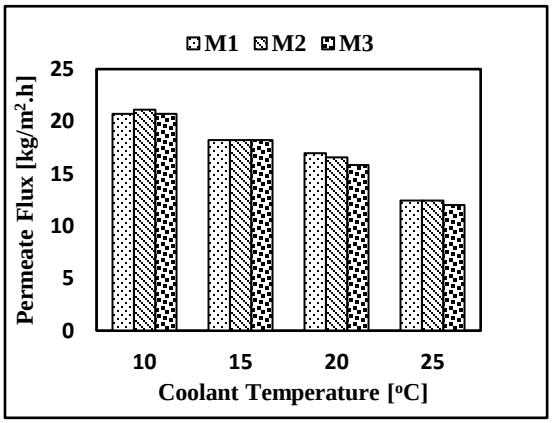

(a) Stage permeate flux for parallel-AGMD

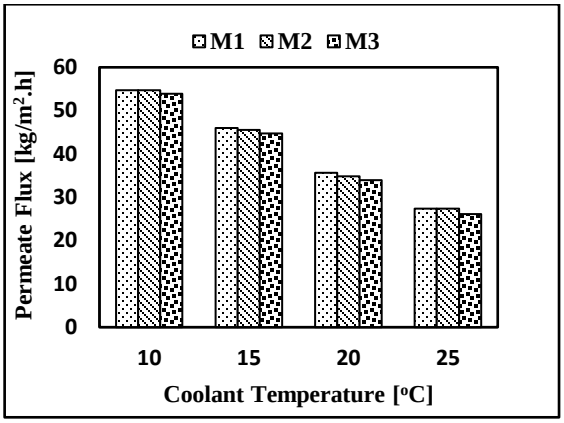

(b) Stage permeate flux for parallel-WGMD

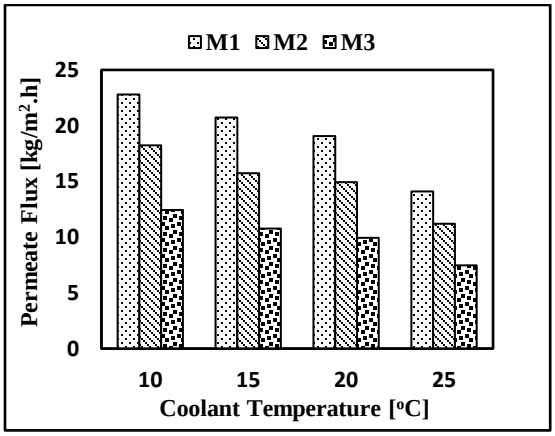

(c) Stage permeate flux for series-AGMD

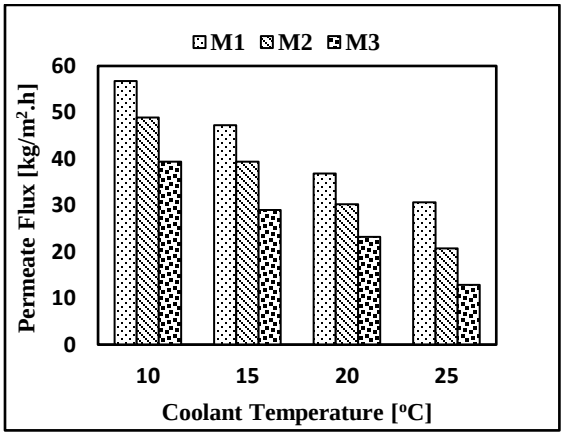

(d) Stage permeate flux for series-WGMD

Figure 5.9: Stage permeates flux variation with cooling water temperature

Conditions: membrane PTFE 0.45 μm, feed temperature 70ºC, feed salinity 150 mg/L, 4 mm gap width, feed and coolant flow rates of 2.3 L/min for each module.

In order to compare the effect of feed temperature and coolant temperature on the flux, the percentage increase in the flux with changing feed and coolant temperatures is calculated for both air gap and water gap multistage systems. Figure 5.10 presents the percentage increase in permeate flux at a constant feed temperature of 70^{o}Cwhen the coolant temperature is decreased from 25^{o}C to 10^{o}C. Figure 5.11 shows the percentage increase in permeate flux at fixed coolant temperature of 20^{o}C when the feed temperature changes from 50^{o}C to 90^{o}C. Reducing the coolant temperature increases the permeate flux for both systems because decreasing the coolant temperature increases the temperature difference and pressure difference across the membrane and the condensation rate increases as well. The percentage increase in flux varies from 63.3 % for parallel air gap to 125.8 % for parallel water gap. On the other hand, increasing the feed temperature increases the permeate flux for air gap and water gap processes because increasing the feed temperature increases the evaporation rate in the feed side and increases the vapor pressure difference across the membrane. The percentage increase in flux changes from 350 % for series water gap to 468.3 % for parallel air gap. We can conclude that, increasing the feed temperature is more effective on increasing the permeate flux than decreasing the coolant temperature.

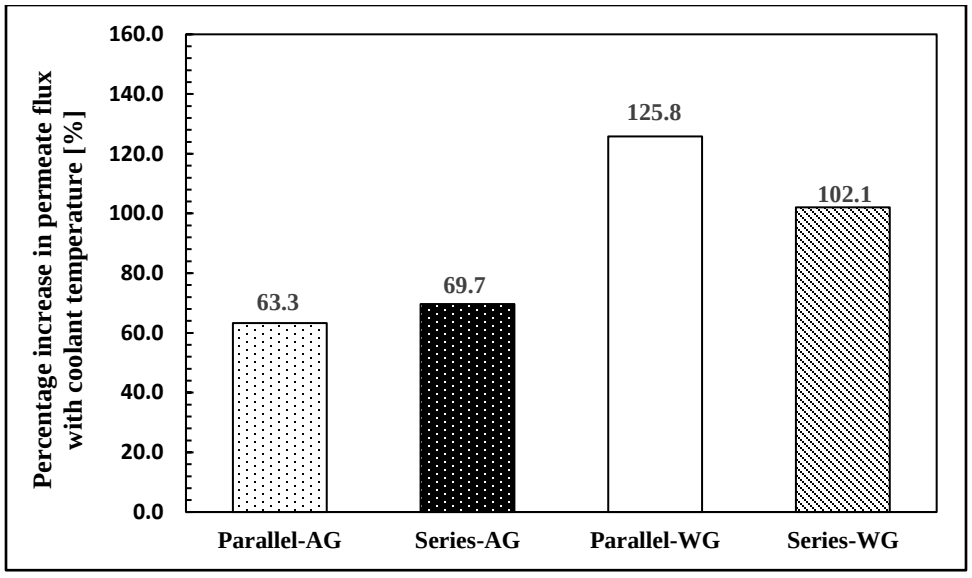

Figure 5.10: The percentage increase in flux when the coolant temperature is decreased from 25ºC to 10ºC

Conditions: membrane PTFE 0.45 µm, feed temperature 70ºC, feed salinity 150 mg/L, 4 mm gap width, feed and coolant flow rates of 2.3 L/min for each module.

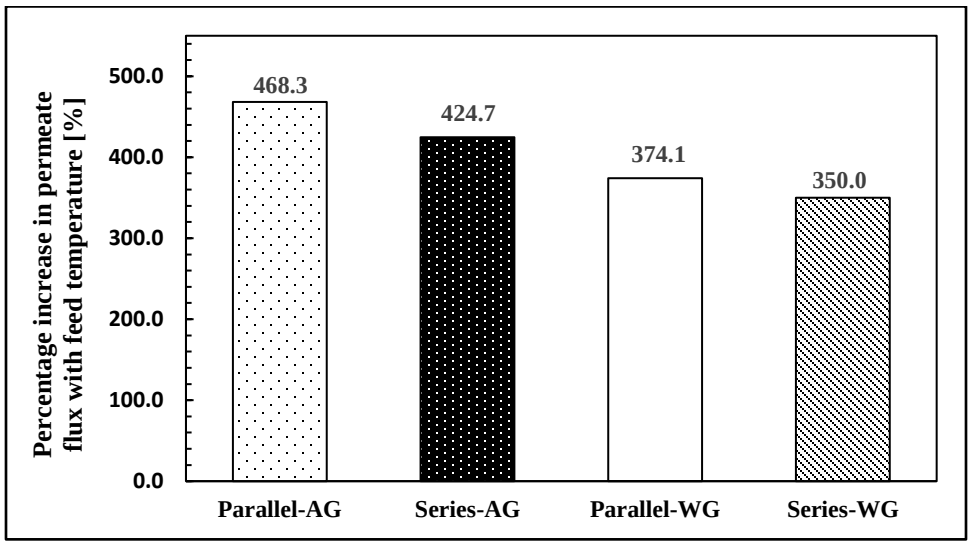

Figure 5.11: The percentage increase in flux when the feed temperature is increased from 50ºC to 90ºC

Conditions: membrane PTFE 0.45 µm, coolant temperature 20ºC, feed salinity 150 mg/L, 4 mm gap width, feed and coolant flow rates of 2.3 L/min for each module.

5.4 Effect of feed flow rate

To study the effect of flow rate on the permeate flux, three different values for feed flow rate are used, 5 L/min, 6 L/min, and 7 L/min (total flow rate for the three modules) for parallel configuration and 1.3 L/min, 2.3 L/min, and 3.3 L/min for series arrangement. The experiments are conducted at constant feed temperature of 70^{o}C, coolant temperature of 20^{o}C, coolant flow rate of 7 L/min (total flow rate for the three modules) in case of parallel and 2.3 L/min for series connection, feed salinity of 150 mg/L, and 4 mm gap width.

Figure 5.12 illustrates the effect of feed flow rate on the permeate flux for both multistage air gap and water gap MD systems. The permeate flux Increases with increasing the feed flow rate for both air gap and water gap processes, because increasing the flow rate enhances the turbulence level, and that leads to better mixing in the boundary layers and leads to higher values of the heat and mass transfer coefficients through the membrane. The maximum value of the permeate flux is about:

- 49.35 kg/m^2.h for multistage air gap membrane distillation system with parallel flow arrangement.
- 104.4 kg/m^2.h for multistage water gap membrane distillation system with parallel flow arrangement.
- 52.6 kg/m^2.h for multistage air gap membrane distillation system with series flow arrangement.
- 116.85 kg/m^2.h for multistage water gap membrane distillation system with series flow arrangement.

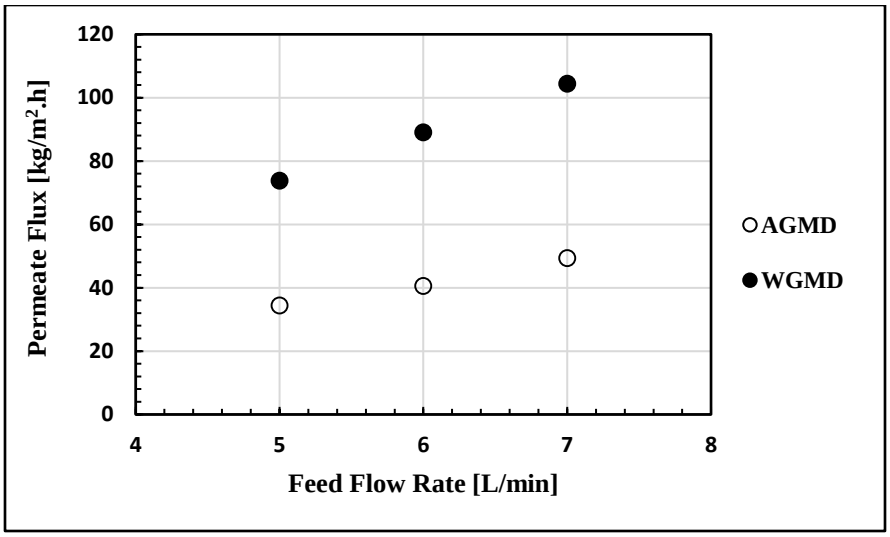

(a) Effect of feed flow rate on the permeate flux for parallel AGMD & WGMD

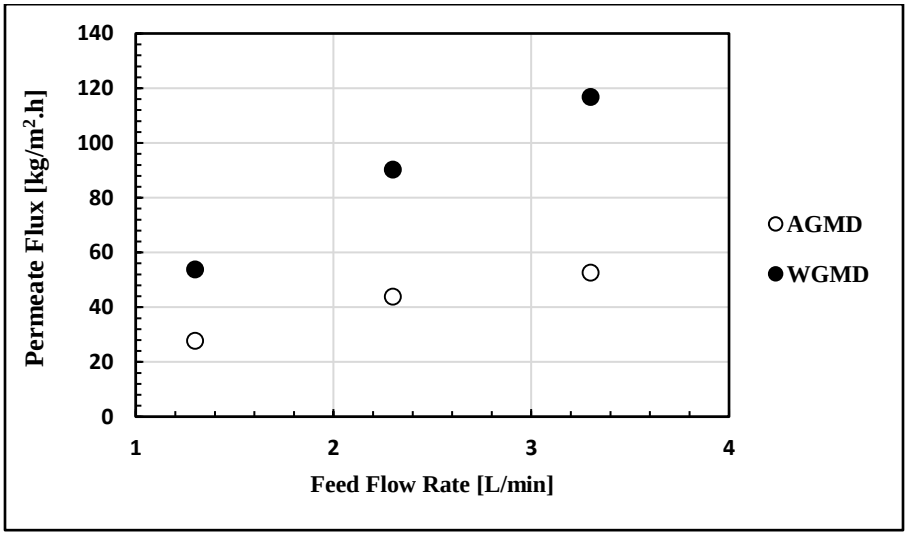

(b) Effect of feed flow rate on the permeate flux for series AGMD & WGMD

Figure 5.12: Effect of feed flow rate on permeate flux for multistage systems

Conditions: membrane PTFE 0.45 μm, feed temperature 70ºC, coolant temperature 20ºC, feed salinity 150 mg/L, 4 mm gap width, coolant flow rate of 2.3 L/min for each module.

5.5 Effect of coolant flow rate

The effect of coolant flow rate on permeate flux is investigated for multi-stage air gap and multi-stage water gap membrane distillation systems with parallel and series flow arrangements. Three different values for coolant flow rate are used, 5 L/min, 6 L/min, and 7 L/min (total flow rate for the three modules) for parallel configuration and 1.3 L/min, 2.3 L/min, and 3.3 L/min for series flow arrangement. The variation of permeate flux with coolant is observed at constant feed temperature of 70^{o}C, coolant temperature of 20^{o}C, 4 mm air gap width, and 150 mg/L feed concentration. The feed flow rate is 7 L/min (total flow rate for the three modules) in case of parallel flow arrangement, and 2.3 L/min for series flow arrangement.

The effect of coolant flow rate on the permeate flux for both multistage air gap and water gap MD systems is shown in Figure 5.13. The permeate flux Increases with increasing the coolant flow rate for both air gap and water gap processes, because increasing the flow rate will enhance the turbulence level in the coolant channels, and that leads to higher values of the heat and mass transfer coefficients in the cold side of condensation plate leading to more heat transfer from the gap and hence better condensation of permeate vapor. The maximum value of the permeate flux is about:

- 49.35 kg/m^2.h for multistage air gap membrane distillation system with parallel flow arrangement.
- 104.4 kg/m^2.h for multistage water gap membrane distillation system with parallel flow arrangement.
- 50.6 kg/m^2.h for multistage air gap membrane distillation system with series flow arrangement.

- 106.9 kg/m^2.h for multistage water gap membrane distillation system with series flow arrangement.

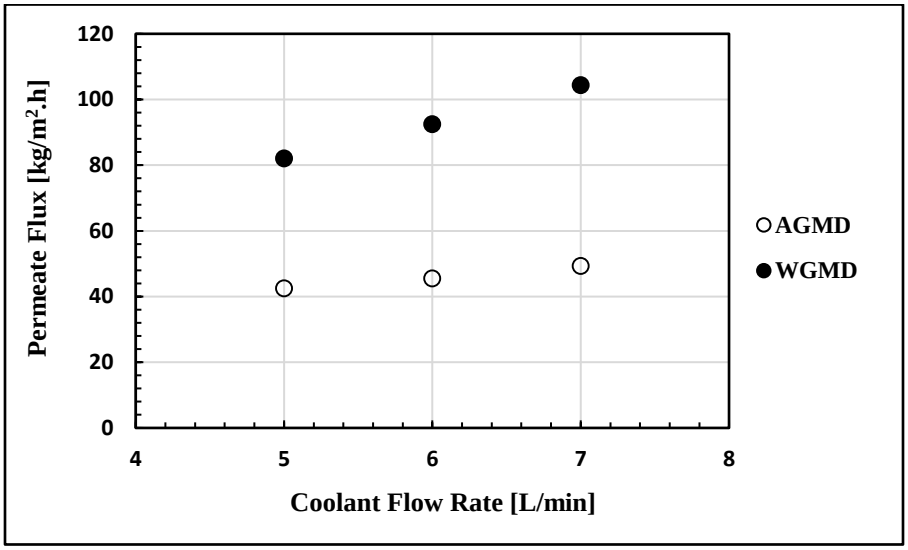

(a) Effect of coolant flow rate on the permeate flux for parallel AGMD & WGMD

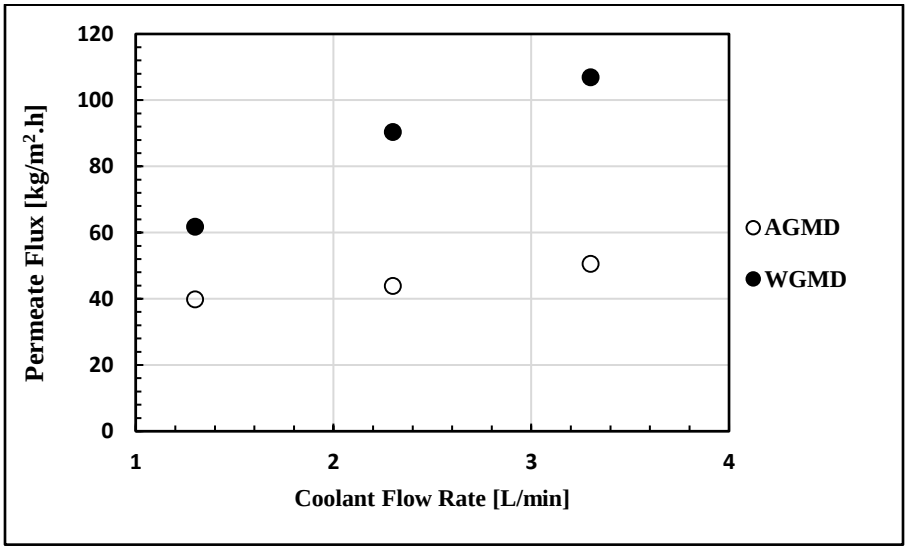

(b) Effect of coolant flow rate on the permeate flux for series AGMD & WGMD

Figure 5.13: Effect of coolant flow rate on permeate flux for multi-stage systems

Conditions: membrane PTFE 0.45 μm, feed temperature 70^{o}C, coolant temperature 20^{o}C, feed salinity 150 mg/L, 4 mm gap width, feed flow rate of 2.3 L/min for each module.

In order to compare the effect of feed flow rate and coolant flow rate on the flux, the percentage change in the permeate flux is calculated when the feed and coolant flow rates are increased from 5 L/min to 7 L/min for parallel flow arrangement and from 1.3 L/min to 3.3 L/min for series flow arrangement. The percentage increase in flux changes from 13.7 % to 24.2 % for increasing the coolant flow rate as in Figure 5.14, and from 29.3 % to 53.9 % for increasing the feed flow rate as in Figure 5.15. That means increasing the feed flow rate is more effective in increasing the permeate flux than increasing the coolant flow rate.

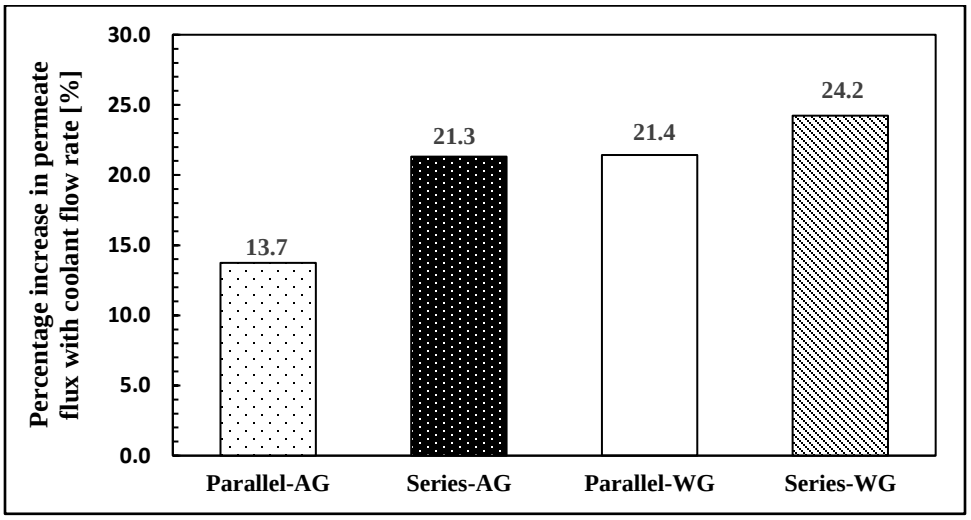

Figure 5.14: The percentage increase in flux with increasing the coolant flow rate

Conditions: membrane PTFE 0.45 μm, feed temperature 70ºC, coolant temperature 20ºC, feed salinity 150 mg/L, 4 mm gap thickness, feed flow rate of 2.3 L/min for each module.

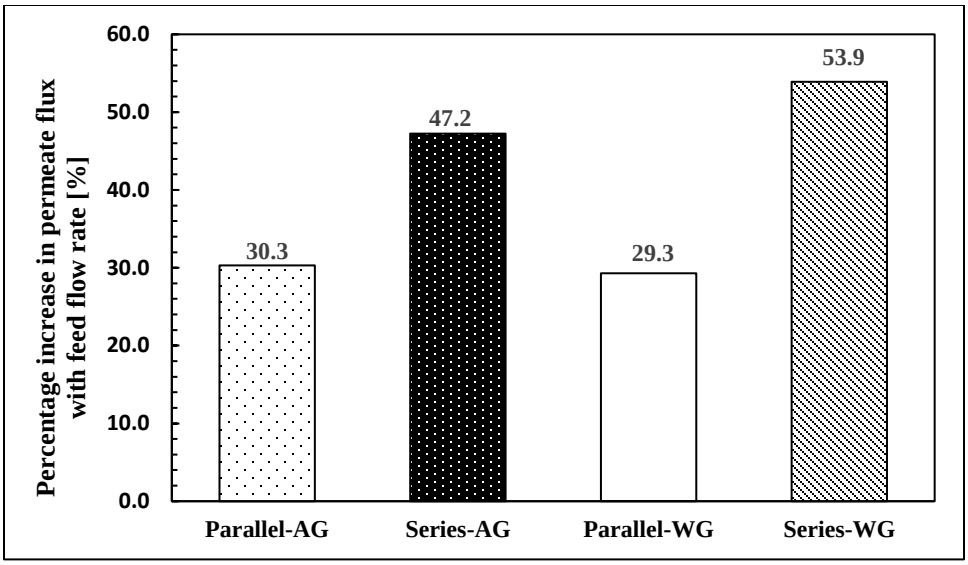

Figure 5.15: The percentage increase in flux with increasing the feed flow rate

Conditions: membrane PTFE 0.45 μm, feed temperature 70ºC, coolant temperature 20ºC, feed salinity 150 mg/L, 4 mm gap thickness, coolant flow rate of 2.3 L/min for each module.

5.6 Effect of feed concentration

The effect of feed salinity on permeate flux is represented in Figure 5.16. Three different concentration feeds (0.15 g/L, 3 g/L, and 30 g/L) are used to study the effect of feed salinity for both air gap and water gap systems with parallel and series configurations at the same operating conditions of 70ºC feed temperature, 20ºC coolant temperature, 7 L/min feed and coolant flow rates (total flow rate for the three modules) for parallel configuration and 2.3 L/min for series flow arrangement, and 4 mm gap thickness. The permeate flux decreases as the feed concentration increasing for both systems, because the salt precipitation on the membrane feed surface increases and that adds additional resistance layer on the membrane surface and prevents the passage of water vapor through the membrane.

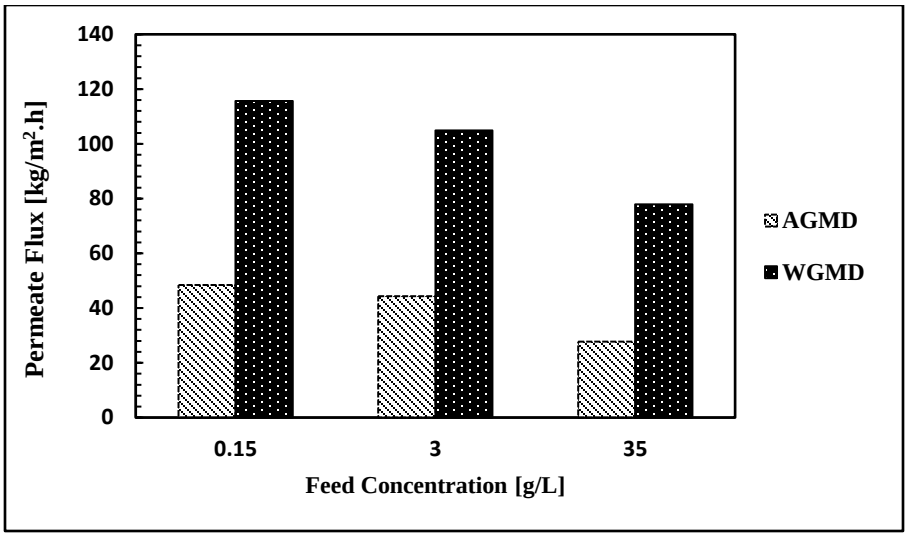

(a) Effect of feed concentration on permeate flux for parallel AGMD & WGMD

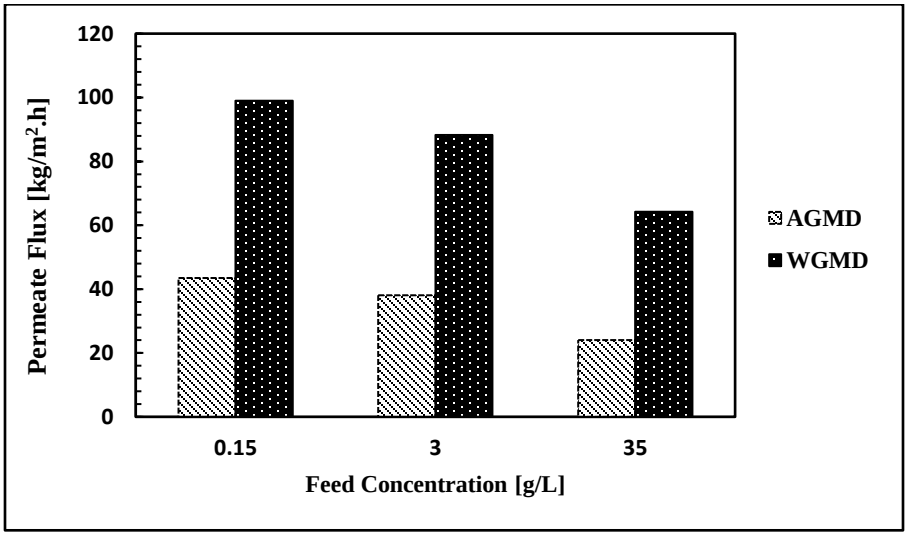

(b) Effect of feed concentration on permeate flux for series AGMD & WGMD

Figure 5.16: Effect of feed concentration on permeate flux

Conditions: membrane PTFE 0.45 μm, feed temperature 70°C, coolant temperature 20°C, 4 mm gap thickness, feed and coolant flow rates of 2.3 L/min for each module.

5.6.1 The Salt Rejection Factor (SRF)

The salt rejection factor (SRF) is a dimensionless parameter utilized to define the quality of permeate as compared to feed salinity. Salt rejection factor is defined as

$$SRF = \frac{\text{Feed Concentration} - \text{Permeate Concentration}}{\text{Feed Concentration}} * 100$$

Figure 5.17 shows the effect of feed concentration on the average salt rejection factor for air gap and water gap systems with parallel and series flow arrangements. As the feed concentration increases from 0.15 g/L to 3 g/L, salt rejection factor increases. When sea water (35 g/L) is used as feed, salt rejection factor was 99.97 %. Salt rejection factor was 97.7 % for feed concentration of 0.15 g/L.

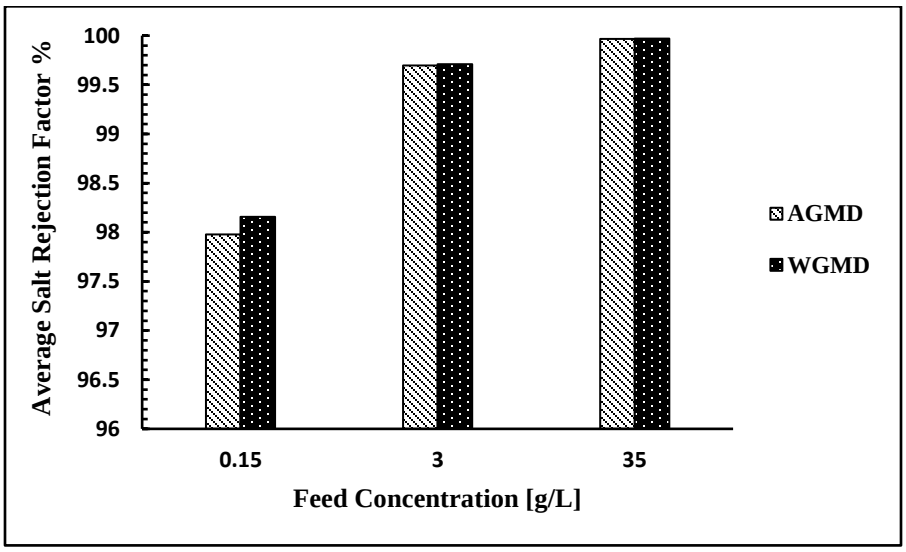

(a) Effect of feed concentration on salt rejection factor for parallel AGMD & WGMD

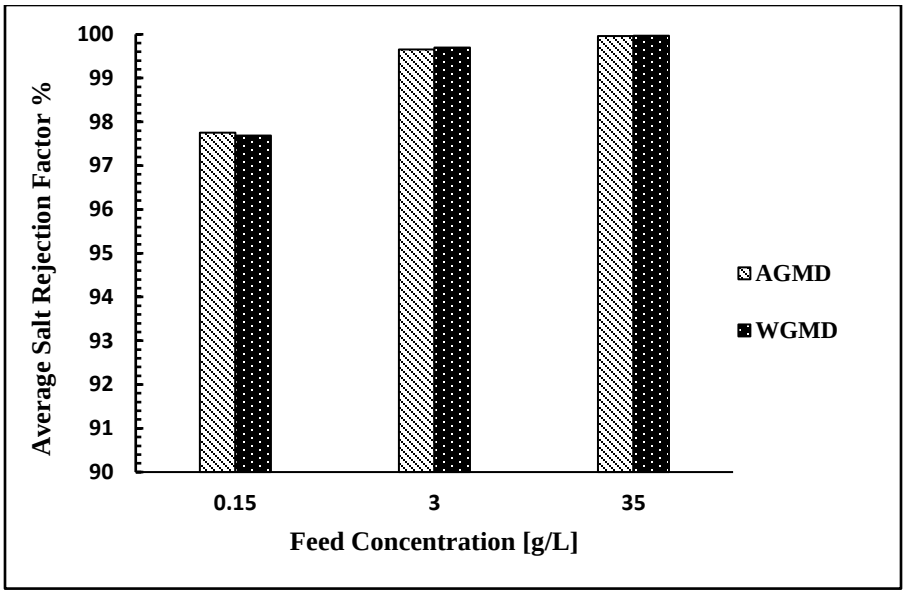

(b) Effect of feed concentration on salt rejection factor for series AGMD & WGMD

Figure 5.17: Effect of feed concentration on salt rejection factor

Conditions: membrane PTFE 0.45 μm, feed temperature 70°C, coolant temperature 20°C, 4 mm gap thickness, feed and coolant flow rates of 2.3 L/min for each module.

5.7 Effect of flow arrangement

The effect of flow arrangement on permeate flux is presented in Figure 5.18. Three different flow arrangements are used in this experiment, namely parallel flow arrangement (parallel feed-parallel coolant), series flow arrangement (series feed-series coolant), and mixed flow arrangement (parallel feed-series coolant, and series feed-parallel coolant). The results show that, parallel flow arrangement produced the highest output flux, where the lower permeate flux was for series flow arrangement.

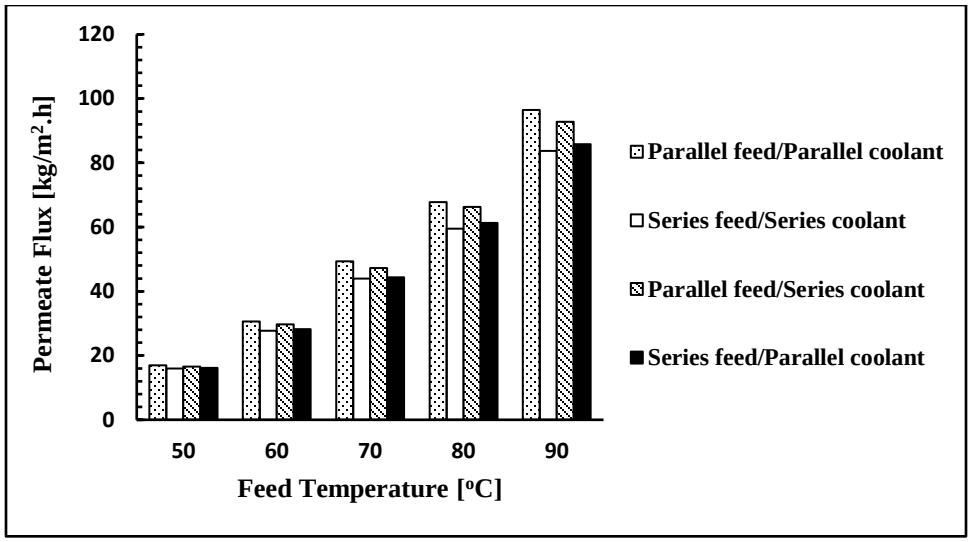

(a) Effect of flow arrangement on permeate flux for AGMD

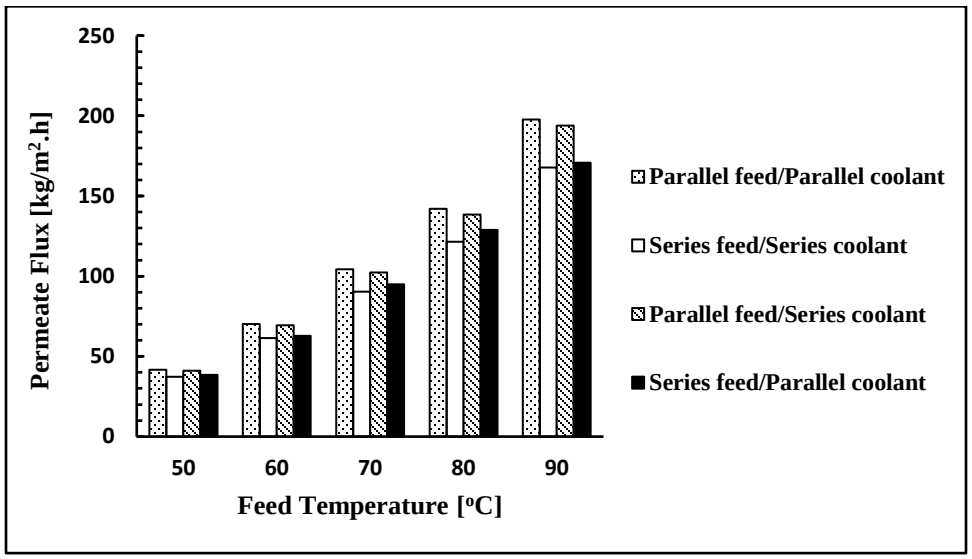

(b) Effect of flow arrangement on permeate flux for WGMD

Figure 5.18: Effect of flow arrangement on permeate flux

Conditions: membrane PTFE 0.45 μm, feed salinity 150 mg/L, coolant temperature 20ºC, 4 mm gap thickness, feed and coolant flow rates of 2.3 L/min for each module.

5.8 Effect of gap width

The gap width is an important design parameter in the evaluating the performance of MS-AGMD and MS-WGMD systems. In order to investigate the influence of gap width on the system flux, an experiment was conducted for three different gap widths; 2 mm, 4 mm and 8 mm. The operating conditions are; PTFE membrane of pore size of 0.45 μm, coolant temperature was fixed at 20^{o}C, feed and coolant flow rates of 7 L/min (total flow rate for the three modules), and feed salinity 150 mg/L. where the feed temperature is changed from 50 to 90^{o}C. Figure 5.19 shows the effect of gap width on permeate flux for MS-AGMD and MS-WGMD configurations. It can be seen that increasing the gap width decreases the permeate flux in both configurations because increasing the gap width means increasing the heat transfer resistance through the gap. Decreasing the gap width from 8 mm to 2 mm increases the permeate flux by a maximum of 75.19 % for MS-WGMD and about 239.7 % for MS-AGMD. So, the conclusion from this experiments is that the AGMD design is more sensitive to the gap width.

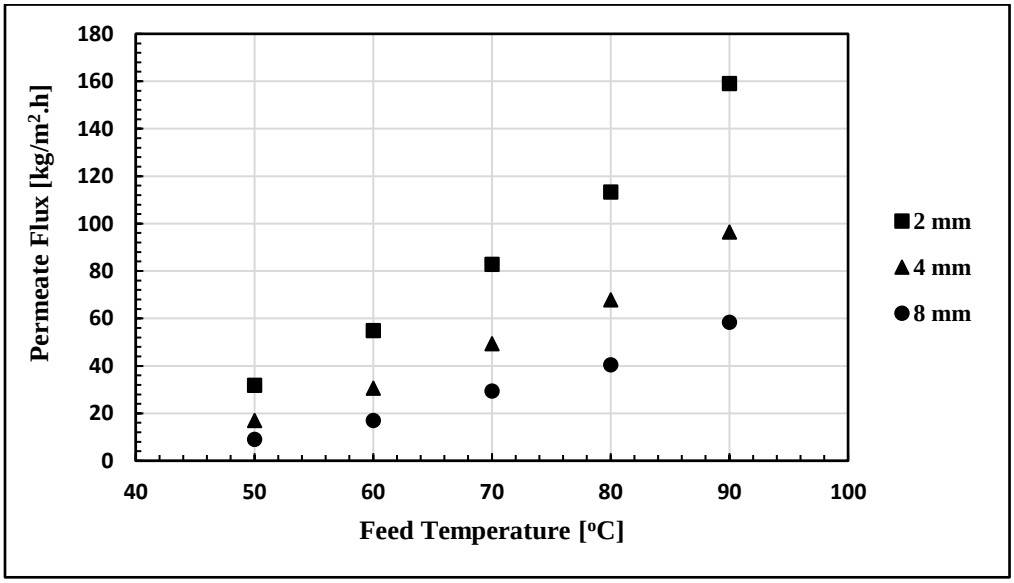

(a) Effect of gap width on permeate flux for AGMD

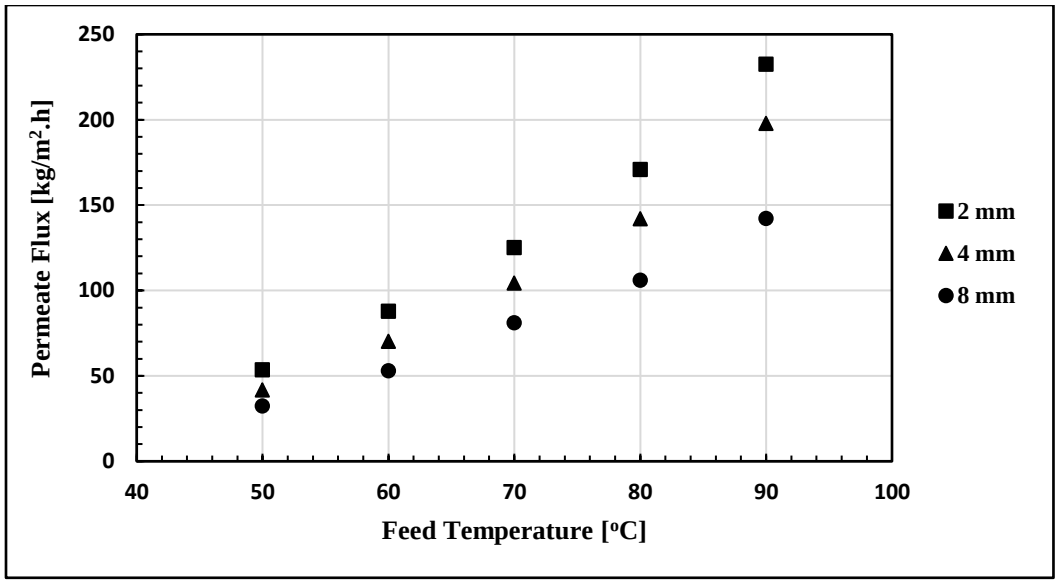

(b) Effect of gap width on permeate flux for WGMD

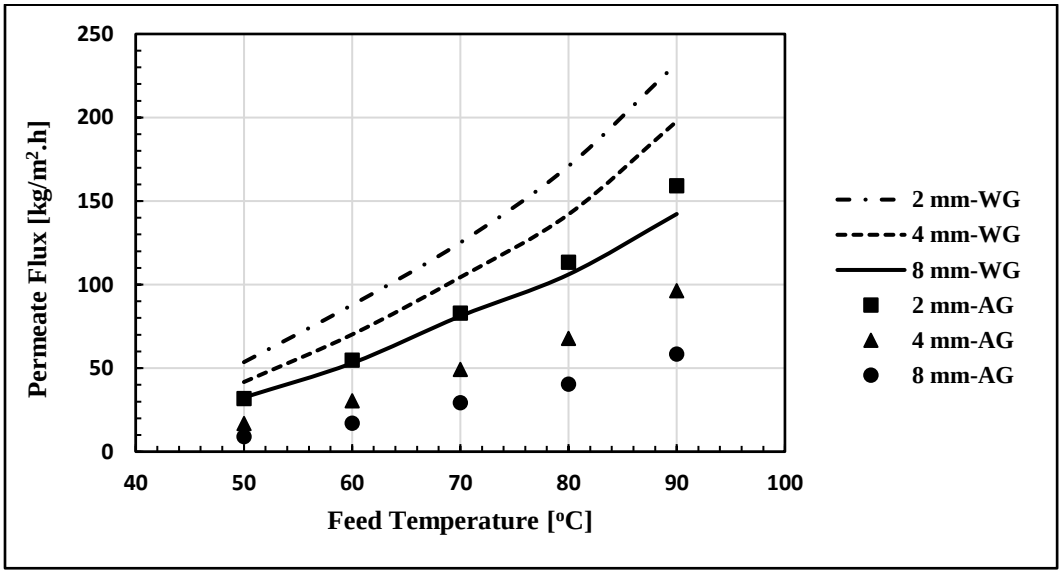

(c) Effect of gap width on permeate flux for AGMD & WGMD

Figure 5.19: Effect of gap width on permeate flux for parallel AGMD & WGMD systems

Conditions: membrane PTFE 0.45 μm, feed salinity 150 mg/L, coolant temperature 20ºC, feed and coolant flow rates of 2.3 L/min for each module.

CHAPTER 6

SOLAR HEATED MD SYSTEM-PRELIMINARY WORK

6.1 Solar heating system

The solar powered MD system is illustrated in Figure 6.1. An evacuated tube solar collector is used for heating the feed water. The performance of the solar collector was tested. The solar collector tank was filled up with water and was kept for 4 days to reach about 100^{o}C before testing. A thermocouple was installed inside the tank. In addition, a Lab View code was developed. The tank was connected to data acquisition system to record temperature readings inside the solar tank every 3 seconds for 24 hours as shown in Figure 6.2. An air gap membrane distillation (AGMD) module is used to investigate the performance of the solar MD system under different feed flow rates. The feed seawater is heated up by the solar collector and then pumped to the MD module using a small centrifugal pump. In this system, the temperatures of the feed and coolant are not controllable but measurable by connecting two thermocouple probes at the inlet and exit of the MD module. Two pressure gauges are used to measure the pressure at the inlet and exit of the MD module in addition to a flow meter for measuring the feed flow rate. The experiment was carried out by collecting a fixed volume of 40 mL of distilled water from the MD module with respect to time for different feed flow rates. The objective was to find the effect of flow rate on permeate flux.

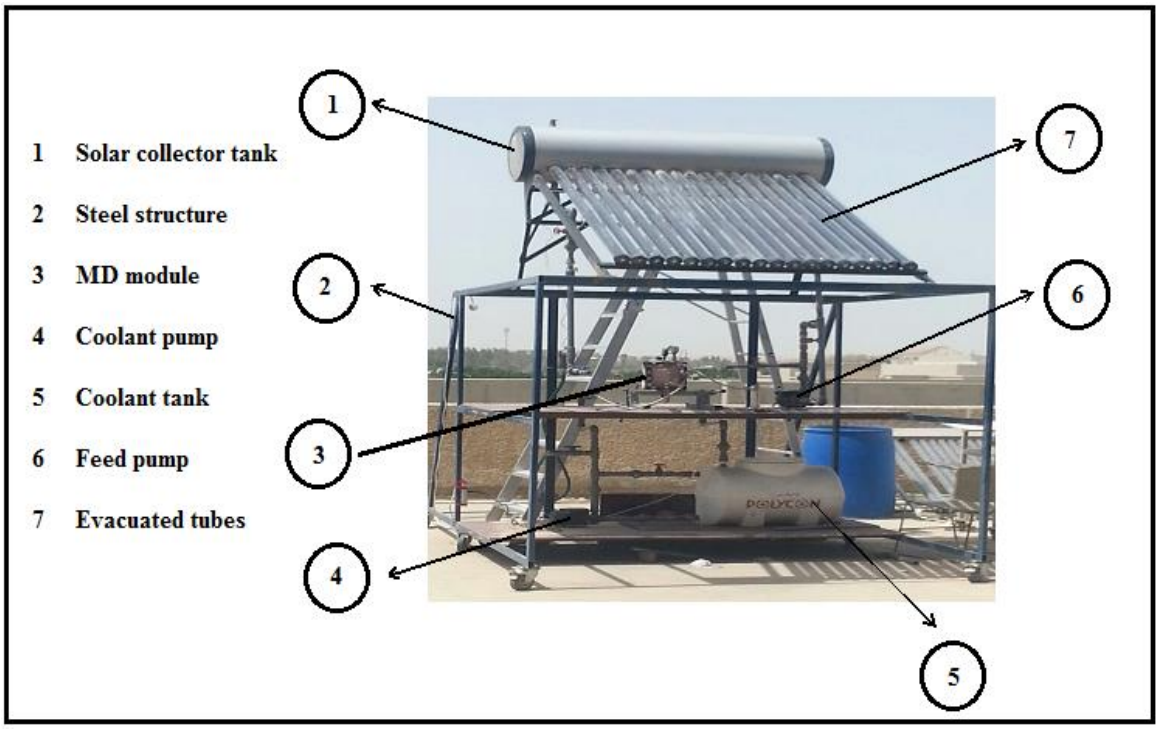

Figure 6.1: Solar-Powered MD system

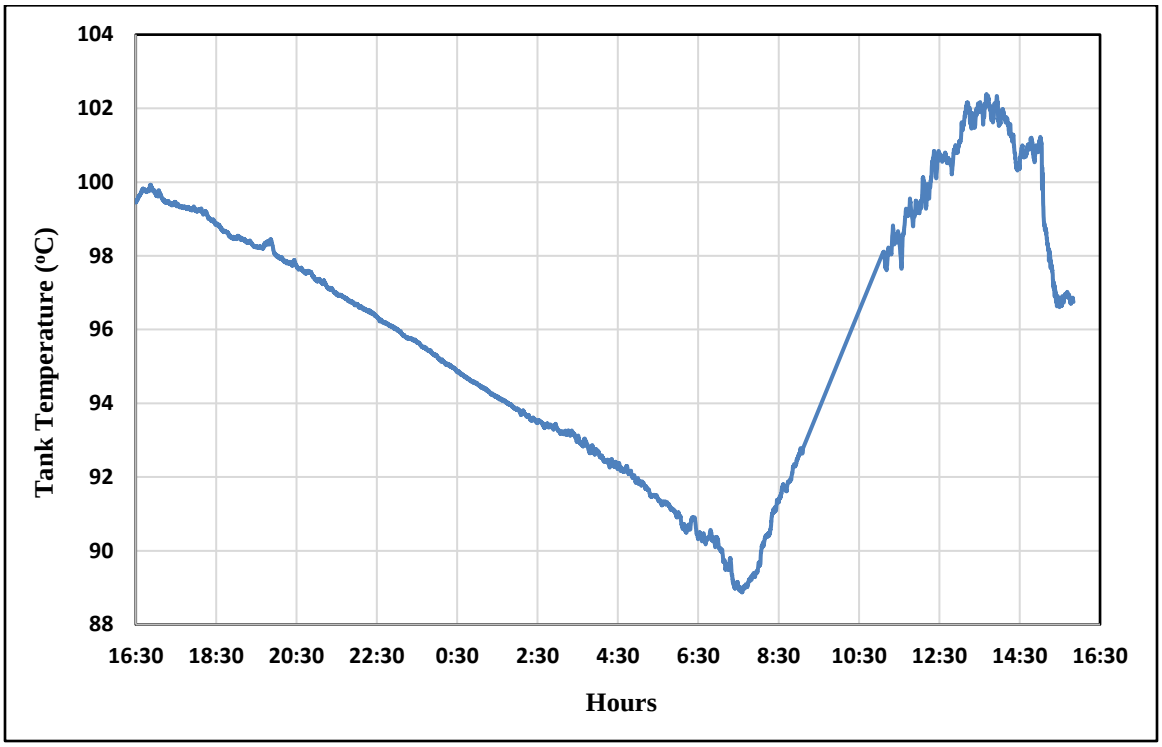

Figure 6.2: Variation of tank temperature with time in May 2015

Figure 6.2 shows a temperature of more than 100°C at the time of day where solar radiation is at its peak (at around 1 pm). Moreover, even at nighttime the temperatures were fairly above 88°C due to insulating the water tank. However, these numbers would decrease slightly as water flows in the piping system. The variation of output flux with feed flow rate is represented in Figure 6.3. The flux seems to be proportional to feed flow rate, with a rise of flow rate correlating to an increase in permeate flux. The salinity of the product was about 48 mg/L and it was decreasing as the feed flow rate decreases, and that gave a high salt rejection factor (about 98 %).

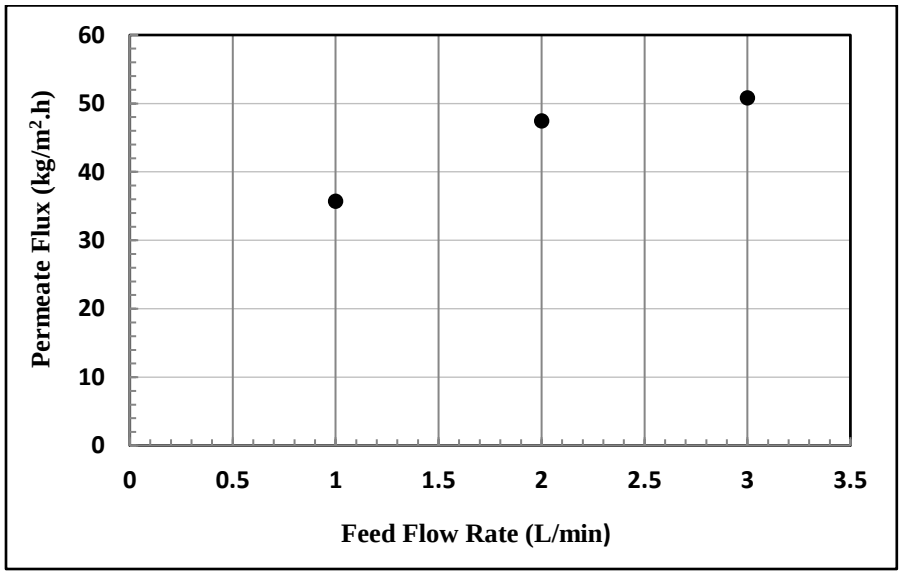

Figure 6.3: The variation of the flux with the feed flow rate for solar system

Conditions: membrane PTFE 0.22 μm, feed salinity 2900 mg/L, coolant temperature 35°C, initial tank temperature 97.3°C, air gap thickness 3 mm

CHAPTER 7

CONCLUSIONS

The performance of multistage air gap and multistage water gap membrane distillation systems for water desalination had been experimentally investigated. In addition, a mathematical model based on the analysis of heat and mass transfer within the MD module has been developed to predict the performance of single stage water gap membrane distillation system under variable operating conditions.

The effect of system operating conditions including the feed inlet temperature, coolant inlet temperature, feed flow rate, coolant flow rate, feed salinity, and gap width on the permeate flux had been studied. Furthermore, the energy analysis and efficiency calculation had been performed.

From the experimental investigation, the following conclusions can be made:

- The permeate flux increases with increasing feed temperature and feed flow rate, and with decreasing the gap width for both air gap and water gap systems. However, it decreased with increasing feed salinity and coolant temperature.
- The output flux for water gap MD system is higher than that for air gap design under the same operating conditions. The ratio of the water gap to air gap permeate flux varies from 2.05 to 2.45 for parallel flow arrangement, and from 2.005 to 2.33 in case of series flow arrangement.
- The permeate flux from parallel flow arrangement is higher than that from series flow arrangement for both air gap and water gap MD systems, and the percentage

increase in flux when the connection is changed from series to parallel changes from 5.99 % to 13.2 % for air gap MD configuration, and from 10.6 % to 15.1 % for water gap MD configuration.

- The salt rejection factor (SRF) was very high reaching almost 99.9 %.
- The gap width is more important in MS-AGMD as compared to MS-WGMD.
- decreasing the gap width from 8 mm to 2 mm increases the permeate flux by a maximum of 75.19 % for MS-WGMD and about 239.7 % for MS-AGMD.
- The power consumed by the heater and chiller increase with increasing the feed temperature due to higher heat transfer and heat losses.
- The power consumption for heater was found to be higher than power consumption of the chiller, for both AGMD and WGMD with parallel and series flow arrangements.
- The power consumption for series connection was higher than that for parallel connection, due to the higher temperature drop in the multistage MD system.
- The power consumed by the heater and chiller for water gap system was found to be higher than power consumption for air gap system.

Finally, the system performance is mostly dominated by the effect of feed temperature and gap width. Other variables have relatively smaller effects on the output flux. The parallel flow arrangement produced higher output flux with lower power consumption.

The results of the theoretical model are in good agreement with the experimental data for the water gap MD system. The model was able to reflect the effects of different operating and design conditions on the MD system performance as validated by the experimental measurements.

References

[1] H. T. El-Dessouky and H. M. Ettouney, *Fundamentals of Salt Warer Desalination*. 2002.

[2] M. T. Kahil, A. Dinar, and J. Albiac, "Modeling water scarcity and droughts for policy adaptation to climate change in arid and semiarid regions," *J. Hydrol.*, vol. 522, pp. 95–109, 2015.

[3] S. Solomon, G.-K. Plattner, R. Knutti, and P. Friedlingstein, "Irreversible climate change due to carbon dioxide emissions.," *Proc. Natl. Acad. Sci. U. S. A.*, vol. 106, no. 6, pp. 1704–9, 2009.

[4] M. H. Sharqawy, J. H. Lienhard V, and S. M. Zubair, "Erratum to Thermophysical properties of seawater: A review of existing correlations and data," *Desalin. Water Treat.*, vol. 29, no. 1–3, pp. 355–355, 2011.

[5] Y. He, X. Lu, Z. Qiu, and J. Zhao, "Shallow water tidal constituents in the Bohai Sea and the Yellow Sea from a numerical adjoint model with TOPEX/POSEIDON altimeter data," *Cont. Shelf Res.*, vol. 24, no. 13–14, pp. 1521–1529, 2004.

[6] K. S. Gallagher, J. P. Holdren, and A. D. Sagar, "Energy-Technology Innovation," *Annu. Rev. Environ. Resour.*, vol. 31, no. 1, pp. 193–237, 2006.

[7] A. Siddiqi and L. D. Anadon, "The water-energy nexus in Middle East and North Africa," *Energy Policy*, vol. 39, no. 8, pp. 4529–4540, 2011.

[8] F. Trieb and H. M??ller-Steinhagen, "Concentrating solar power for seawater desalination in the Middle East and North Africa," *Desalination*, vol. 220, no. 1–3, pp. 165–183, 2008.

[9] A. M. Alklaibi and N. Lior, "Transport analysis of air-gap membrane distillation," *J. Memb. Sci.*, vol. 255, no. 1–2, pp. 239–253, 2005.

[10] M. Al-bahou, Z. Al-Rakaf, H. Zaki, and H. Ettouney, "Desalination experience in Kuwait," *Desalination*, vol. 204, no. 1–3 SPEC. ISS., pp. 403–415, 2007.

[11] F. N. Alasfour, M. A. Darwish, and A. O. Bin Amer, "Thermal analysis of ME-TVC+MEE desalination systems," *Desalination*, vol. 174, no. 1, pp. 39–61, 2005.

[12] A. D. Khawaji, I. K. Kutubkhanah, and J. M. Wie, "Advances in seawater desalination technologies," *Desalination*, vol. 221, no. 1–3, pp. 47–69, 2008.

[13] B. M. Hamieh, J. R. Beckman, and M. D. Ybarra, "Brackish and seawater desalination using a 20 ft2 dewvaporation tower," *Desalination*, vol. 140, no. 3, pp. 217–226, 2001.

[14] M. A. Anderson, A. L. Cudero, and J. Palma, "Capacitive deionization as an

electrochemical means of saving energy and delivering clean water. Comparison to present desalination practices: Will it compete?," *Electrochimica Acta*, vol. 55, no. 12. pp. 3845–3856, 2010.

[15] V. G. Gude, N. Nirmalakhandan, and S. Deng, "Renewable and sustainable approaches for desalination," *Renew. Sustain. Energy Rev.*, vol. 14, no. 9, pp. 2641–2654, 2010.

[16] M. Wolf, "Solar energy utilization by physical methods.," *Science*, vol. 184, no. 4134, pp. 382–6, 1974.

[17] L. García-Rodríguez, A. I. Palmero-Marrero, and C. Gómez-Camacho, "Comparison of solar thermal technologies for applications in seawater desalination," *Desalination*, vol. 142, no. 2, pp. 135–142, 2002.

[18] H. M. Qiblawey and F. Banat, "Solar thermal desalination technologies," *Desalination*, vol. 220, no. 1–3, pp. 633–644, 2008.

[19] E. Tzen, G. Zaragoza, and D. C. Alarcón Padilla, *Solar desalination*, vol. 3. Elsevier Ltd., 2012.

[20] M. M. A. Shirazi, D. Bastani, A. Kargari, and M. Tabatabaei, "Characterization of polymeric membranes for membrane distillation using atomic force microscopy," *Desalin. Water Treat.*, vol. 51, no. 31–33, pp. 6003–6008, 2013.

[21] N. N. Li, A. G. Fane, W. S. W. Ho, and T. Matsuura, *Advanced Membrane Technology and Applications*. 2011.

[22] A. Criscuoli, M. C. Carnevale, and E. Drioli, "Evaluation of energy requirements in membrane distillation," *Chem. Eng. Process. Process Intensif.*, vol. 47, no. 7, pp. 1098–1105, 2008.

[23] K. W. Lawson and D. R. Lloyd, "Membrane distillation," *Journal of Membrane Science*, vol. 124, no. 1. pp. 1–25, 1997.

[24] A. M. Alklaibi and N. Lior, "Membrane-distillation desalination: Status and potential," *Desalination*, vol. 171, no. 2, pp. 111–131, 2005.

[25] E. U. Khan and A. R. Martin, "Water purification of arsenic-contaminated drinking water via air gap membrane distillation (AGMD)," *Period. Polytech. Mech. Eng.*, vol. 58, no. 1, pp. 47–53, 2014.

[26] V. D. Alves and I. M. Coelhoso, "Orange juice concentration by osmotic evaporation and membrane distillation: A comparative study," *J. Food Eng.*, vol. 74, no. 1, pp. 125–133, 2006.

[27] E. Drioli and A. Criscuoli, "Membrane distillation," *WATER WASTEWATER Treat. Technol. – Vol. III - Membr. Distill.*, vol. III, 1997.

[28] A. Alkhudhiri, N. Darwish, and N. Hilal, "Membrane distillation: A comprehensive

review," *Desalination*, vol. 287, pp. 2–18, 2012.

[29] E. Paso, D. Office, J. Walton, H. Lu, C. Turner, S. Solis, and H. Hein, "Solar and waste heat desalination College of Engineering University of Texas at El Paso Bureau of Reclamation," *Security*, no. April, 2004.

[30] S. Madaeni, "The application of membrane technology for water disinfection," *Water Res.*, vol. 33, no. 2, pp. 301–308, 1999.

[31] C. Gostoli and G. C. Sarti, "Separation of liquid mixtures by membrane distillation," *J. Memb. Sci.*, vol. 41, no. C, pp. 211–224, 1989.

[32] G. L. Liu, C. Zhu, C. S. Cheung, and C. W. Leung, "Theoretical and experimental studies on air gap membrane distillation," *Heat Mass Transf.*, vol. 34, no. 4, pp. 329–335, 1998.

[33] D. U. Lawal and A. E. Khalifa, "Experimental investigation of an air gap membrane distillation unit with double-sided cooling channel," *Desalin. Water Treat.*, no. MAY, pp. 1–15, 2015.

[34] M. Khayet and C. Cojocaru, "Artificial neural network modeling and optimization of desalination by air gap membrane distillation," *Sep. Purif. Technol.*, vol. 86, pp. 171–182, 2012.

[35] M. Khayet and C. Cojocaru, "Air gap membrane distillation: Desalination, modeling and optimization," *Desalination*, vol. 287, no. 0, pp. 138–145, 2012.

[36] A. Alkhudhiri, N. Darwish, and N. Hilal, "Treatment of high salinity solutions: Application of air gap membrane distillation," *Desalination*, vol. 287, pp. 55–60, 2012.

[37] A. S. Alsaadi, N. Ghaffour, J.-D. Li, S. Gray, L. Francis, H. Maab, and G. L. Amy, "Modeling of air-gap membrane distillation process: A theoretical and experimental study," *J. Memb. Sci.*, vol. 445, pp. 53–65, 2013.

[38] H. Geng, H. Wu, P. Li, and Q. He, "Study on a new air-gap membrane distillation module for desalination," *Desalination*, vol. 334, no. 1, pp. 29–38, 2014.

[39] Q. He, P. Li, H. Geng, C. Zhang, J. Wang, and H. Chang, "Modeling and optimization of air gap membrane distillation system for desalination," *Desalination*, vol. 354, pp. 68–75, 2014.

[40] A. Khalifa, D. Lawal, M. Antar, and M. Khayet, "Experimental and theoretical investigation on water desalination using air gap membrane distillation," *Desalination*, vol. 376, pp. 94–108, 2015.

[41] A. E. Khalifa and D. U. Lawal, "Performance and Optimization of Air Gap Membrane Distillation System for Water Desalination," *Arab. J. Sci. Eng.*, vol. 40, no. 12, pp. 3627–3639, 2015.

[42] V. V. Ugrozov, I. B. Elkina, V. N. Nikulin, and L. I. Kataeva, “Theoretical and experimental research of liquid-gap membrane distillation process in membrane module,” *Desalination*, vol. 157, no. 1–3, pp. 325–331, 2003.

[43] M. Essalhi and M. Khayet, “Application of a porous composite hydrophobic/hydrophilic membrane in desalination by air gap and liquid gap membrane distillation: A comparative study,” *Sep. Purif. Technol.*, vol. 133, pp. 176–186, 2014.

[44] V. V. Ugrozov and L. I. Kataeva, “Mathematical modeling of membrane distiller with liquid gap,” *Desalination*, vol. 168, no. 1–3, pp. 347–353, 2004.

[45] L. Francis, N. Ghaffour, A. A. Alsaadi, and G. L. Amy, “Material gap membrane distillation: A new design for water vapor flux enhancement,” *J. Memb. Sci.*, vol. 448, pp. 240–247, 2013.

[46] A. E. Khalifa, “Water and air gap membrane distillation for water desalination - An experimental comparative study,” *Sep. Purif. Technol.*, vol. 141, pp. 276–284, 2015.

[47] J. G. Lee and W. S. Kim, “Numerical study on multi-stage vacuum membrane distillation with economic evaluation,” *Desalination*, vol. 339, no. 1, pp. 54–67, 2014.

[48] J. G. Lee, Y. D. Kim, S. M. Shim, B. G. Im, and W. S. Kim, “Numerical study of a hybrid multi-stage vacuum membrane distillation and pressure-retarded osmosis system,” *Desalination*, vol. 363, pp. 82–91, 2015.

[49] Y. D. Kim, K. Thu, and S. H. Choi, “Solar-assisted multi-stage vacuum membrane distillation system with heat recovery unit,” *Desalination*, vol. 367, pp. 161–171, 2015.

[50] B. L. Pangarkar and S. K. Deshmukh, “Theoretical and experimental analysis of multi-effect air gap membrane distillation process (ME-AGMD),” *J. Environ. Chem. Eng.*, vol. 3, no. 3, pp. 2127–2135, 2015.

[51] H. W. Chung, J. Swaminathan, D. M. Warsinger, and J. H. Lienhard V, “Multistage vacuum membrane distillation (MSVMD) systems for high salinity applications,” *J. Memb. Sci.*, vol. 497, pp. 128–141, 2016.

[52] Y. Xing, C. Qi, H. Feng, Q. Lv, G. Xu, H. Lv, and X. Wang, “Performance study of a pilot-scale multi-effect vacuum membrane distillation desalination plant,” *Desalination*, 2016.

[53] H. Geng, J. Wang, C. Zhang, P. Li, and H. Chang, “High water recovery of RO brine using multi-stage air gap membrane distillation,” *Desalination*, vol. 355, pp. 178–185, 2015.

[54] X. Zhang, Z. Guo, C. Zhang, and J. Luan, “Exploration and optimization of two-stage vacuum membrane distillation process for the treatment of saline wastewater produced by natural gas exploitation,” *Desalination*, vol. 385, pp. 117–125, 2016.

[55] P. A. Hogan, Sudjito, a. G. Fane, and G. L. Morrison, “Desalination by solar heated membrane distillation,” *Desalination*, vol. 81, pp. 81–90, 1991.

[56] M. R. Qtaishat and F. Banat, “Desalination by solar powered membrane distillation systems,” *Desalination*, vol. 308, pp. 186–197, 2013.

[57] N. Ghaffour, J. Bundschuh, H. Mahmoudi, and M. F. a. Goosen, “Renewable energy-driven desalination technologies: A comprehensive review on challenges and potential applications of integrated systems,” *Desalination*, vol. 356, pp. 94–114, 2015.

[58] F. Salata and M. Coppi, “A first approach study on the desalination of sea water using heat transformers powered by solar ponds,” *Appl. Energy*, vol. 136, pp. 611–618, 2014.

[59] A. Chafidz, S. Al-Zahrani, M. N. Al-Otaibi, C. F. Hoong, T. F. Lai, and M. Prabu, “Portable and integrated solar-driven desalination system using membrane distillation for arid remote areas in Saudi Arabia,” *Desalination*, vol. 345, pp. 36–49, 2014.

[60] R. Schwantes, A. Cipollina, F. Gross, J. Koschikowski, D. Pfeifle, M. Rolletschek, and V. Subiela, “Membrane distillation: Solar and waste heat driven demonstration plants for desalination,” *Desalination*, vol. 323, pp. 93–106, 2013.

[61] C. D. Ho, C. H. Huang, F. C. Tsai, and W. T. Chen, “Performance improvement on distillate flux of countercurrent-flow direct contact membrane distillation systems,” *Desalination*, vol. 338, no. 1, pp. 26–32, 2014.

[62] M. Essalhi and M. Khayet, “Self-sustained webs of polyvinylidene fluoride electrospun nanofibers at different electrospinning times: 1. Desalination by direct contact membrane distillation,” *Journal of Membrane Science*, 2013.

[63] Y. Yun, R. Ma, W. Zhang, A. G. Fane, and J. Li, “Direct contact membrane distillation mechanism for high concentration NaCl solutions,” *Desalination*, vol. 188, no. 1–3, pp. 251–262, 2006.

[64] L. Martínez-Díez and M. . Vázquez-González, “Temperature and concentration polarization in membrane distillation of aqueous salt solutions,” *J. Memb. Sci.*, vol. 156, no. 2, pp. 265–273, 1999.

[65] S. Srisurichan, R. Jiraratananon, and A. G. Fane, “Mass transfer mechanisms and transport resistances in direct contact membrane distillation process,” *J. Memb. Sci.*, vol. 277, no. 1–2, pp. 186–194, 2006.

[66] T.-C. Chen, C.-D. Ho, and H.-M. Yeh, “Theoretical modeling and experimental analysis of direct contact membrane distillation,” *J. Memb. Sci.*, vol. 330, pp. 279–287, 2009.

[67] M. Khayet, “Membranes and theoretical modeling of membrane distillation: A review,” *Adv. Colloid Interface Sci.*, vol. 164, no. 1–2, pp. 56–88, 2011.

[68] M. Khayet and T. Matsuura, *Membrane Distillation: Principles and Applications*. 2011.

[69] M. Qtaishat, T. Matsuura, B. Kruczek, and A. Khayet, “Heat and mass transfer analysis in direct contact membrane distillation,” *Desalination*, vol. 219, pp. 272–292, 2008.

[70] J. Phattaranawik, R. Jiraratananon, and A. G. Fane, “Effect of pore size distribution and air flux on mass transport in direct contact membrane distillation,” *J. Memb. Sci.*, vol. 215, no. 1–2, pp. 75–85, 2003.

[71] W. Kast and C. R. Hohenthanner, “Mass transfer within the gas-phase of porous media,” *Int. J. Heat Mass Transf.*, vol. 43, no. 5, pp. 807–823, 2000.

[72] Z. Ding, R. Ma, and A. G. Fane, “A new model for mass transfer in direct contact membrane distillation,” *Desalination*, vol. 151, no. 3, pp. 217–227, 2003.

[73] R. B. Bird, W. E. Stewart, and E. N. Lightfoot, *Transport Phenomena*. 1960.

[74] F. A. Banat and J. Simandl, “Removal of benzene traces from contaminated water by vacuum membrane distillation,” *Chem. Eng. Sci.*, vol. 51, no. 8, pp. 1257–1265, 1996.

[75] S. B. Iversen, V. K. Bhatia, K. Dam-Johansen, and G. Jonsson, “Characterization of microporous membranes for use in membrane contactors,” *J. Memb. Sci.*, vol. 130, no. 1–2, pp. 205–217, 1997.

[76] J. Zhang, S. Gray, and J. De Li, “Predicting the influence of operating conditions on DCMD flux and thermal efficiency for incompressible and compressible membrane systems,” *Desalination*, vol. 323, pp. 142–149, 2013.

Vitae

Name	: Suhaib Mustafa Alawad Ahmed
Nationality	: Sudanese
Date of Birth	: 22-Oct-1990
Email	: su.mu085@gmail.com
Address	: Jabra, Khartoum, Sudan
Academic Background:	Master of Science (MSc.), December 2016, Mechanical Engineering Department, King Fahd University of Petroleum & Minerals, Dhahran, Saudi Arabia. Bachelor of Science (BSc.), September 2013, Mechanical Engineering Department, University of Khartoum, Khartoum, Sudan.